Master's thesis

NTNU
Norwegian University of Science and Technology
Faculty of Engineering
Department of Structural Engineering

Magne Stangeland Hårr & Gaute Kjeka

Macroporosity and water penetration measurements of sprayed concrete:

Open vs closed macroporosity, size, shape, orientation and anisotropy

Master's thesis in structural engineering
Supervisor: Stefan Jacobsen
Co-supervisor: Nicholas Henry Trussell, Iman Asadi and Martin Kristoffersen

June 2022

NTNU
Norwegian University of Science and Technology

Magne Stangeland Hårr & Gaute Kjeka

Macroporosity and water penetration measurements of sprayed concrete:

Open vs closed macroporosity, size, shape, orientation and anisotropy

Master's thesis in structural engineering
Supervisor: Stefan Jacobsen
Co-supervisor: Nicholas Henry Trussell, Iman Asadi and Martin Kristoffersen
June 2022

Norwegian University of Science and Technology
Faculty of Engineering
Department of Structural Engineering

NTNU
Kunnskap for en bedre verden

Department of Structural Engineering
Faculty of Engineering
NTNU – Norwegian University of Science and Technology

ACCESSIBILITY

Open

MASTER'S THESIS 2022

SUBJECT AREA: TKT4950	DATE: 9th June 2022	NO. OF PAGES: 72 + Appendix

TITLE:

Macroporosity and water penetration measurements of sprayed concrete: Open vs closed macroporosity, size, shape, orientation and anisotropy

Makroporøsitet- og vanninntrengingmålinger i sprøytebetong: Åpen vs. lukket makroporøsitet, størrelse, form, orientering og anisotropi

BY:
Magne Stangeland Hårr
Gaute Kjeka

SUMMARY:
The purpose of the presented work was to investigate macroporosity and permeability of sprayed concrete. This entailed (1) examining open and closed macroporosity measured by the PF method, (2) comparing air contents in different types of concrete, measured by the PF method and image analysis (IMA), (3) investigating size, shape and orientation distributions with IMA and (4) performing water penetration tests normal and parallel to spraying direction. A literature review was carried out, and results from previous studies were presented together with the results of the experimental tests in this project. The PF method, image analysis and water penetration test were carried out in accordance with SINTEF's full PF procedure, ASTM C457 and NS-EN 12390-8, respectively, but certain adaptations were made.

Sprayed concrete has high open macroporosity, and the open macroporosity increases for increasing set accelerator dosage. The PF method measures higher air content than IMA in conventional concrete, whereas IMA measures the highest air content in sprayed concrete, zero-slump concrete, high strength concrete and cast "sprayed concrete". Open macroporosity has previously been suggested as an explanation for the deviation in air content measured by the PF method and IMA. However, open macroporosity can not solely explain this deviation.

Total macroporosity in sprayed concrete increases with addition of set accelerator and increased flow rate in the hose, but the total macroporosity is higher in cast concrete than in sprayed concrete with the same mix design. The macropores become more elongated by the spraying process and addition of set accelerator, and they tend to orient perpendicular to the spraying direction. The shape of the macropores seems to be unaffected by spraying angle, spraying distance and mix design.

Water penetrated sprayed concrete more easily normal to spraying direction than parallel to spraying direction. The sprayed concrete with high set accelerator dosage was more permeable than the sprayed concrete with low set accelerator dosage. However, pure spray of set accelerator (defined as "spitting") and lamination damages seem to influence water penetration more than set accelerator dosage.

RESPONSIBLE TEACHER: Stefan Jacobsen

SUPERVISORS: Stefan Jacobsen, Nicholas Henry Trussell, Iman Asadi and Martin Kristoffersen

CARRIED OUT AT: Department of Structural Engineering

Abstract

The purpose of the presented work was to investigate macroporosity and permeability of sprayed concrete. This entailed (1) examining open and closed macroporosity measured by the PF method, (2) comparing air contents in different types of concrete, measured by the PF method and image analysis (IMA), (3) investigating size, shape and orientation distributions with IMA and (4) performing water penetration tests normal and parallel to spraying direction. A literature review was carried out, and results from previous studies were presented together with the results of the experimental tests in this project. The PF method, image analysis and water penetration test were carried out in accordance with SINTEF's full PF procedure, ASTM C457 and NS-EN 12390-8, respectively, but certain adaptations were made.

Sprayed concrete has high open macroporosity, and the open macroporosity increases for increasing set accelerator dosage. The PF method measures higher air content than IMA in conventional concrete, whereas IMA measures the highest air content in sprayed concrete, zero-slump concrete, high strength concrete and cast "sprayed concrete". Open macroporosity has previously been suggested as an explanation for the deviation in air content measured by the PF method and IMA. However, open macroporosity can not solely explain this deviation.

Total macroporosity in sprayed concrete increases with addition of set accelerator and increased flow rate in the hose, but the total macroporosity is higher in cast concrete than in sprayed concrete with the same mix design. The macropores become more elongated by the spraying process and addition of set accelerator, and they tend to orient perpendicular to the spraying direction. The shape of the macropores seems to be unaffected by spraying angle, spraying distance and mix design.

Water penetrated sprayed concrete more easily normal to spraying direction than parallel to spraying direction. The sprayed concrete with high set accelerator dosage was more permeable than the sprayed concrete with low set accelerator dosage. However, pure spray of set accelerator (defined as "spitting") and lamination damages seem to influence water penetration more than set accelerator dosage.

Sammendrag

Hensikten med oppgaven var å undersøke makroporøsitet og permeabilitet til sprøytebetong. Dette innebar å (1) undersøke åpen og lukket makroporøsitet målt med PF-metoden, (2) sammenligne luftinnhold i ulike betongtyper målt med PF-metoden og bildeanalyse (IMA), (3) undersøke fordelinger av størrelse, form og orientering til makroporer med IMA, og (4) utføre vanninntrengingforsøk normalt på og parallelt med sprøyteretningen. Et litteraturstudium ble gjennomført, og resultater fra tidligere studier ble presentert sammen med resultatene fra forsøkene i dette prosjektet. PF-metoden, bildeanalyse og vanninntrenging ble gjennomført i samsvar med henholdsvis SINTEFs PF-prosedyre, ASTM C457 og NS-EN 12390-8, men prosedyrene ble justert.

Sprøytebetong har mye åpen makroporøsitet, og den åpne makroporøsiteten øker ved økende mengde størkningsakselerator. PF-metoden måler høyere luftinnhold enn IMA i konvensjonell betong, mens IMA måler høyest luftinnhold i sprøytebetong, jordfuktig betong, høyfast betong og støpt "sprøytebetong". Åpen makroporøsitet har tidligere blitt foreslått som en forklaring på avviket i luftinnhold målt med PF-metoden og IMA. Det ble likevel funnet at åpen makroporøsitet ikke kan forklare dette avviket alene.

Total makroporøsitet i sprøytebetong øker ved tilsetning av størkningsakselerator og økt strømningshastighet i slangen, men total makroporøsitet er høyere i støpt betong enn i sprøytebetong med samme betongsammensetning. Makroporene blir mer avlange i sprøyteprosessen og ved tilsetning av størkningsakselerator, og de ser ut til å orientere seg normalt på sprøyteretningen. Det virker som at formen til makroporene er upåvirket av sprøytevinkel, sprøyteavstand og betongsammensetning.

Vann trenger lettere inn i sprøytebetong normalt på sprøyteretningen enn parallelt med sprøyteretningen. Sprøytebetong med mye størkningsakselerator var mer permeabel enn sprøytebetong med lite størkningsakselerator. Det ser likevel ut til at sprøyting av kun størkningsakselerator (definert som "spytting") og lamineringsskader påvirker vanninntrenging mer enn mengde størkningsakselerator.

Preface and acknowledgements

This master's thesis was written spring semester 2022, and it was carried out in close collaboration with Nicholas Trussell's PhD and the SUPERCON project.

We are particularly thankful to our main supervisor, Stefan Jacobsen, who has enthusiastically provided both theoretical and practical guidance at short notice the whole semester. We would further like to thank our three co-supervisors. Nicholas Henry Trussell has always been available and repeatedly given substantial guidance in the laboratory and meetings. We would also like to thank him for allowing us to analyze and present data from his PhD project. Iman Asadi and Martin Kristoffersen have given useful feedback and continuous encouragement during progress meetings throughout the semester.

An important part of this thesis is a literature review of porosity measurements on different types of concretes. We are thankful to Synnøve Adelheid Myren, Øyvind Bjøntegaard and Ola Skjølsvold for sending us raw data from previous studies.

We would like to show gratitude to Per Øystein Nordtug, who have assisted and trained us for various lab activities and other practical matters. We would further acknowledge Erik Johansen for the active participation and supervision during sawing of sprayed concrete panels and water penetration experiments in the SINTEF lab. Ingvild Runningen at Department of Materials Science and Engineering provided training and guidance with regards to polishing, which we are very grateful for.

Trondheim, 9th June 2022

Magne Stangeland Hårr and Gaute Kjeka

Contents

List of Tables

List of Figures

Abbreviations frequently used in this thesis

A	Air
AEA	Air entraining agent
Agg.	Aggregate
FA	Fly ash
HA	Hardening accelerator
IMA	Image analysis
LF	Limestone filler
NPRA	Norwegian Public Roads Administration
OA	Optical analysis
PF	Pore Fraction
PFc	Closed macroporosity measured with the full PF method
PFo	Open macroporosity measured with the full PF method
PFt	Total macroporosity (i.e. PFt = PFo + PFc)
RH	Relative humidity
SC	Sprayed concrete
SRA	Shrinkage reducing agent
TSA	Trondheim set accelerator
TSM	Trondheim spraying mechanics

1 Introduction

1.1 Background

Sprayed concrete is used mostly for rock support, tunneling, in repair work and in structures where it is difficult to use formwork [1]. In tunnels, sprayed concrete may be used as both immediate support and permanent tunnel lining [2]. To improve durability and stability of sprayed concrete tunnel linings, requirements for thickness of sprayed concrete have increased [3]. One example is that the Norwegian Public Roads Administration increased the minimum thickness of sprayed concrete in tunnels from 60 mm to 80 mm in 2010 [4, 5]. Because of this and more tunnel projects than earlier in Norway, the consumption of sprayed concrete has increased.

Since the production of sprayed concrete is high, it is important to ensure a sufficient durability of sprayed concrete structures. Nearly all the deterioration mechanisms of concrete involve transport of water through the concrete [6]. Therefore, it is important to make the tunnel lining watertight. It will be a great synergy if the sprayed concrete can be made impermeable and durable for the service life period of the tunnel.

Macrovoids and porosity in sprayed concrete linings influence permeability and strength of the sprayed concrete, and hence influence two of the main properties of the sprayed concrete lining. Two common methods for measuring macroporosity in hardened concrete in Norway is the PF method and image analysis (IMA). However, the methods are based on very different principles and yield different values for the same concrete [7]. The PF method is based on capillary suction and filling of pores, whereas IMA is based on optically visible pores in a specific plane section of the concrete.

In optical macroporosity measurements, irregularly shaped air voids have been observed in sprayed concrete [8, 9]. Irregularly shaped and elongated air voids oriented in the same direction might lead to different permeability of sprayed concrete in different directions. It is already known that sprayed concrete has different strength properties parallel and normal to spraying direction, which is so far believed to be caused by fiber alignment perpendicular to the spraying direction [10]. This motivates to further analyze a possibility for anisotropic properties in porosity and permeability as well.

This thesis is a part of the research project “Sprayed sUstainable PErmanent Robotized CONcrete tunnel lining (SUPERCON)" financed by the Research Council of Norway (project no. 294724), in cooperation with industrial partners Andersen Mek. Verksted, BASF, Bever Control, Bekaert, Elkem, Entreprenørservice, NORCEM, SWECO Norge, Veidekke and Wacker Chemicals Norway. Research partners in SUPERCON are NGI, NTNU and SINTEF. The following project owners support the project; Bane NOR, Nye Veier and the Norwegian Public Roads Administration. In the SUPERCON project, the main focus is to “provide new competence for research institutions and industry to produce Sprayed sUstainable Permanent Robotized CONncrete tunnel linings, which meet modern demands for functionality, sustainability and eco-friendliness in future

infrastructure projects" [11]. A paper with some of the data presented in this thesis may be published. The master's thesis is also a continuation of Magne Stangeland Hårr and Gaute Kjeka's specialization project from fall 2021 [12].

1.2 Objectives

The objectives of the thesis is to:

- Review literature on air content measurements with the PF method and with image analysis (IMA) on sprayed concrete and other types of concrete.
- Review literature on the relation between macroporosity measurements with the aforementioned methods, open macroporosity and the possibility for water transport through sprayed concrete tunnel linings.
- Compare total air void measurements from the PF method and IMA.
- Evaluate the open macroporosity in sprayed concrete and compare it to other types of concrete.
- Characterize size, shape and orientation of the macropores with IMA.
- Analyze anisotropy effect of sprayed concrete based on water penetration and porosity measurements.

1.3 Scope

The experimental program is based on concrete from four different series, Flekkefjord, Trondheim set accelerator (TSA), Trondheim spraying mechanics (TSM) and Svorkmo, with different parameters varying. The laboratory work that has been conducted in association with this thesis is shown in Table 1 and 2.

There have been made macroporosity measurements, both with the PF method and with image analysis (IMA) of sprayed concrete with different spraying mechanics, mix designs and set accelerator dosage. Size, shape, and orientation was recorded for each air void in the IMA. It has also been executed water penetration experiments on sprayed concrete with different accelerator dosage, both normal and parallel to spraying direction.

Table 1: Overview of the production and testing of sprayed concrete in 2020 and 2021.

Activity	Date	Performed by
Concrete production Flekkefjord	18th February 2020	Ribe Betong
Concrete production Trondheim	16th June 2020	Unicon
Concrete production Svorkmo	16th March 2021	Unicon
Spraying in Flekkefjord	18th February 2020	
Spraying in Trondheim	16-17th June 2020	
Spraying in Svorkmo	16th March 2021	
Coring and sample preparation		SINTEF
The full PF method	3 months after spraying	Nicholas Henry Trussell, Magne Stangeland Hårr
Polishing and sample preparation for IMA	Spring 2021	Nicholas Henry Trussell
IMA	Summer 2021	Magne Stangeland Hårr

Table 2: Overview of testing of sprayed concrete in 2022. Only concrete from two mixes in the Flekkefjord series and one mix from the Svorkmo series was tested for water penetration and prepared for binary images.

Activity	Date	Performed by
Sawing of sprayed concrete panels, 3% and 10% Flekkefjord mixes	9-10th March 2022	SINTEF, Gaute Kjeka, Magne Stangeland Hårr
Water penetration	Spring 2022	Gaute Kjeka, Magne Stangeland Hårr
Polishing and sample preparation for binary images	Spring 2022	Gaute Kjeka, Magne Stangeland Hårr

The scope is limited to wet sprayed, air entrained concrete mixes with alkali free set accelerator, typically used in hard rock tunnel linings in Norway. All the concrete was sprayed on panels. Only macroporosity is analyzed, whereas the gel and capillary porosity is not considered in this thesis.

2 Literature review

2.1 Sprayed concrete

Sprayed concrete is concrete that is pumped to a nozzle, where accelerator and compressed air is added, and placed by spraying at a surface where it sets instantly. Compared to conventional concrete, sprayed concrete has a considerably higher matrix volume. The matrix phase consists of cement, pozzolan, water, admixtures and particles with diameter smaller than 0.125 mm [13]. Sprayed concrete may have a matrix volume higher than 400 l/m^3, as compared to 300-320 l/m^3 in conventional structural concrete [14]. The high matrix volume ensures sufficient pumpability and sprayability. Sprayability is defined by Trussell and Jacobsen as the "ability of a specific concrete mix to be sprayed and obtain satisfactory production and in-situ properties after pumping, addition of accelerator at the nozzle and spraying with a specific spraying set up and specific settings" [15, p. 22].

Coarse aggregate may fall off when the sprayed concrete hits the surface, which is referred to as rebound loss. Consequently, the maximum aggregate size is usually 8 mm in sprayed concrete and the mixes usually contain silica fume as it has been found that rebound is reduced by reducing maximum aggregate size and by using condensed silica fume [16]. At least 90 weight-% of the aggregate should be smaller than 8 mm in Norway [1, 2].

The addition of accelerator reduces the quality of the concrete [1]. Consequently, the quality of the initial fresh concrete must be high in order to satisfy requirements with regards to strength and durability. Sprayed concrete in subsea tunnels in Norway is required to have a strength class of B40 and durability class of M45 or better [1].

2.2 Porosity in concrete

Concrete is a porous material. Pores of different sizes give the concrete different properties, and they are usually divided into three different categories: gel pores, capillary pores and macropores/air voids. Gel pores are defined as pores smaller than 2 nm [17, 18]. In this thesis, the definition of capillary pores and macropores presented by Yun et al. (2010) [19, 20] will be used. Their definition is that air voids are larger than 10 µm. Consequently, the size of the capillary pores is between 2 nm and 10 µm. Yun et al. (2010) also distinguishes between entrained air and entrapped air [19]. In this thesis, entrained air consists of the air voids smaller than 1000 µm, while entrapped air consists of the air voids larger than 1000 µm.

In conventional concrete, macropores (i.e. air voids) are formed when air is whipped into the concrete during mixing and during inadequate compaction [17]. Air voids may also form due to addition of air entraining admixtures (AEA), and these air voids are usually spherical in shape and considered as entrained air according to the definitions of Yun et al. (2010) [19]. In sprayed concrete with AEA, most of the air content can be lost in the spraying process, according to Beaupré [21]. Air entraining admixtures are used to ensure sufficient protection

against frost and make the fresh concrete more workable. Entrapped air is caused by poor compaction [17, 22], and it is considered unfavourable, since it reduces the strength of concrete. During hydration, CSH-gel is formed and the gel also contains small pores, i.e. gel pores [17, 18]. Capillary pores in the hardened concrete includes parts of the space that was filled with water in the fresh concrete [17]. As the hydration process continues, the volume of capillary pores is decreasing and the volume of gel pores is increasing, because the amount of CSH-gel is increasing and the gel is consuming water [17, 23].

Air voids affect the properties of concrete. For instance, studies show that for each 1% of air content in conventional/structural concrete, its strength is reduced by 5% [24]. An explanation to this is that forces will be distributed over a smaller cross-sectional area and stresses consequently increases. In case of frost, air voids may function as empty spaces in concrete which the freezing water in capillary pores may freely expand into and depressurize [25]. This concept is shown in Figure 1 [26]. To maximize this positive effect, the air voids should be as evenly distributed in the concrete as possible. This is needed to achieve the lowest possible average distance for the freezing water to travel from capillary pores to an air void.

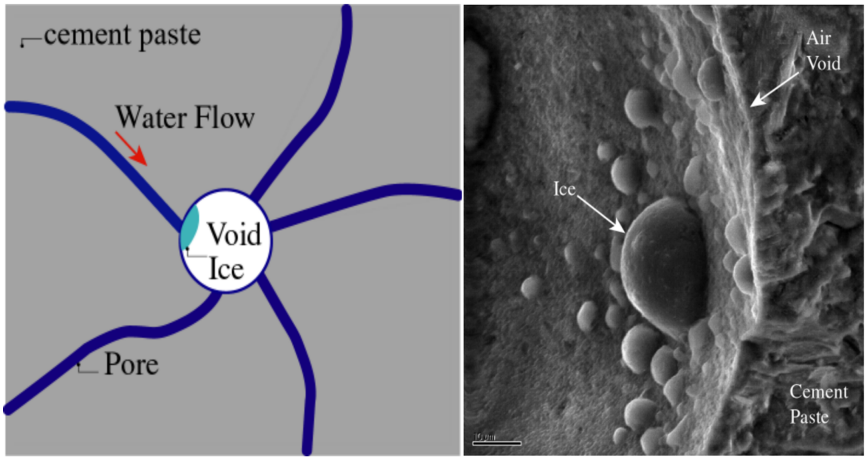

Figure 1: When water freezes, it is transported into an air void where it may expand without creating cracks in the concrete. Figure and photo from Mehta and Monteiro [26].

2.3 Capillary suction

Water may be absorbed into concrete in the same way water level rises in a small tube. This phenomenon is called capillary suction. It happens due to formation of a water meniscus in the pore towards the wet side of the concrete, which pulls the water into the pore [27]. The uptake of water in concrete due to suction is proportional to the square root of time, up to a knee point (see Figure 2). The capillary suction ("underpressure") in the water in the pore may be calculated with the equation:

$$p = 2 \cdot \sigma_w / r_c \tag{1}$$

where p = pressure in the water in the pore, $\sigma_w = 0.073$ N/m (for water at 20°C) is the surface

tension between liquid and gas, and r_c = pore radius. Equation 1 shows that for increasing pore radius, the capillary suction decreases. The macropores are too large to be filled by capillary suction but they are filled when the concrete is saturated with pressure. This is the idea behind the PF method, which is described in more detail in subsection 3.3.

Figure 2 shows the water uptake in concrete as a function of time. Before the knee point in this figure, the pores are filled by capillary suction. Hall and Hoff describe a model of how water water uptake is in this phase [28]. Water is sucked into the concrete by capillary forces, and during the process it may invade blind pore paths or fill pores from all sides, such that the air may not escape. These air pockets will not be filled with water during the suction phase, and there will become a pressure inside them, expressed as in Equation 1 [28].

The filling after the kneepoint in Figure 2 is much slower, and Hall and Hoff [28] suggest that the dominant transport mechanism in this part of the curve is diffusion. Because of different sizes and shapes of the trapped air pockets, they will have different pressures. The solubility of gas increases for increased pressure (Henry's Law). Since the pressure of the trapped air is higher than the pressure at the surface of the concrete, there will be a gradient in concentration of dissolved gas (air) between the entrapped air and the surface. The concentration gradient drives a diffusion process that governs the filling of pores after the kneepoint [28]. Note that this "entrapped air" is not the same entrapped air as explained in subsection 2.2 and subsection 2.7. Erik Sellevold proposes a different mechanism for the filling of pores after the knee point [29]. He suggests that the smallest air pores have capillary suction, and that they are filled slowly due to suction. According to Sellevold, the water must be "pulled through" the capillary pores to fill the small air voids by suction [29]. For this reason, the filling is slow.

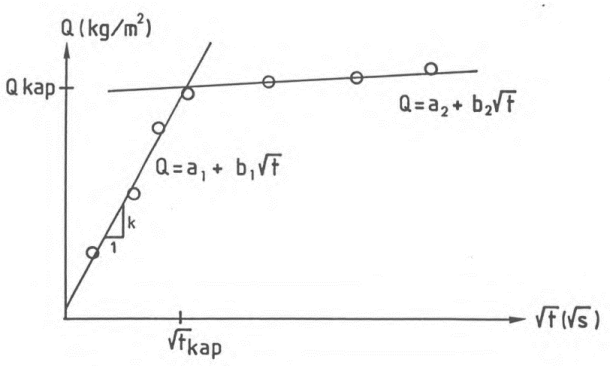

Figure 2: Absorption of water into concrete. The figure is from [30].

2.4 Open, closed and total macroporosity

A well known way of measuring porosities in concrete is the PF method. SINTEF has proposed an extended variant of the PF method, "the full PF procedure", which distinguishes between suction porosity, open macroporosity and closed macroporosity. The procedure is described in subsection 3.3. The principles of the full PF procedure is to first let the gel and capillary pores fill with water with one sided capillary suction. The samples are then submerged in water

and further pressure saturated. The pores that are filled with water during submersion after one sided suction are regarded as open macropores, see Equation 6. Closed macroporosity is defined as the pores that are further filled by pressure saturation after submersion, see Equation 7. Total macroporosity is defined as the sum of open and closed macroporosity. Note that the traditional PF procedure skips one sided capillary suction. Hence, the traditonal PF procedure only measures closed macroporosity, and the open macroporosity is then a part of the suction porosity. In this thesis, the following abbreviations are frequently used: PFo (open macroporosity), PFc (closed macroporosity) and PFt (total macroporosity).

According to Equation 1 and Hall and Hoff's theory [28], open macroporosity is not filled by capillary suction nor external pressure. During submersion and filling of open macroporosity, water may enter the concrete from all sides as opposed to the one sided suction where capillary pores are filled. Sellevold found that the duration of capillary suction is important for suction porosity and open macroporosity, especially in high quality concrete (i.e. w/b = 0.35) [7]. In high quality concrete, the suction porosity increased by 0.4 vol-% when the duration of suction increased from 2 to 7 days, which reduces the open macroporosity with the same amount. Usually, open macroporosity is around 0.5% and lower. Higher values indicate continuous macropores [31]. This is most common for dry compacted concretes and sprayed concrete [31].

2.5 Previous studies with open macroporosity measurements

The studies with open macroporosity measurements found in literature are presented here. The open macroporosity values from these studies are presented in subsection 4.1. The studies include several types of concrete, and the objective is to compare sprayed concrete with other types of concrete. The following studies have been reviewed:

- Myren and Bjøntegaard (2014) [32]
- Tandberg (2014) [33]
- Justnes et al. (2007) [34]
- Hermansen (2018) [35]
- Bjelland and Moi (2021) [36]
- Rønnes (2015) [37]

Myren and Bjøntegaard [32], and Tandberg [33] measured open macroporosity in sprayed concrete. It should be emphasized that Tandberg [33] measured open macroporosity of the samples Karl Gunnar Holter presents in his doctoral thesis [38], and that these samples have been subjected to 25-50 freeze-thaw cycles before the PF test. The mixes in Justnes et al. contain high amounts of filler [34]. Hermansen used mixes with high fly ash content [35], Rønnes used mixes with slag [37], and Bjelland and Moi used concrete with high fly ash and slag content [36]. Note that the open macroporosity was not published in the papers of Myren and

Bjøntegaard [32] and Justnes et al. [34]. The open macroporosity for the samples in these two papers were calculated for this master's thesis based on the raw data from the papers. There were also some differences in duration of capillary suction, submersion and pressure saturation, as well as saturation pressure in the investigated studies. These are presented in Table 3.

Table 3: Differences in duration of capillary suction, submersion and pressure saturation, as well as saturation pressures in the investigated studies.

Reference	Duration of capillary suction [days]	Duration of submersion [days]	Duration of pressure saturation [days]	Saturation pressure [MPa]
Myren & Bjøntegaard (2014) [32]	4	3	1	5
Tandberg (2014) [33]	4	3	3	5
Justnes et al. (2007) [34]	5	3	3	8
Hermansen (2018) [35]	4	3	1	5
Bjelland & Moi (2021) [36]	4	3	1	5
Rønnes (2015) [37]	4	3	1	5

Salvador et al. [39] have studied water accessible porosity, which includes gel porosity, capillary porosity and open macroporosity. Since they used a different procedure than in subsection 3.3, the porosities are not directly comparable to porosities measured by the PF method, but qualitatively their results could be interesting. They examined the relation between accelerator dosage and water accessible porosity in mortars [39]. Equation 2 shows their definition of water accessible porosity.

$$w_p = \frac{w_s - w_d}{w_d} \tag{2}$$

w_s is the weight of mortar after 3 days of submersion, while w_d is the weight of mortar dried at 60°C for 5 days. The measurements were done when the age of the mortar was 7 and 28 days. Note that Salvador et al. dried the mortar after submersion [39].

According to Salvador et al. the water accessible porosity depends on the accelerator dosage, and the water accessible porosity increases with increasing accelerator dosages [39]. A suggested explanation is that "fast setting does not allow enough time for the matrix to consolidate properly and eliminate the entrapped air, leading to higher porosities" [39, p. 126].

Macroporosity may also be measured with image analysis (IMA). IMA measures macroporosity optically and will not take into consideration which transport mechanism that fills the pores, as opposed to the PF method. Thus, it is assumed that IMA measures the total macroporosity, both open and closed. The traditional procedure of the PF method will only measure closed macroporosity, as it does not include one sided suction before submersion. A comparison of the methods is presented in the next subsection.

2.6 PF method vs IMA - comparison of previous studies

Studies where both PF method and IMA were used, show that the two methods give different values for total air content. Jacobsen et al. (1993) distinguishes between open and closed macroporosity as a possible explanation for different measured air contents with the traditional PF procedure and with IMA [40]. Studies by Sellevold and Farstad [7] and Shpak [41] indicate that the PF method gives larger total air content than IMA for conventional concrete, whereas studies by Jacobsen et al. (1993) [40], Sætre [42] and Holter [38] show that IMA gives the largest total air content in zero slump, high strength and sprayed concrete. In Mørtsell [43], Jacobsen et al. (1996) [44] and Myren and Bjøntegaard [32], none of the methods clearly measures larger air content than the other method. These results are presented in Table 4 and 5, and compared with Trussell's results in subsection 4.2.

Here, some of the differences of the studies in Table 4 and 5 will be mentioned. Table 4 and 5 show that air void measurements from the PF test often are based on more test specimens than the air void measurements from IMA. Furthermore, the PF test measures porosity in three dimensions, and image analysis measures the porosity in two dimensions. In other words, the PF measurements may be more representative for the entire concrete core.

Some of the mixes in Table 4 and 5 contain air entraining admixture (AEA), whereas others do not. Jacobsen et al. (1996) [44] and Shpak [41] used AEA in the mixes marked with an "A" in the name of the mix. It was added AEA in all of Sætre's [42] and Mørtsell's [43] mixes, while only "Mix 1" from both factories in Jacobsen et al. (1993) [40] contains AEA. Myren and Bjøntegaard did not use AEA in their mixes [32]. The details of the mix designs that Sellevold [7, 23] used are unknown.

The image analysis was conducted differently in the studies in Table 4 and 5. It is distinguished between OA (optical analysis) and IMA. OA means that air voids were counted manually, and IMA means that the air voids are counted by an image analysis program. In this thesis, they will both be regarded as IMA. All the studies followed the ASTM C457 standard, except for the study by Myren and Bjøntegaard [32] which followed the NS-EN 480-11 standard [45]. Sellevold (1986) [23] and Sellevold and Farstad (2005) [7] did not specify which standard they followed when they executed the IMA. In the studies by Jacobsen et al. (1993) [40], Jacobsen et al. (1996) [44], Sellevold (1986) [23] and Sellevold and Farstad (2005) [7] the image analysis was conducted by counting points manually, whereas Shpak [41], Sætre [42], Mørtsell [43] and Holter [38] have used MATLAB scripts developed by Fonseca and Scherer [46] to automatically count air voids. Air contents from Sellevold (1986)/Sellevold and Farstad (2005) were extracted from Figure 2 in [7] using an online graph-reader (WebPlotDigitizer).

The PF procedure in the studies varies, but the concrete specimens were dried at 105°C in all studies. In Holter's study, the samples were submerged for 7 days and pressure saturated for 3 days [38]. In Sætre's study, both submersion and pressure saturation lasted for at least 2 days [42]. Myren and Bjøntegaard submerged the specimens for 3 days and pressure saturated

for 1 day [32]. Shpak submerged the samples for 7 days and pressure saturated them for 2 days [41]. Mørtsell did not specify the details of the PF procedure [43]. The measurements in Mørtsell [43] were however performed by Andrei Shpak, and it may be assumed that the PF procedure in Shpak [41] and Mørtsell [43] is similar. Jacobsen et al. (1993) [40] and Jacobsen et al. (1996) [44] do not specify the durations of submersion and pressure saturation, but refer to the PF procedure in Sellevold (1986) [23]. The proposed procedure in Sellevold (1986) [23] is 3 days of submersion and 4 hours of pressure saturation. The saturation pressures are given in Table 4-5.

Table 4: Total air content measured with the PF method and IMA for different samples found in literature. Empty cells indicate that the data could not be found in the reference. Information about the number of samples in the references is slightly difficult to compare, because different words such as sections, samples and cores are used to provide information about the samples. These studies only measured closed air content with the PF method (no one sided suction before submersion).

Reference	Type of concrete	Mix name	Saturation pressure $[MPa]$	Air PF (closed) [%]	No. of samples PF	Air IMA (total) [%]	No. of samples IMA	PF (closed)/IMA
Jacobsen (1996) [44]	High strength	1 030-08 QD	10	1.3		1.0	2 sections	1.30
	High strength	5 035-08 ND	10	1.8		2.0	2 sections	0.90
	High strength	6 035-08 ND A	10	7.8		13.2	2 sections	0.59
	Conventional	7 035-00 ND2	10	2.4		3.5	2 sections	0.69
	Conventional	8 049-00 ND3 A	10	3.7		5.8	2 sections	0.64
	Conventional	9 040-00 ND	10	2.0		2.5	2 sections	0.80
	Conventional	10 040-05 ND	10	2.3		2.0	2 sections	1.15
	Conventional	11 040-05 ND A	10	4.2		5.3	2 sections	0.79
Shpak (2020) [41]	Conventional	0.40-33 A	5	6.0	4 discs	3.8	2 sections	1.58
	Conventional	0.40-33 0	5	2.1	4 discs	1.6	2 sections	1.31
	Conventional	0.45-33 A	5	5.9	4 discs	3.9	2 sections	1.51
	Conventional	0.45-33 0	5	2.4	4 discs	1.3	2 sections	1.85
	Conventional	0.293-33 A	5	5.2	4 discs	4.3	2 sections	1.21
	Conventional	0.293-33 0	5	1.9	4 discs	1.3	2 sections	1.46
	Conventional	0.45-00 A	5	5.4	4 discs	3.8	2 sections	1.42
Sætre (2014) [42]	High strength	1. B70 reference	5	3.1	3 samples	4.1	1 sample	0.76
	High strength	2. 0.5% steel	5	2.4	3 samples	3.7	1 sample	0.65
	High strength	3. 1.5% steel	5	1.8	3 samples	3.8	1 sample	0.47
	High strength	4. 1.5% poly.	5	2.7	3 samples	3.7	1 sample	0.73
	High strength	5. 1.5% basalt	5	3.7	3 samples	4.6	1 sample	0.80
Jacobsen (1993) [40]	Zero-slump	Factory A - Mix 1	10	4.2	3 cores	4.8	1 core	0.88
	Zero-slump	Factory A - Mix 2	10	6.9	3 cores	12.1	1 core	0.57
	Zero-slump	Factory B - Mix 1	10	3.4	2 cores	7.1	1 core	0.48
	Zero-slump	Factory B - Mix 2	10	5.6	2 cores	7.9	1 core	0.71

Table 5: Total air content measured with PF and IMA for different samples found in literature. Information about the number of samples in the references is slightly difficult to compare, because different words such as sections, samples and cores are used to provide information about the samples. Apart from Myren and Bjøntegaard [32] and Holter [38], these studies only measured closed air content with the PF method (no one sided suction before submersion).

Reference	Type of concrete	Mix name	Saturation pressure $[MPa]$	Air PF (closed) [%]	No. of samples PF	Air IMA (total) [%]	No. of samples IMA	PF (closed)/IMA
Sellevold (1986/2005) [7, 23]	Conventional	1	10	2.7	6 chunks	1.7	6 sections	1.64
	Conventional	2	10	3.4	6 chunks	2.4	6 sections	1.40
	Conventional	3	10	4.3	6 chunks	3.0	6 sections	1.41
	Conventional	4	10	4.4	6 chunks	3.3	6 sections	1.32
	Conventional	5	10	5.2	6 chunks	4.8	6 sections	1.08
	Conventional	6	10	7.9	6 chunks	6.0	6 sections	1.32
	Conventional	7	10	8.0	6 chunks	7.3	6 sections	1.10
	Conventional	8	10	8.8	6 chunks	7.3	6 sections	1.21
Mørtsell (2019) [43]	Conventional	B45MF40 A1-1	5 (assumed)	5.3	2 samples	5.9	2 samples	0.90
	Conventional	B45MF40 A1-2	5 (assumed)	3.8	2 samples	5.2	2 samples	0.73
	Conventional	B45MF40 A1-3	5 (assumed)	5.3	2 samples	6.6	2 samples	0.80
	Conventional	B45MF40 A2-1	5 (assumed)	6.3	2 samples	5.1	2 samples	1.23
	Conventional	B45MF40 A2-2	5 (assumed)	3.7	2 samples	4.1	2 samples	0.91
	Conventional	B45MF40 A2-3	5 (assumed)	5.2	2 samples	5.2	2 samples	0.99
	Conventional	B45MF40 A2-4	5 (assumed)	6.3	2 samples	4.9	2 samples	1.28
	Conventional	B45MF40 R1	5 (assumed)	6.8	2 samples	5.9	2 samples	1.14
	Conventional	B45MF40 R2	5 (assumed)	6.5	2 samples	7.2	2 samples	0.90
	Conventional	B45MF40 R3	5 (assumed)	5.8	2 samples	6.2	2 samples	0.94
	Conventional	B45MF40 R4	5 (assumed)	4.9	2 samples	5.1	2 samples	0.96
	Conventional	B45MF40 Y-1	5 (assumed)	5.7	2 samples	6.3	2 samples	0.90
	Conventional	B45MF40 Y-2	5 (assumed)	6.0	2 samples	5.7	2 samples	1.04
	Conventional	B45MF40 Y-3	5 (assumed)	4.5	2 samples	5.1	2 samples	0.88
	Conventional	B45MF40 Y-4	5 (assumed)	4.6	2 samples	4.0	2 samples	1.14
	Conventional	B45MF40 Y-5	5 (assumed)	4.8	2 samples	5.4	2 samples	0.87
	Conventional	B45MF40 Y-6	5 (assumed)	5.0	2 samples	4.6	2 samples	1.08
Myren & Bjøntegaard (2014) [32]	Cast	Steel fibre, cast	5	5.6	2 cores	6.6	2 cores	0.85
	Sprayed	Steel fibre, sprayed	5	3.8	2 cores	2.9	2 cores	1.31
	Cast	Macro pp fibre, cast	5	4.1	2 cores	5.0	2 cores	0.82
	Sprayed	Macro pp fibre, sprayed	5	3.6	2 cores	3.1	2 cores	1.16
Holter (2015) [38]	Sprayed	Average	5	4.5	27 specimens	5.7	5 specimens	0.79

2.7 Total air content and size of macropores (IMA) in sprayed concrete

There are few studies of macroporosity in sprayed concrete, but it is known that the air content is affected by the spraying process, the pumping process, AEA and set accelerator [12, 19, 32, 47]. The intention of this subsection is to get an overview of typical air contents in sprayed concrete and how different parameters influence it. Five studies will be presented, where total air content in sprayed concrete have been measured by IMA in all of them. In Appendix C.1, there is a complete overview of total air content from the studies presented here. It will be distinguished between four categories of SC (sprayed concrete):

- SC with accelerator
- SC without accelerator
- Cast SC (pumped)
- Cast SC (not pumped)

Both the SC with accelerator and SC without accelerator were sprayed through a nozzle. Cast SC was not sprayed and does not contain set accelerator. Cast SC has otherwise a typical sprayed concrete mix design.

Yun et al. (2019) [48] measured air content in accordance with ASTM C457 in cast SC (not pumped), cast SC (pumped) and SC with accelerator, as shown in Figure 4a. Moreover, Yun et al. (2010) [19] and Choi et al. [20] have measured the total air content in cast SC (not pumped) and in SC with accelerator. The experiments were done in accordance with ASTM C457 [49], and the air contents are presented in Figure 4b. Choi et al. [20] also presents the entrained and entrapped air for some of the mixes, see Table 6. All measured air voids are smaller than 6000 μm in Yun et al. (2010) [19], Yun et al. (2019) [48] and Choi et al. [20]. In the aforementioned studies, some of the mixes contain silica fume (SF), air entraining admixture (A or AE), fiber (F), polymer (P), viscosity admixture (V), fly ash (FA), metakaolin (MK) and ground-granulated blast furnace slag (GGBFS), see Appendix C.1.

Talukdar and Heere [47] have also measured total air content according to ASTM C457, see Figure 4d. Note that none of their mixes contained accelerator, and their mixes are defined as SC without accelerator in this thesis. In Figure 4c, Myren and Bjøntegaard's [32] measurements are presented. They followed the NS-EN 480-11 standard. Some of their mixes are SC with accelerator, whereas others are cast SC (not pumped).

The total air contents from literature are presented in box plots in Figure 4. Figure 3 shows how the different quartiles, median and mean is marked in the box plots. Quartiles are calculated by the "QUARTILE.EXC" function in Excel.

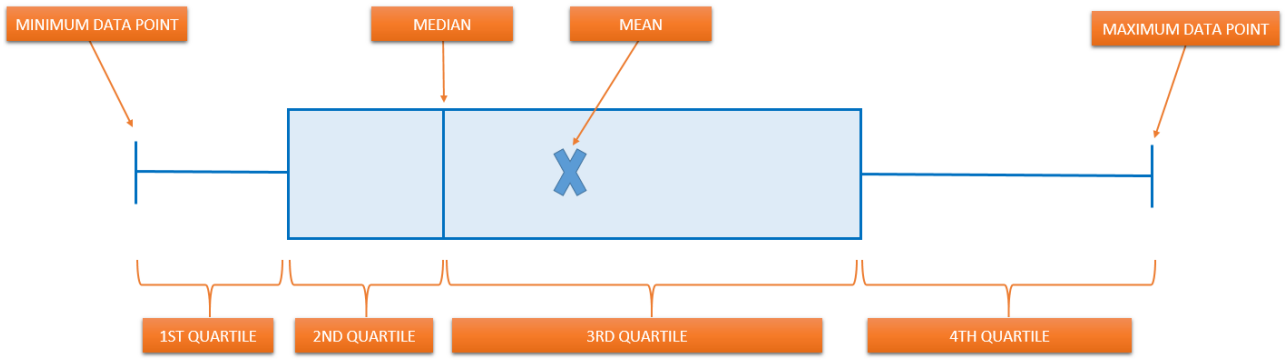

Figure 3: Figure explaining how box and whisker charts work. [50]

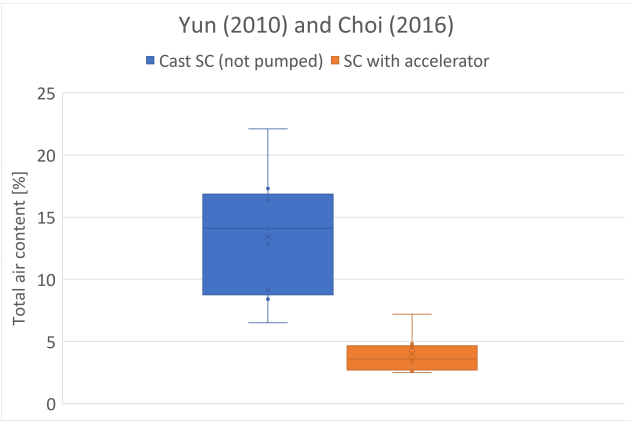

(a) Total air content from Yun et al. (2010) [19] and Choi et al. [20].

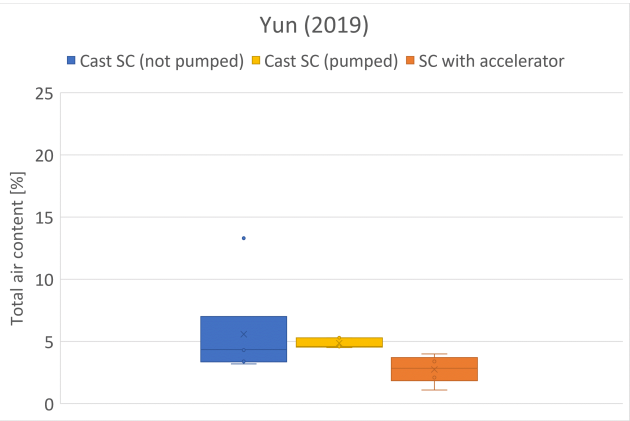

(b) Total air content from Yun et al. (2019) [48].

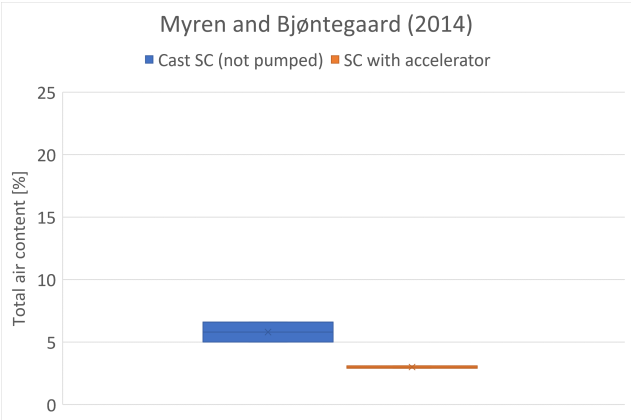

(c) Total air content from Myren and Bjøntegaard [32].

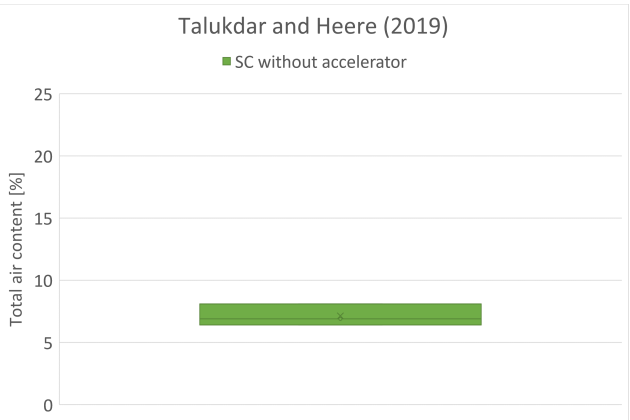

(d) Total air content from Talukdar and Heere [47].

Figure 4: Box plots with total air content in the different studies.

From Figure 4, it may be seen that SC with accelerator has lower air content than cast SC (pumped) and cast SC (not pumped). SC with accelerator has air contents in the range 1.1-7.2%. Cast SC (not pumped) has a very big spread. SC without accelerator has air contents in the range 6.4-8.1%. In Table 6, it is presented entrained and entrapped air from Choi et al. [20]. Entrained air varies from 2.9-4.2% and entrapped air varies from 0.5-0.8% for SC with accelerator and AEA. Table 6 also shows that an increasing silica fume content reduces the entrained air in sprayed concrete containing AEA.

Table 6: Entrained and entrapped air from the study by Choi et al. [20]. In the mix names, BS means "before shotcreting" (i.e. not pumped) and AS means "after shotcreting" (i.e. pumped). Silica fume content is given in the mix name, e.g. SF4.5 means 4.5% silica fume in the mix.

Reference	Mix	Entrained air $<1000\ \mu m$ [%]	Entrapped air $>1000\ \mu m$ [%]
Choi (2016) [20]	SF0-BS	4.2	4.9
	SF4.5-BS	4.4	4.0
	SF9-BS	4.7	1.8
	SF0-AS	1.9	0.7
	SF4.5-AS	2.2	0.6
	SF9-AS	2.0	0.5
	SF0-A-BS	12.3	4.1
	SF4.5-A-BS	12.6	1.6
	SF9-A-BS	9.1	3.7
	SF0-A-AS	4.2	0.6
	SF4.5-A-AS	3.7	0.8
	SF9-A-AS	2.9	0.5

2.8 Shape and orientation of air voids in concrete

It has previously been observed elongated air voids with irregular shape in sprayed concrete [8, 9]. An interesting parameter to investigate in relation with this is the threshold for percolating pores, with regards to the elongation of the pores. Percolation means that the pores are connected and there is a continuous path from one side of a specimen to the other. It is known in material science that the threshold for percolation is dependent on factors such as shape, orientation, size and distribution of particles and pores [51]. More elongated and irregular shaped pores have a lower percolation threshold, which motivates further analysis of these parameters for macroporosity in concrete.

Garboczi et al. have calculated geometrical percolation thresholds for porous materials with ellipsoids of different aspect ratios [52]. Aspect ratio is defined as “the length of the symmetry axis of the ellipsoid, a, over the length of the axis perpendicular to the symmetry axis, b” [52, p. 2]. The calculation of percolation thresholds was done by considering a cube of a material and generating two randomly placed ellipsoids one million times. Each time, one ellipsoid is generated along the x-axis, then the other is generated, randomly placed and with random orientation, but with same aspect ratio. Count was kept if the two overlapped. The volume fraction for percolation, p_c, was then calculated. If the volume of air voids is equal to or higher than p_c, percolation is unavoidable, provided that the aspect ratio is equal for all air voids. The following percolation thresholds were presented by Garboczi et al. [52] (only aspect ratio up to 3 is considered, as there are few air voids in concrete that are more elongated than that):

Table 7: Percolation thresholds for aspect ratios up to 3 [52].

Aspect ratio	a	b	p_c
1	0.025	0.025	0.2854
1.5	0.030	0.020	0.2795
2	0.020	0.010	0.2618
3	0.030	0.010	0.2244

There are few studies of orientation of air voids in sprayed concrete, but there are some studies of anisotropy in strength. Segura-Castillo et al. observed a strong anisotropy in tensile residual response of sprayed concrete [10]. Specimens which were loaded parallel to the spraying direction exhibited 3.5 times higher loads than those which were loaded perpendicular to the spraying direction. The reason for this is assumed to be that fibres tend to align perpendicular to the spraying direction, which has been found and reported several times [53, 54, 55, 56]. In Segura-Castillo et al. [10], the orientation number perpendicular to the spraying direction was measured to be 3 times bigger than the number parallel to the spraying direction. The fact that fibers tend to orient normal to the spraying direction and that fiber orientation affects the properties of concrete, motivates for further analysis on whether pores and other constituents have the same tendencies. Due to the nature of compaction and setting of sprayed concrete, it is not unreasonable to believe that there may also be an anisotropy with regards to permeability as well.

2.9 Water penetration and permeability

As mentioned earlier, nearly all the deterioration mechanisms of concrete involve transport of water [6]. Thus, water penetration and permeability have an important impact on the durability of concrete. Permeability is measured by subjecting a concrete sample, that is sealed on the sides, to a constant hydrostatic pressure on the top, and measuring percolating water as outflow rate at the bottom (Darcy flow test). One other way to evaluate permeability of concrete is by water penetration test. This test is based on applying hydrostatic pressure on the top surface of a cubic/cylindrical sample, and measuring the water ingress after a given time interval, often 72 hours.

Although water permeability is an important material parameter, there are few current standardized methods for measuring it and using it as a quality criterion for concrete [57]. One disadvantage with permeability measurements of concrete is high coefficient of variation. Moreover, the tests are time consuming and works best for lower quality concretes. There are also other parameters that are easier to measure/control that highly affect permeability, such as absorption, pore distribution, resistivity and w/b ratio [57]. Nonetheless, for research purposes and for characterizing differences, water permeability tests are still interesting, as they give an indication of how different parameters may affect the permeability.

For evaluating water permeability, there are some important factors that must be taken into consideration. The moisture condition and moisture history is important for deciding which transport mechanism is governing (suction/permeation). Drying may cause collapse of C-S-H sheets and shrinkage cracking [57]. This is particularly an issue when drying at high temperature, such as 110°C. Suction porosity is also known to decrease after high temperature drying, because capillary pores become bigger [31]. It should also be noted that permeating water may react with unhydrated cement and move particles from one place to another, resulting in reduced permeability [57]. There is also a relation between the permeability and the age of concrete. The permeability is reduced as the age of the concrete increases [6, 58]. However, Sjölander and Ansell found that curing time did not affect the water penetration through sprayed concrete [59].

Permeability of concrete is often expressed by a coefficient, K_{darcy}. The coefficient is obtained from a Darcy flow test. The results from a water penetration test can be converted such that the coefficient of permeability is calculated without doing the Darcy flow test. This relationship was developed by O. Valenta [6]. Equation 3 shows the relation between the coefficient of permeability [m/s] and the penetration depth in the water penetration test:

$$K_{valenta} = \frac{e^2 v}{2ht} \tag{3}$$

where e is the penetration depth in concrete [m], h is hydraulic height [m], t is time under pressure [s] and v is the fraction of the volume of concrete occupied by discrete pores that are only filled by applying pressure [6]. Note that the K_{darcy} and $K_{valenta}$ are in principle the same. Vuorinen [60] found that the relationship between these two permeability coefficients was not one to one. He proposed a new coefficient of permeability, $K_{vuorinen}$, which is an estimation for the coefficient for rate of flow (K_{darcy}) based on $K_{valenta}$ from the water penetration test.

$$log(K_{vuorinen}) = \frac{log(K_{valenta}) + 4.70}{0.583} \tag{4}$$

A small literature review was conducted in order of checking Equation 4 on other concretes where both water penetration and water permeability tests were performed. The results from this review are shown in Table 8:

Table 8: Coefficient of permeability calculated from both water penetration (with Vuorinen conversion) and water permeability test. The measurements are based on sprayed concrete panels from Opsahl [8] and conventional concrete from Skutnik [61]. In Skutnik's study [61], admixture A represents a cement-based admixture and B represents a super plasticizer. The table also shows the relation between the calculated permeability coefficients.

Study	Mix	No. of samples	$K_{valenta}$	$K_{vuorinen}$	K_{darcy}	$\frac{K_{valenta}}{K_{darcy}}$	$\frac{K_{vuorinen}}{K_{darcy}}$
Opsahl	Mix II0	1	1.7E-11	3.8E-11	5.0E-12	3.3	7.5
(1985) [8]	Mix II1,0	6	5.8E-12	6.1E-12	1.4E-12	4.1	4.4
Skutnik	No admixture	3	1.3E-12	4.4E-13	4.5E-14	28	9.8
(2020) [61]	With A	3	3.1E-12	2.1E-12	2.5E-13	12	8.5
	With B	3	7.9E-13	2.0E-13	1.1E-13	7.1	1.8
	With A + B	3	6.5E-13	1.5E-13	7.0E-14	9.3	2.1

$K_{vuorinen}$ was closer than $K_{valenta}$ to the darcy permeability coefficient, K_{darcy}, in Skutnik's study [61], but not in Opsahl's study [8]. As Equation 3 shows, the air content affects $K_{valenta}$. In the study by Opsahl, the applied air content was measured by optical analysis [8], whereas the air in the study by Skutnik was measured in fresh concrete [61]. Note that the $K_{vuorinen}$ from both studies and the $K_{valenta}$ in Opsahl's study were calculated for this master's thesis.

The permeability and water penetration test can be used to evaluate watertightness of concrete. According to NS-EN 3420-L5 [62] from 1986, the concrete is considered watertight if one of the following criteria are satisfied:

- The coefficient of permeability, K_{darcy}, is less than $1 \cdot 10^{-11}$.
- Water penetration depth is less than 25 mm when the pressure is 0.3 MPa for 24 hours, followed by 0.5 MPa for 24 hours and then 0.7 MPa for 24 hours.

2.10 Trussell's study

In the specialization project of Hårr and Kjeka [12], results from image analysis (IMA) of Trussell's samples from Flekkefjord and Trondheim set accelerator (TSA) were analyzed. The main findings were:

- Macroporosity increases with addition of set accelerator.
- For concrete with an air entraining admixture, macroporosity is lower when concrete is sprayed, compared to cast, especially in the area of 200-700 microns.
- Concrete which is cast has a much higher portion of spherical and less elongated air voids than sprayed concrete (Figure 36). Both cast and sprayed concrete contained AEA. Of the cast concrete in TSA, 34-38% of the macroporosity was of spherical pores, whereas in the sprayed concretes with accelerator, 5-7% of the macroporosity consisted of spherical pores.

- Sprayed concrete which contains set accelerator has more elongated air voids than sprayed concrete without accelerator (Figure 35). Of the sprayed concrete in Flekkefjord without accelerator, 14-26% of the macroporosity was of spherical pores, whereas the sprayed concrete with accelerator had 4-9% spherical pores.
- There was no percolation in macropores according to IMA, except in one mix, Ff10-2m90deg, which had large lamination damages.

3 Methods

3.1 Concrete proportioning and constituents

The experimental tests of this thesis were conducted in association with Nicholas Trussell's PhD, and were performed on sprayed concrete from three locations: Flekkefjord, Trondheim and Svorkmo. The experiments are divided into four series where different parameters were investigated, and the series were Flekkefjord, Trondheim set accelerator (TSA), Trondheim spraying mechanics (TSM) and Svorkmo. Set accelerator dosage was varying in Flekkefjord and TSA. In TSM, spraying distance and spraying angle were varying. In Svorkmo, different batched mix designs were investigated. An overview of all the mixes is shown in Table 10.

Name codes are used to distinguish the different samples. The name code gives information about where the sample was sprayed, if it contains fiber or not, set accelerator dosage, spraying distance, spraying angle and other information:

- F: Flekkefjord, T: Trondheim, S: Svorkmo
- f: fiber, nf: no fiber
- set accelerator dosage (0%, 3%, 3.5%, 6%, 7%, 10%)
- spraying distance (1.5m, 2m, 2.5m, 3.5m)
- spraying angle (90deg, 67deg, 45deg)

For instance, the Ff3-2m90deg was sprayed in Flekkefjord, and contains fibers and 3% set accelerator. The spraying distance was 2 metres, while the spraying angle was 90 degrees.

Table 11 - 15 show placed concrete proportions for the different mixes. The mixes intend to represent typical sprayed concrete mixes which are used in tunnel linings in Norway today. Standard FA cement is used in every mix, and the cement content varied from 374 to 488 kg/m^3. The matrix volume varied from 393-463 l/m^3. The maximum aggregate size (D_{max}) is 8 mm, in all of the series. Aggregate in Flekkefjord was 0/8 mm granitic sand (crushed) with density of 2645 kg/m^3 and water absorption of 0.46% by mass. In Trondheim and Svorkmo, it was used 0/4 mm crushed gabbro (3030 kg/m^3, 0.2% free water, 0.8% absorbed water) and 0/8 mm natural sand (2710 kg/m^3, 4.2-5.8% free water, 0.6% absorbed water). Aggregate size distributions are given in Table 9. All the samples from Flekkefjord, Svorkmo and TSM contained steel fibres. The length of the steel fibres was 35 mm, and the diameter was 0.55 mm, except for one of the mix designs in Svorkmo, Sf7-1,5m90deg-ref1,2. The steel fibres in this exception had a length of 30 mm and a diameter of 0.38 mm. Master Builders Masterroc SA 188 was used as set accelerator in Flekkefjord and Svorkmo, and SA 168 was used in Trondheim.

Table 9: Particle size distributions for the aggregate used in this project. Values are given as mass-% passing through the sieve. The same aggregate was used in Trondheim and Svorkmo.

Sieve size [mm]		11.2	8	4	2	1	0.5	0.25	0.125	0.063
Flekkefjord	0/8 Agg.	100	98	82	72	53	25	8	2	1
Trondheim	0/8 Agg.	100	98.2	84.5	70.6	55.2	39.2	22.3	9.1	2.
& Svorkmo	0/4 Agg.	100	99.8	89.2	58.9	38.4	26.2	18	12.4	8.1

w/c, w/b and m was calculated for each mix:

$$w/c = \frac{m_w}{m_c}, \qquad w/b = \frac{m_w}{m_c + m_p}, \qquad m = \frac{m_w}{m_c + \Sigma k \cdot m_p} \tag{5}$$

where m_w is mass of water, m_c is mass of cement, m_p is mass of pozzolan and k is the activity factor. m (mass ratio) is the effective w/b ratio. According to the NS-EN 206 standard [63], the k-factors are different for concrete with mass ratio lower and higher than 0.45. K-factor of 0.7 for fly ash, 0.3 for limestone powder and 2 for silica fume was used, regardless of mass ratio. The w/b ratio for all mixes varied from 0.43 to 0.52. Table 11-15 show that the accelerator dosage affects the w/c, w/b and m ratios. For instance, the w/c ratio in Ff0-2m90deg is 0.45, whereas Ff10-2m90deg has a w/c ratio of 0.51.

In Table 11-15, the constituents have been adjusted for measured hardened air content (with IMA) and addition of set accelerator. It is assumed that the volume of accelerator (dry) is zero, because the accelerator is dissolved in water. Total water content is the sum of added water and water from aggregate and admixtures.

The concrete was sprayed perpendicular on inclined panels. However, the Ff0-2m90deg samples were sprayed vertically down on a horizontal panel. Tnf0-Cast was pumped without accelerator through the nozzle, but it was not sprayed. A blockage in the accelerator line was discovered while spraying the 6% Flekkefjord panels. Accordingly, the Ff6-2m90deg* has in reality zero accelerator.

Table 10: Overview of the different concrete mixes. *0% set accelerator.

Test series	Mix	Mix name code	no
Flekkefjord	zero set accelerator	Ff0-2m90deg	1
	3% set accelerator	Ff3-2m90deg	2
	6% set accelerator*	Ff6-2m90deg*	3
	10% set accelerator	Ff10-2m90deg	4
Trondheim set accelerator	zero set accelerator cast	Tnf0-Cast	5
	3.5% set accelerator	Tnf3,5-1,5m90deg	6
	7% set accelerator	Tnf7-1,5m90deg	7
Trondheim spraying mechanics	1.5 m spraying distance	Tf7-1,5m90deg	8
	2.5 m spraying distance	Tf7-2,5m90deg	9
	3.5 m spraying distance	Tf7-3,5m90deg	10
	67° spraying angle	Tf7-1,5m67deg	11
	45° spraying angle	Tf7-1,5m45deg	12
Svorkmo	Reference mix	Sf7-1,5m90deg-ref1,1	13
	Reference mix - different fibre	Sf7-1,5m90deg-ref1,2	14
	without shrinking reducing agent	Sf7-1,5m90deg-noSRA	15
	without hardening accelerator	Sf7-1,5m90deg-noHA	16
	mix with polymer	Sf7-1,5m90deg-polymer	17
	mix with fly ash	Sf7-1,5m90deg-FA	18
	mix with lime powder	Sf7-1,5m90deg-LF	19
	mix with low matrix volume	Sf7-1,5m90deg-380M	20

Table 11: Placed concrete composition for the Flekkefjord mixes. Mass is given in kg/m^3, and placed volume is given in $litres/m^3$. *0% set accelerator.

Mix	Ff0-2m90deg		Ff3-2m90deg		Ff6-2m90deg*		Ff10-2m90deg	
	Mass	Volume	Mass	Volume	Mass	Volume	Mass	Volume
Std FA cement	461.7	154.4	455.2	152.3	461.5	154.4	442.5	148.0
Water	206.1	206.1	210.3	210.3	206.0	206.0	220.5	220.5
Silica fume	19.2	8.7	19.0	8.6	19.2	8.7	18.4	8.4
Super plasticiser	4.8	4.6	4.7	4.5	4.8	4.6	4.6	4.4
AEA	0.5	0.5	0.4	0.4	0.4	0.4	0.4	0.4
Set accelerator (dry)	0.0	0.0	7.7	0.0	0.0	0.0	24.9	0.0
Agg. (<0.125 mm)	21.8	8.3	21.5	8.1	21.8	8.3	20.9	7.9
Air (IMA)		41.3		47.6		41.6		58.0
Agg. (>0.125 mm)	1506.5	570.6	1485.5	562.7	1506.0	570.4	1444.0	547.0
Steel fibres	45.0	5.6	44.4	5.5	45.0	5.6	43.1	5.4
Total water content	210.0		233.4		210.0		254.0	
w/c	0.45		0.47		0.45		0.51	
w/b	0.44		0.45		0.44		0.49	
m (effective w/b)	0.42		0.43		0.42		0.47	

Table 12: Placed concrete composition for the Trondheim set accelerator mixes. Mass is given in kg/m^3, and placed volume is given in $litres/m^3$.

Mix	Tnf0-Cast		Tnf3,5-1,5m90deg		Tnf7-1,5m90deg	
	Mass	Volume	Mass	Volume	Mass	Volume
Std FA cement	437.4	146.3	439.4	147.0	437.1	146.2
Water	163.2	163.2	172.8	172.8	180.6	180.6
Silica fume	42.8	19.5	43.0	19.6	42.8	19.5
Super plasticiser	3.8	3.6	3.8	3.6	3.8	3.6
AEA	0.6	0.6	0.6	0.6	0.6	0.6
Retarder	0.4	0.4	0.4	0.4	0.4	0.4
Set accelerator (dry)	0.0	0.0	9.6	0.0	19.0	0.0
0 – 4 Agg. (<0.125 mm)	22.1	7.3	22.2	7.3	22.1	7.3
0 – 8 Agg. (<0.125 mm)	135.0	49.6	135.7	49.9	134.9	49.6
Air (IMA)		62.2		49.0		45.2
0 – 4 Agg. (>0.125 mm)	156.1	51.5	156.8	51.7	156.0	51.5
0 – 8 Agg. (>0.125 mm)	1348.8	495.9	1355.0	498.2	1347.9	495.6
Steel fibres	0.0	0.0	0.0	0.0	0.0	0.0
Total water content	232.2		242.2		249.7	
w/c	0.53		0.55		0.57	
w/b	0.48		0.50		0.52	
m (effective w/b)	0.44		0.46		0.48	

Table 13: Placed concrete composition for the Trondheim spraying mechanics mixes. Mass is given in kg/m^3, and placed volume is given in $litres/m^3$.

Mix	Tf7-1,5m90deg		Tf7-2,5m90deg		Tf7-3,5m90deg		Tf7-1,5m67deg		Tf7-1,5m45deg	
	Mass	Volume	Mass	Volume	Mass	Volume	Mass	Volume	Mass	Volume
Std FA cement	430.2	143.9	432.7	144.7	428.9	143.4	431.4	144.3	429.2	143.5
Water	176.9	176.9	177.9	177.9	176.4	176.4	177.4	177.4	176.5	176.5
Silica fume	42.9	19.5	43.1	19.6	42.7	19.4	43.0	19.5	42.7	19.4
Super plasticiser	3.7	3.5	3.7	3.6	3.7	3.5	3.7	3.5	3.7	3.5
AEA	0.6	0.6	0.6	0.6	0.6	0.6	0.6	0.6	0.6	0.6
Retarder	0.6	0.5	0.6	0.5	0.6	0.5	0.6	0.5	0.6	0.5
Set accelerator (dry)	18.8	0.0	18.9	0.0	18.7	0.0	18.8	0.0	18.7	0.0
0 – 4 Agg. (<0.125 mm)	21.6	7.1	21.8	7.2	21.6	7.1	21.7	7.2	21.6	7.1
0 – 8 Agg. (<0.125 mm)	132.0	48.5	132.8	48.8	131.6	48.4	132.4	48.7	131.7	48.4
Air (IMA)		60.3		54.9		63.2		57.7		62.6
0 – 4 Agg. (>0.125 mm)	152.9	50.5	153.7	50.7	152.4	50.3	153.3	50.6	152.5	50.3
0 – 8 Agg. (>0.125 mm)	1318.9	484.9	1326.5	487.7	1314.8	483.4	1322.5	486.2	1315.7	483.7
Steel fibres	29.8	3.7	30.0	3.7	29.7	3.7	29.9	3.7	29.8	3.7
Total water content	242.0		242.0		242.0		242.0		242.0	
w/c	0.56		0.56		0.56		0.56		0.56	
w/b	0.51		0.51		0.51		0.51		0.51	
m (effective w/b)	0.47		0.47		0.47		0.47		0.47	

Table 14: Placed concrete composition for four of the Svorkmo mixes. Mass is given in kg/m^3, and placed volume is given in $litres/m^3$.

Mix	Sf7-1,5m90deg-ref1,1		Sf7-1,5m90deg-ref1,2		Sf7-1,5m90deg-noSRA		Sf7-1,5m90deg-noHA	
	Mass	Volume	Mass	Volume	Mass	Volume	Mass	Volume
Std FA cement	473.5	158.3	479.2	160.3	487.6	163.1	480.1	160.6
Fly ash	0.0	0.0	0.0	0.0	0.0	0.0	0.0	0.0
Lime powder	0.0	0.0	0.0	0.0	0.0	0.0	0.0	0.0
Water	137.1	137.1	140.1	140.1	141.1	141.1	149.6	149.6
Silica fume	19.7	9.0	19.9	9.0	20.3	9.2	20.0	9.1
Super plasticiser	4.2	4.0	4.3	4.1	4.3	4.1	4.3	4.1
AEA	0.7	0.6	0.7	0.7	0.7	0.7	0.7	0.6
Retarder	1.0	0.9	1.1	1.0	1.1	1.0	1.1	1.0
SRA	2.5	2.7	2.5	2.7	0.0	0.0	2.5	2.7
Set accelerator (dry)	18.6	0.0	18.9	0.0	19.2	0.0	18.9	0.0
Hardening accelerator	8.1	7.1	8.2	7.2	8.2	7.3	0.0	0.0
Etonis 3500 W	0.0	0.0	0.0	0.0	0.0	0.0	0.0	0.0
0 – 4 Agg. (<0.125 mm)	21.4	7.1	21.5	7.1	21.7	7.2	21.6	7.1
0 – 8 Agg. (<0.125 mm)	135.2	49.7	137.8	50.7	138.5	50.9	136.7	50.2
Air (IMA)		71.8		55.9		51.2		57.6
0 – 4 Agg. (>0.125 mm)	151.3	49.9	151.5	50.0	153.2	50.6	152.4	50.3
0 – 8 Agg. (>0.125 mm)	1350.7	496.6	1376.7	506.1	1383.2	508.5	1365.0	501.8
Steel fibres	40.3	5.1	40.8	5.2	41.3	5.3	40.8	5.2
Total water content	232.1		236.9		238.1		239.3	
w/c	0.49		0.49		0.49		0.50	
w/b	0.47		0.47		0.47		0.48	
m (effective w/b)	0.45		0.46		0.45		0.46	

Table 15: Placed concrete composition for four of the Svorkmo mixes. Mass is given in kg/m^3, and placed volume is given in $litres/m^3$.

Mix	Sf7-1,5m90deg-polymer		Sf7-1,5m90deg-FA		Sf7-1,5m90deg-LF		Sf7-1,5m90deg-380M	
	Mass	Volume	Mass	Volume	Mass	Volume	Mass	Volume
Std FA cement	452.4	151.3	373.8	125.0	405.2	135.5	387.1	129.5
Fly ash	0.0	0.0	97.4	42.4	0.0	0.0	0.0	0.0
Lime powder	0.0	0.0	0.0	0.0	100.0	36.5	0.0	0.0
Water	144.2	144.2	137.1	137.1	131.9	131.9	110.6	110.6
Silica fume	19.0	8.6	19.6	8.9	21.3	9.7	16.0	7.3
Super plasticiser	4.1	3.9	4.2	4.0	4.6	4.3	3.4	3.2
AEA	0.6	0.6	0.7	0.6	0.7	0.6	0.5	0.5
Retarder	0.5	0.4	0.8	0.8	0.5	0.4	0.4	0.4
SRA	2.4	2.6	2.5	2.7	2.7	2.9	2.0	2.2
Set accelerator (dry)	17.8	0.0	18.6	0.0	16.1	0.0	15.2	0.0
Hardening accelerator	8.1	7.2	8.0	7.0	8.1	7.2	7.9	7.0
Etonis 3500 W	20.2	18.8	0.0	0.0	0.0	0.0	0.0	0.0
0 – 4 Agg. (<0.125 mm)	21.5	7.1	21.0	6.9	21.7	7.1	25.9	8.6
0 – 8 Agg. (<0.125 mm)	134.3	49.4	134.0	49.3	135.5	49.8	147.4	54.2
Air (IMA)		57.5		69.1		60.8		69.7
0 – 4 Agg. (>0.125 mm)	151.6	50.0	148.4	49.0	153.0	50.5	183.2	60.5
0 – 8 Agg. (>0.125 mm)	1341.7	493.3	1338.7	492.2	1353.3	497.5	1472.5	541.4
Steel fibres	40.5	5.2	40.0	5.1	40.6	5.2	39.5	5.0
Total water content	238.2		231.1		226.7		205.8	
w/c	0.53		0.62		0.56		0.53	
w/b	0.51		0.47		0.43		0.51	
m (effective w/b)	0.49		0.48		0.47		0.49	

3.2 Pumping and spraying

The pumping and spraying process influences the hardened concrete properties, and a description of these processes will be given here. Before spraying, fresh concrete is filled in a hopper and pumped to the nozzle by a piston pump. Compressed air propels the concrete to the substrate. In addition, set accelerator is added at the nozzle in order to ensure immediate setting. Table 16 shows the kind of pump and spraying machine, hose size, nozzle size and flow rate that were used at the different spraying locations. Spraying setup is shown in Figure 5 and 6.

The concrete pumping is percussive and clogging may occur, whereas the flow of accelerator is continuous. This may cause only accelerator to be sprayed in some cases. This phenomenon is defined as spitting in this thesis. Spitting may cause large lamination damages perpendicular to the spraying direction because of too high concentration of accelerator. Lamination damage is characterized by layers in the concrete with non-compacted concrete, which is more porous than the rest of the concrete. Spitting may be controlled by flow rate, viscosity/workability and age of the fresh concrete, as well as friction inside the pipe. Lamination damages could also occur because of initial rebound of the concrete closest to the adhesion surface.

Table 16: Overview of spraying and pumping equipment.

	Flekkefjord	Trondheim	Svorkmo
Spraying machine	AMV 7450 shotcrete robot	Normet Spraymec NorRunner 140 DVC shotcrete robot	Normet Spraymec NorRunner 140 DVC shotcrete robot
Concrete pump	Olin pump	Normet pump	Normet pump
Hose diameter	75 mm	75 mm	100 mm
Nozzle diameter	40 mm	40 mm	40 mm
Concrete flow rate	$10\,m^3/h$	$14\,m^3/h$	$24\,m^3/h$

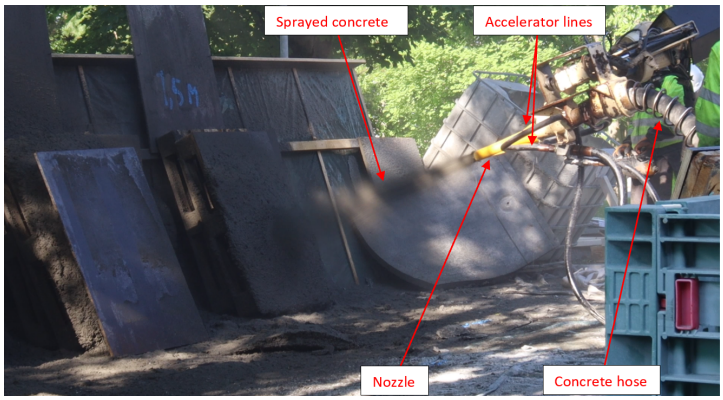

Figure 5: A panel which was sprayed with 1,5m distance, perpendicular to the panel surface. Photo: Nicholas Henry Trussell.

Figure 6: A panel which was sprayed 67/23 degrees to the panel surface. Photo: Nicholas Henry Trussell.

3.3 The full PF method

The full PF procedure was used in Trussell's PhD project and this master's project. The durations of each step in the list below was slightly altered from the SINTEF procedure [31]. The tests were performed on discs of 25 mm thickness and 98 mm diameter. Two discs from each mix in Table 10 were used. The full PF test was executed in the following order:

1. Drying the specimens in an oven at 105°C for 3 days (W_1)

2. One sided capillary suction for 4 days[1] ($W_{1.5}$)
3. Water saturation for 4 days by water submersion (W_2)
4. Weighing in water and air to determine volume (V)
5. Pressure saturation in water under 5 MPa pressure for 3 days (W_3)

For the capillary suction, a tray was prepared with a steel net plate in it, and water was filled about 1 mm above the steel plate. The samples were then placed in the tray with one sided contact with water, and weighed for given time intervals.

As mentioned in subsection 2.4, the suction porosity is defined to be the pores which are filled from only one sided suction. The open macropores are assumed to be filled with water during unpressurized submersion, and the closed macropores are filled by pressure saturation. In standard procedures and comparable studies, the duration of capillary suction is often 4 days. For this reason, the calculation of open macroporosity in this study is based on the measurements of capillary suction at 4 days. Note that the duration of capillary suction actually was 6 days for the Trondheim samples and 7 days for the Flekkefjord and Svorkmo samples, but results based on these measurements are only presented in Figure 15 and Figure 16.

The following macroporosities were calculated:

$$PFo = \frac{W_2 - W_{1.5}}{V} \tag{6}$$

$$PFc = \frac{W_3 - W_2}{V} \tag{7}$$

$$PFt = \frac{W_3 - W_{1.5}}{V} \tag{8}$$

where $W_{1.5}$ = weight after one sided capillary suction, W_2 = weight after submersion, W_3 = weight after pressure saturation and V = volume.

3.4 Preparing the samples for IMA [2]

The samples that were used in the image analysis (IMA) were from concrete cylinders. These cylinders were drilled as 100 mm diameter cores through the approximately 100 mm thick panels parallel to the spraying direction. They were wet sawn along the cylinder length axes and over the diameters into two equal half cylinders. IMA was performed on both half cylinders, giving two images per mix in Table 10. The grinding and polishing were done in accordance with ASTM C457, section 8 [49]. The polishing machine Struers Tegramin 30 was used to polish the

[1] The capillary suction lasted for 6-7 days, but the measurements at 4 days were used in comparison with other studies.

[2] This subsection is based on a subsection from Hårr and Kjeka [12].

surface of the samples before the IMA. The samples were polished with diamond discs with the following grits: 220 grits, 600 grits and 1200 grits. The aim of the polishing with these grits was to achieve a light-reflecting surface and sharp edges around the air voids in the images to be analyzed.

Figure 7: Parts of core used for PF and IMA. The outer discs were used for PF and the half cylinders for IMA.

The polished surface was coloured black with a permanent marker (Edding 390), and the voids were filled with the white powder barium sulphate, $BaSO_4$. The $BaSO_4$ powder was filled gently into the air voids by hand, carefully inspecting the surface to remove any particles left on the surfaces outside the air voids. The barium sulphate was supplied by Chiron and the product number is Al013989. The particle size of the powder was 1-4 µm. The scanning was executed with Epson Perfection V600 Photo at 2400 ppi with a plastic foil between the readily prepared surface and the glass plate of the table scanner.

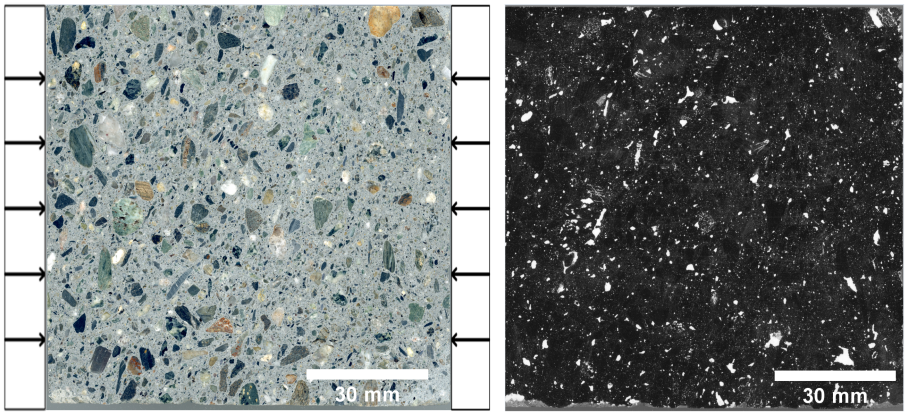

Figure 8: One of the samples before and after colouring it black and white. Arrows indicate spraying direction.

Some steel fibres had the potential to harm the discs, and were consequently removed from the sample. The white powder filled the voids where the steel fibres had been. In these cases, the top layer of the sample was removed and the sample was polished again, or the steel fibre damage was removed by cropping. The principles of cropping are shown in Figure 9.

3.5 Measuring macroporosity size distributions with IMA [3]

The images were analyzed with a series of MATLAB scripts by Fonseca and Scherer [46]. The scripts are slightly adjusted for efficiency and cooperation with an existing Excel template from Andrei Shpak's PhD [41]. The Excel file calculates accumulated air void size distributions of macrovoids with equivalent spherical diameter $D = 2\sqrt{\frac{A}{\pi}}$, where A is the area of the pore.

The first script, readimage.m, in Appendix B.1, loads the image file and crops it. All of the images had the edges cropped away (as shown in the left image in Figure 9). Some of the samples had large lamination damages, due to spitting. For these, the whole sample was analyzed first, including the damage. The damage was later cropped away, and the sample was reanalyzed to give a clearer view of the undamaged concrete, as shown in Figure 9.

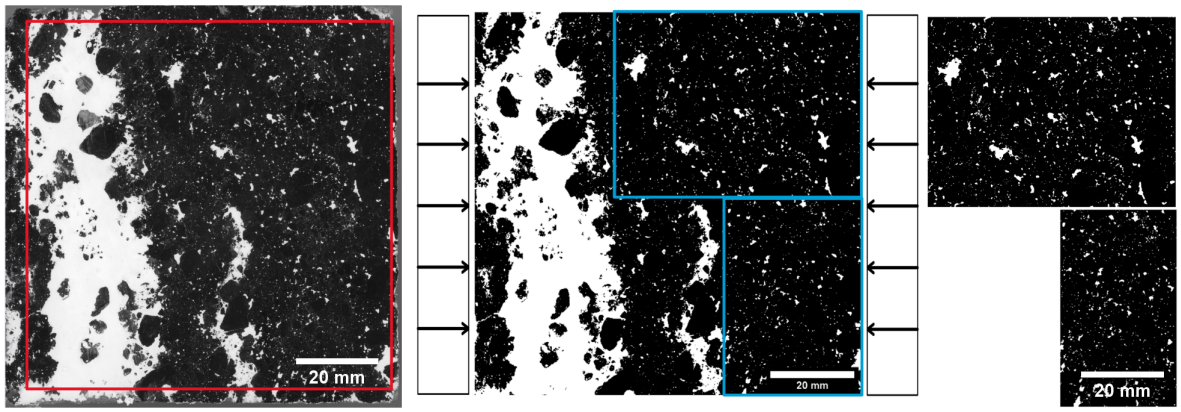

Figure 9: From left: Black and white image after scanning, binarized image processed through MATLAB and final cropped image. Red lines indicate cropping from the edges and blue lines indicate cropping of "common concrete". The images were analyzed both with and without lamination damage. Arrows indicate spraying direction.

The second script, basicanalysis.m, in Appendix B.2, binarizes the image using Otsu's method to determine the grayscale threshold [64]. Further it calculates the total air content in accordance with ASTM C457 [49].

The third script, reconstructspheres.m, in Appendix B.3, assigns each air void an equivalent diameter. The air voids are further binned to a diameter range of 13 microns, starting at 10-23 microns, as 10 microns is the pixel size and therefore the smallest detectable void.

Vectors containing the binned air void sizes and number densities for each void, up to the largest measured void, is written to an Excel template. The Excel file automatically analyzes the data and creates a cumulative air volume distribution plot for the sample. It is the same Excel file that was used by Marte Brun in her master's thesis [65] and Andrei Shpak in his doctoral thesis [41].

[3] This subsection is based on a subsection from Hårr and Kjeka [12].

3.6 Measuring shape and orientation with IMA [4]

To determine shape parameters for the macroporosity, the image-analyzing software JMicroVision v1.3.4 was used. The software extracts objects similarly as the MATLAB scripts by Fonseca and Scherer [46]. The thresholding is done using Otsu's method. JMicroVision, however, has a limit of 10 pixels to determine something as an air void. Therefore, the lowest detectable void size has an equivalent diameter of 36 microns. Voids that are on the cropping border are excluded, as the whole shape is not included.

The L/W ratio is determined by fitting the smallest rectangle possible around an air void, where the longest side is the length (L) and the shorter side is the width (W), see Figure 10. Thus, the L/W ratio is equal to or higher than 1 by definition. An air void is considered spherical if the L/W ratio is lower than 1.1.

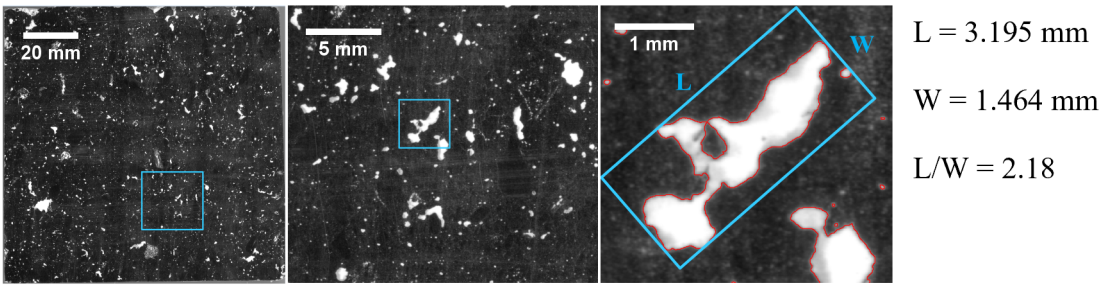

Figure 10: Example of determining L/W-ratio for an air void in the sample Tf7-1,5m90deg-2.

Orientation was also determined using JMicroVision v1.3.4. The software extracts orientation as the angle between the horizontal line of the image and the length-axis of the air void, counterclockwise. The voids with orientation between 0-30° and 150-180° are regarded as oriented parallel to the spraying direction. The voids oriented between 60-120° are regarded as oriented normal to the spraying direction. The remaining voids (30-60° and 120-150°) are regarded as having no orientation, see Figure 11.

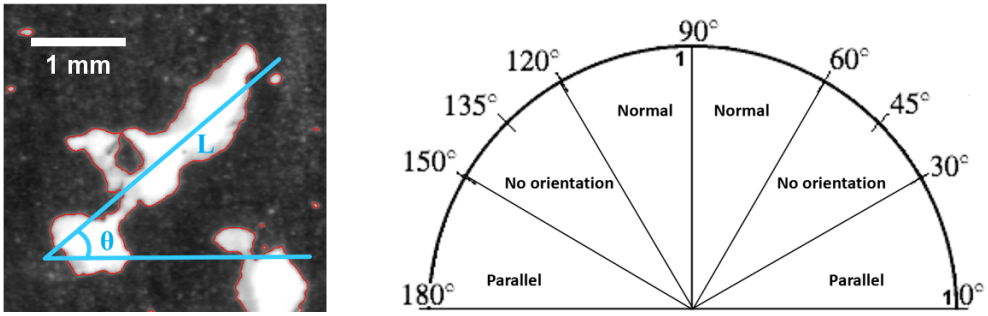

Figure 11: The orientation, θ, is measured as the angle counterclockwise between the horizontal axis and the length axis. Spraying direction is parallel to the horizontal axis.

[4] This subsection is based on a subsection from Hårr and Kjeka [12].

3.7 Water penetration

The intention of the test in this master's project is to measure water penetration normal and parallel to the spraying direction in mixes with different accelerator dosages. In the water penetration test, it was used 12 cubes from the Ff3-2m90deg mix, 10 cubes from the Ff10-2m90deg mix and 4 discs from the Sf7-1,5m90deg-ref1,2 mix. These mixes will be referred to as the 3% mix, the 10% mix and the ref1,2 mix, respectively. From the 3% panel, 8 cubes were tested parallel to the spraying direction, and 4 cubes were tested normal to the spraying direction. From the 10% panel, 6 cubes were tested parallel to the spraying direction, and 4 cubes were tested normal to the spraying direction. All the discs from the ref1,2 mix were tested parallel to the spraying direction.

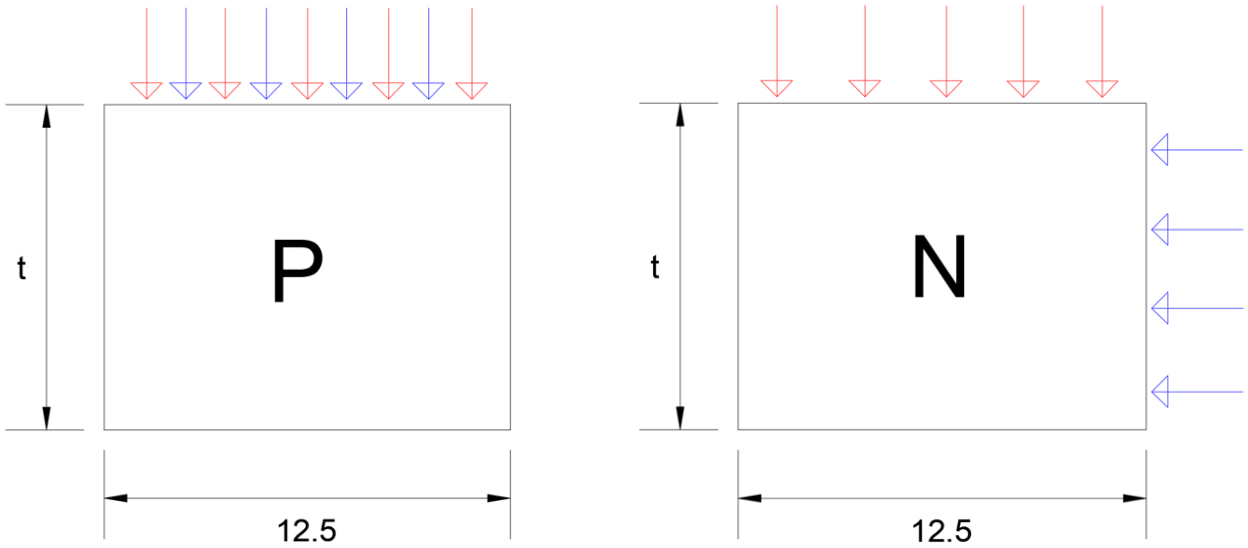

(a) Water penetration parallel to the spraying direction (P-cube).

(b) Water penetration normal to the spraying direction (N-cube).

Figure 12: Spraying direction and water penetration direction in P-cubes and N-cubes. Red arrows indicate water penetration direction and blue arrows indicate spraying direction. The width of the cube is 12.5 cm and t is the thickness.

The water penetration procedure was based on NS-EN 12390-8 [66], procedure 14.633 in Handbook R210 from the Norwegian Public Roads Administration [67], the EN-ISO 7031 standard [68] and Rilem's CPC 13.1 [69]. The dimensions of the N-cubes and P-cubes are given in Table 17. In Figure 12, the water penetration and spraying directions for the P- and N-cubes are given. The water pressure was applied to a side with dimensions 125x125 mm^2 for all but three cubes. For the Svorkmo discs, water pressure was applied parallel to the spraying direction to a circular surface of 150 mm diameter. According to Farstad, the size of the specimen does not affect water penetration [70].

From the time of spraying until the preparations for the water penetration test, the sprayed concrete panels from Flekkefjord had been stored in air indoors, while the Svorkmo samples

had been stored in water. At the time of testing, the age of the samples was approximately 2 years and 1 month for the 3% and 10% mix, and 1 year and 1 month for the ref1,2 samples. The specimens were stored in a tub for at least two weeks prior the the water penetration test. In the tub, there was water at the bottom, and the cubes were stored in the air above the water. A wet cloth was hanging from the upper edge of the tub to ensure high relative humidity. The top of the tub was covered in plastic such that the air remained humid. Relative humidity was measured to be above 90% in the tub, and the temperature was 20°C. The penetration surface was roughened with a wire brush before the test. Table 17 shows pressures and durations for the different samples. A rubber ring was used to limit the water penetration area, and the internal diameter of this ring was 60 mm. The test setup is shown in Figure 13.

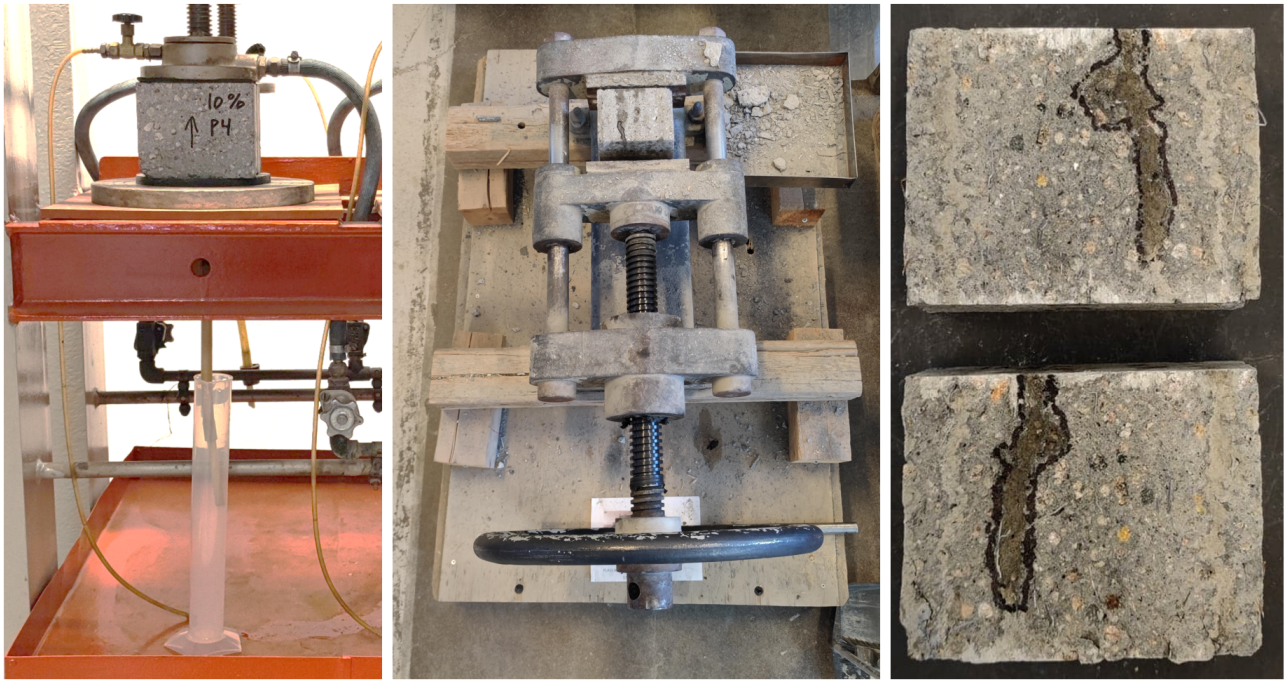

Figure 13: The test setup for water penetration. First image (from left): Water is penetrating from the top. The sample is sealed with a hollow rubber disc on the top and the bottom. A container was placed at the bottom to see if water penetrated all the way through the sample. Second image: The sample was split with a manual splitting device, such that both lamination and water penetration front could be seen on the split surface. Third image: Two split surfaces with penetration fronts.

After removing the samples from the water penetration apparatus and before splitting, the excessive water on the surface was wiped. To examine the water front, the specimens were split perpendicularly to the surface which the pressure was applied. Splitting was carried out immediately after the end of water penetration. The water front was marked on the split surfaces, no later than 2 minutes after splitting.

A permeability coefficient, $K_{valenta}$, was calculated based on the maximum penetration depth (see Equation 3). One of the parameters in this equation is v, which is the fraction of volume occupied by discrete pores only filled by applying pressure. For v, the PFc values from samples of the same mix, but a different panel, was used. $K_{vuorinen}$ was then calculated (see Equation 4.

Four of the water penetration cubes were polished, and coloured black and white after they had been split. The four cubes were 3%P6, 3%N6, 10%P5 and 10%N5. The polishing machine Struers Tegramin-30 and silicon carbide paper was used. The silicon carbide paper had grits of 320, 800, 1200, 2000 and 4000 with a grain size of 46 μm, 22 μm,15 μm, 10 μm and 5 μm, respectively.

Table 17: Overview of pressure, duration and specimen size for the water penetration tests. S1-S4 are discs, whereas the other samples are cubes. Four of the specimens where tested at two different pressures, and the duration of each pressure are given in a parenthesis in the table in these cases. *Note that 3%P7, 3%P8 and 10%P6 originally were N-cubes, but they were tested as P-cubes instead.

Sample	Pressure [MPa]	Time [h]	Dimensions [mm]	Thickness [mm]
3%N2	0.3	72	125x125	100
3%N4	0.1	48	125x125	100
3%N5	0.3	72	125x125	100
3%N6	0.3	72	125x125	100
3%P1	0.5 (70h) & 0.7 (24h)	94	125x125	100
3%P2	0.3	72	125x125	125
3%P3	0.5	3	125x125	100
3%P4	0.1	48	125x125	115
3%P5	0.3	72	125x125	125
3%P6	0.3	72	125x125	125
3%P7*	0.5	70	125x100	125
3%P8*	0.5 (70h) & 0.7 (24h)	94	125x100	125
10%N2	0.1	1.75	125x125	100
10%N3	0.1	1.75	125x125	100
10%N4	0.1	24	125x125	100
10%N5	0.1	1.75	125x125	100
10%P1	0.3	6.33	125x125	125
10%P2	0.3	6.33	125x125	125
10%P3	0.1	1.75	125x125	125
10%P4	0.1	24	125x125	100
10%P5	0.1	1.75	125x125	100
10%P6*	0.1	1.75	125x100	125
S1 (Ref1,2)	0.5	70	d = 150	50
S2 (Ref1,2)	0.5	70	d = 150	50
S3 (Ref1,2)	0.5 (70h) & 0.7 (24h)	94	d = 150	50
S4 (Ref1,2)	0.5 (70h) & 0.7 (24h)	94	d = 150	50

4 Results and analysis

In this section, the results from both experimental testing and literature are presented and analyzed. Keep in mind that PFo is open macroporosity, PFc is closed macroporosity and PFt is total macroporosity.

4.1 Open macroporosity measured with the full PF method

In Figure 14, the open macroporosity from the Trussell study and literature is presented. According to SINTEF, mixes with more than 0.5 vol-% open macroporosity may contain continuous macropores [31]. Figure 14 shows that the open macroporosity is higher than 0.5 vol-% in mixes from Trussell, Tandberg [33] and Bjelland and Moi [36]. Hence, they might have continuous macropores. Open macroporosity in sprayed concrete with accelerator was in the range 0.8-1.6 vol-% in Trussell's study.

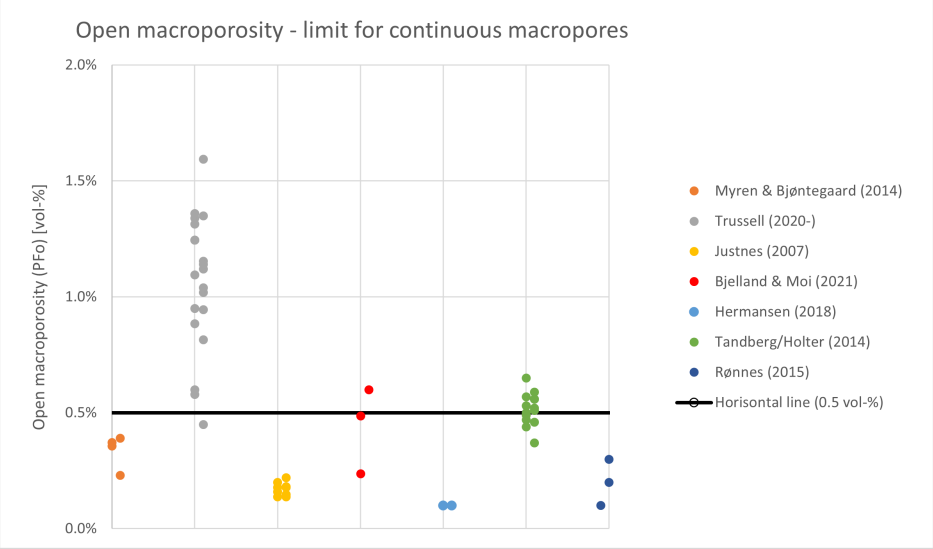

Figure 14: Open macroporosity in vol-% from Trussell's study and in literature. The horizontal line is the limit for continuous macroporosity [31].

SINTEF's procedure [31] defines the open macroporosity as the water uptake during water submersion after 4 days of capillary suction. Figure 15 and 16 show the difference in open macroporosity measured with 6 and 7 days of suction, compared to 4 days. The mixes without accelerator have the lowest open macroporosity regardless of the suction durations. They also have the smallest decrease (vol-%) in open macroporosity from 4 days to 6 or 7 days. On average, open macroporosity decreases with 38% from 4 to 7 days and 36% from 4 to 6 days. All the samples with accelerator still have more than 0.5 vol-% of open macroporosity after 6 or 7 days of suction. Sf7-1,5m90deg-polymer has the highest open macroporosity measured with 4 days of suction, but loses around 1 vol-% between 4 days and 7 days.

Figure 17 shows the relation between the degree of open macroporosity (PFo/PFt) and dosage of set accelerator. The degree of open macroporosity increases for higher accelerator dosages,

from 0.14 to 0.24 in the Flekkefjord series and from 0.10 to 0.21 in the TSA series. In Myren and Bjøntegaard [32], the PFo/PFt increased from 0.04 to 0.09 in the series with steel fibres, but the series with macro pp remained quite the same on 0.09 (green columns).

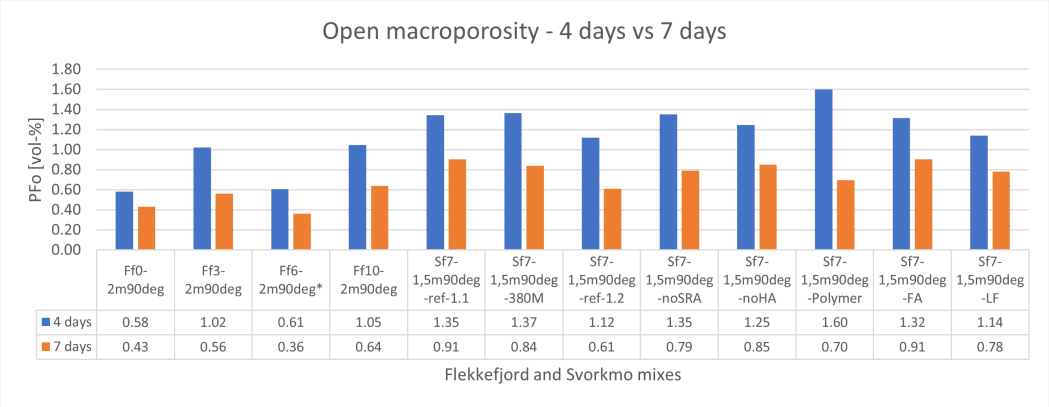

Figure 15: Open macroporosity in the Flekkefjord and Svorkmo test series based on 4 and 7 days of capillary suction.

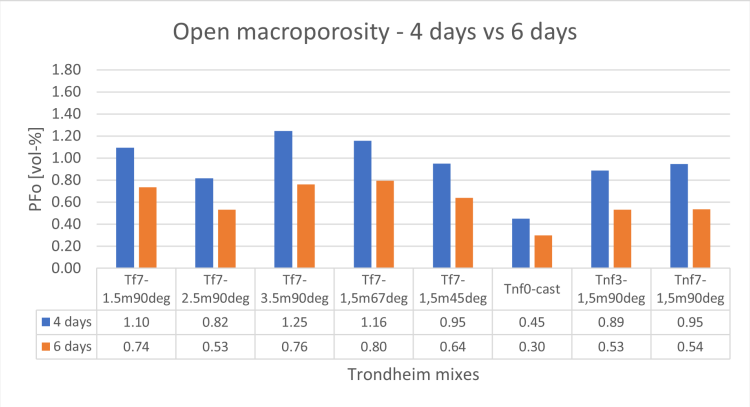

Figure 16: Open macroporosity in Trondheim (TSA and TSM) based on 4 and 6 days of capillary suction.

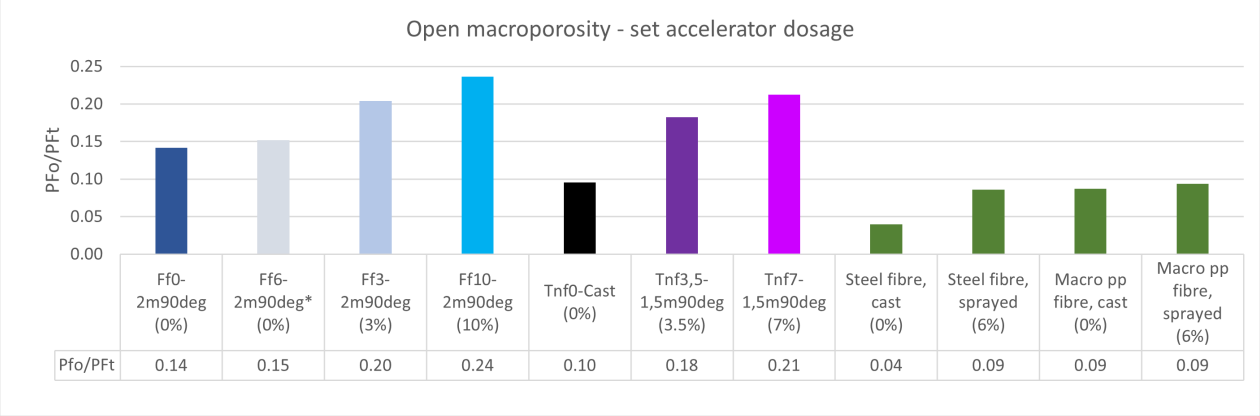

Figure 17: Set accelerator dosage vs open macroporosity/total macroporosity. There are seven mixes from Trussell's study (Flekkefjord and TSA) and four mixes from Myren and Bjøntegaard's study [32]. Below each mix name, the accelerator dosage is written in the parenthesis.

According to Figure 18a and 18b, the degree of open macroporosity seems to increase with higher w/b ratio when each series is considered separately. There is too much spread to conclude whether AEA affects the degree of open macroporosity (PFo/PFt), see Figure 18c. There is a tendency that degree of open macroporosity decreases by higher strengths (Figure 18d), when looking at each series separately. Note that cylinder strength was measured in Trussell's study. The cylinder strength was converted to cube strength by using the conversion factors in table NA.2 in NS-EN 206 [63]. The series by Bjelland and Moi [36] deviates from the rest, having a high degree of open macroporosity (30%-40%).

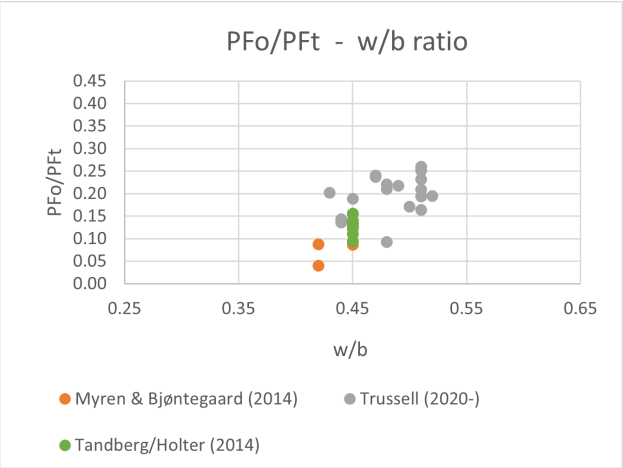

(a) w/b ratio vs the degree of open macroporosity to the total macroporosity in sprayed concrete and "cast sprayed" concrete.

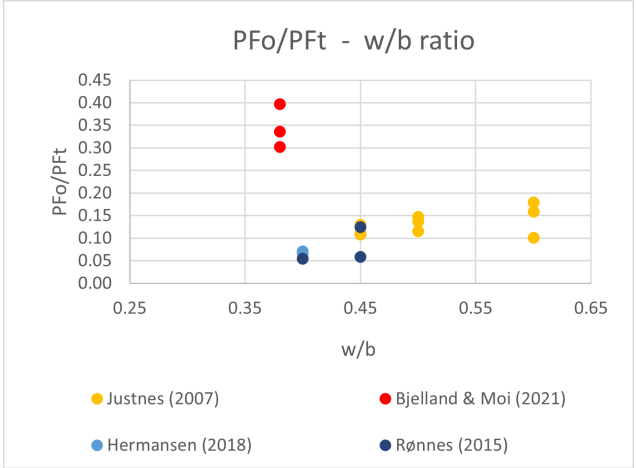

(b) w/b ratio vs the degree of open macroporosity to the total macroporosity in different concrete types.

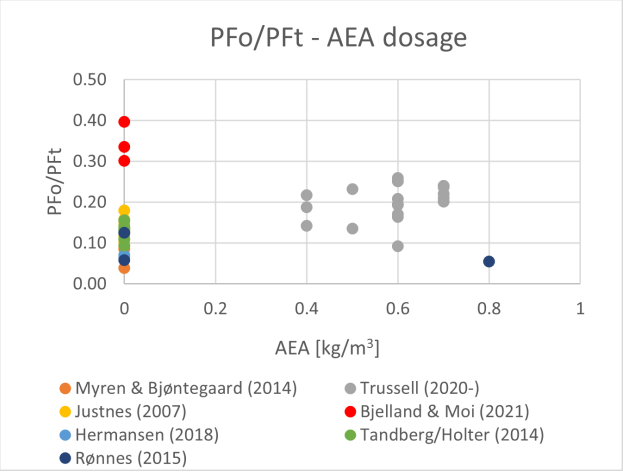

(c) AEA dosage vs the degree of open macroporosity to the total macroporosity.

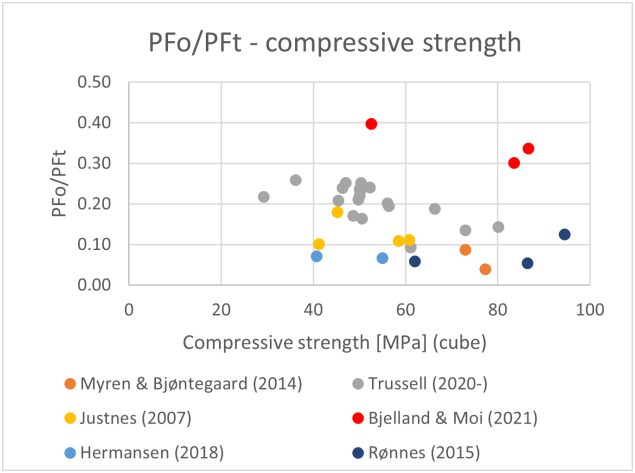

(d) Compressive strength (cube) vs the degree of open macroporosity to the total macroporosity.

Figure 18: w/b ratio, AEA content and compressive strength vs the degree of open macroporosity to the total macroporosity.

4.2 Comparison of air content measured with PF and IMA

Figure 19, 20 and 21 show the relation between macroporosity measured with IMA and with the PF method in the Trussell study. If only the closed macroporosity is included, the IMA

measures higher macroporosity for all of the samples (blue columns). When total macroporosity is considered, the IMA measures the highest macroporosity for all the samples except Ff3-2m90deg (orange columns). The PFc/IMA ratios are in the span from 0.57 to 0.93, and the PFt/IMA ratios are in the range from 0.70 to 1.05. PFt/IMA is 0.98-0.99 for Ff0-2m90deg, Tnf3,5-1,5m90deg, Tnf7-1,5m90deg and Sf7-1,5m90deg-noSRA. Consequently, the PF method and IMA measures almost the same total macroporosity in these mixes.

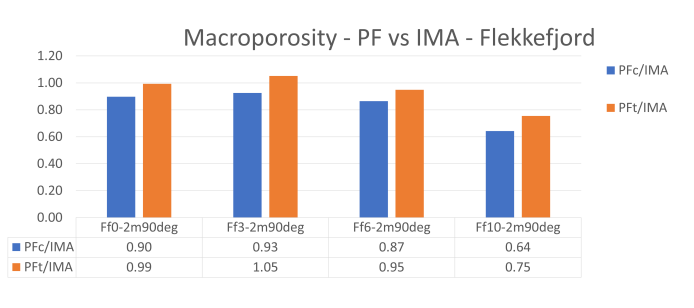

Figure 19: Relation between macroporosities measured with the PF method and with image analysis (IMA) on the Flekkefjord samples.

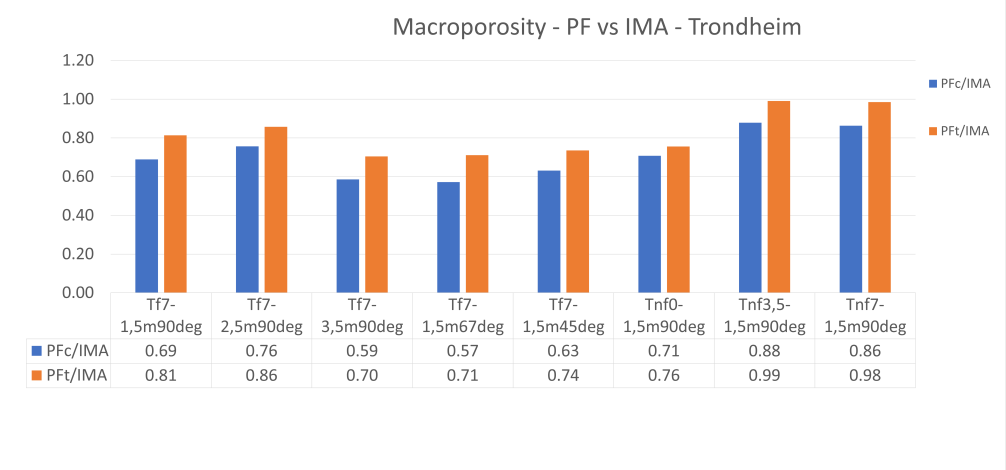

Figure 20: Relation between macroporosities measured with the PF method and with image analysis (IMA) on the Trondheim samples.

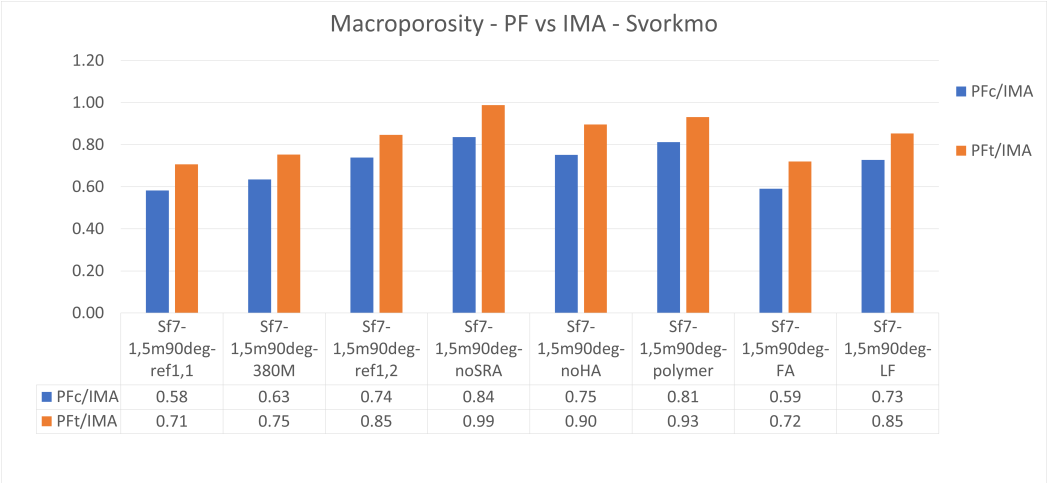

Figure 21: Relation between macroporosities measured with the PF method and with image analysis (IMA) on the Svorkmo samples.

Figure 22 and 23 are box and whisker charts showing the PFc/IMA relations from the literature, as well as from Trussell's study. Sellevold (1986/2005) [7, 23] and Shpak [41] are studies of conventional concrete, and have ratios solely above 1. Sætre (high strength) [42], Jacobsen et al. (1993) (zero slump) [40] and Trussell (sprayed) measured higher macroporosity with IMA than with the PF method. 50% of the mixes in Myren and Bjøntegaard's study [32] are sprayed concretes, and 50% are cast concretes. The sprayed concretes have a PFc/IMA ratio higher than 1, and the cast concretes have a PFc/IMA ratio lower than 1 [32]. Mørtsell's [43] measurements of conventional concrete are quite evenly distributed around 1, whereas Jacobsen et al. (1996) [44] (high strength, conventional) has a large scatter.

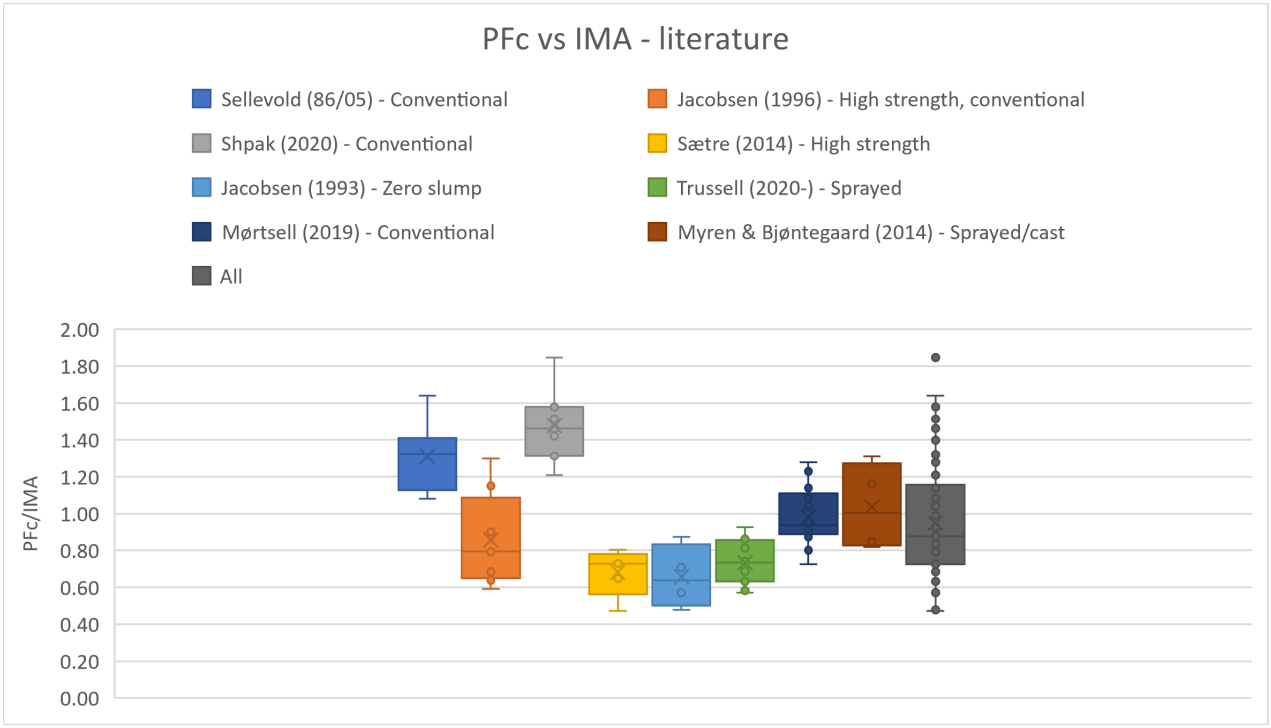

Figure 22: Box plot comparing PFc/IMA ratio for literature and Trussell's study.

Figure 23 shows that conventional concrete tends to have a higher PFc/IMA ratio than the high strength, sprayed and zero slump concretes. There is however a big spread.

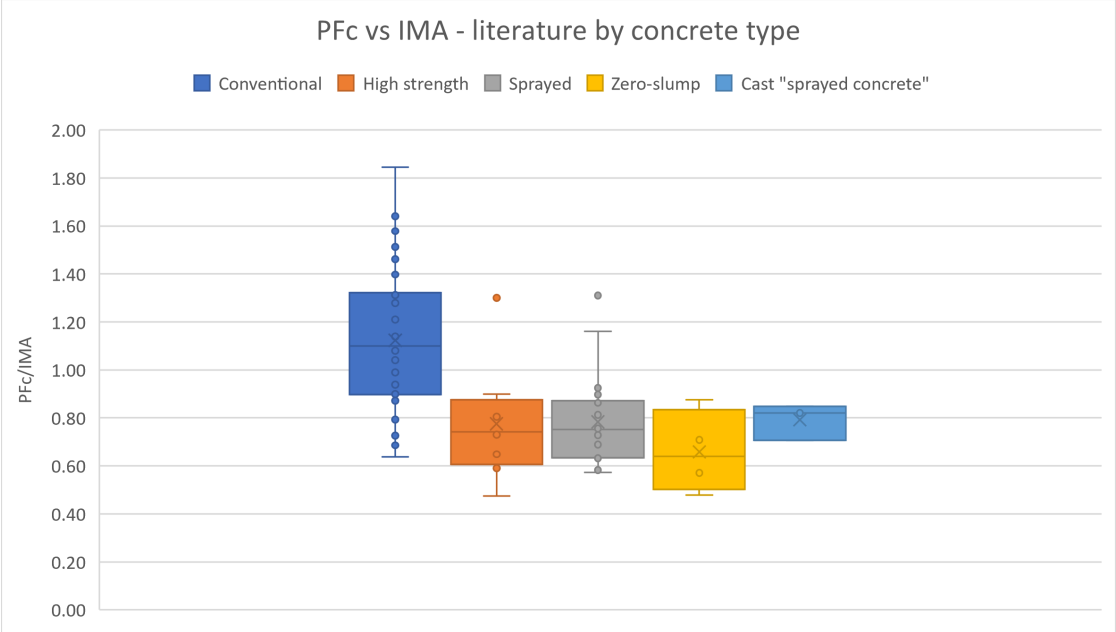

Figure 23: Box plot comparing PFc/IMA ratio for literature and Trussell's study, sorted for different types of concrete.

Both the samples which were saturated with 5 MPa pressure and those which were saturated with 10 MPa pressure, have averages of PFc/IMA close to 1 (Figure 24). The samples with 5 MPa pressure have slightly lower PFc/IMA ratio.

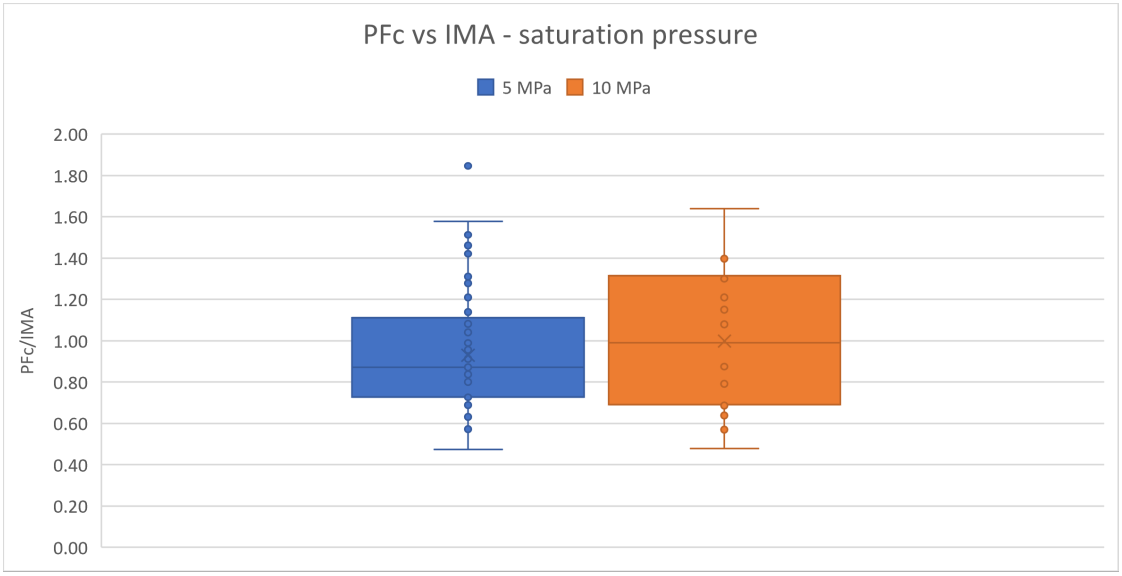

Figure 24: Box plot comparing PFc/IMA ratio for literature and Trussell's study, sorted for different saturation pressures.

According to Figure 25a, 25b and 25c, there is little relation between PFc/IMA ratio and w/b ratio, AEA content and compressive strength.

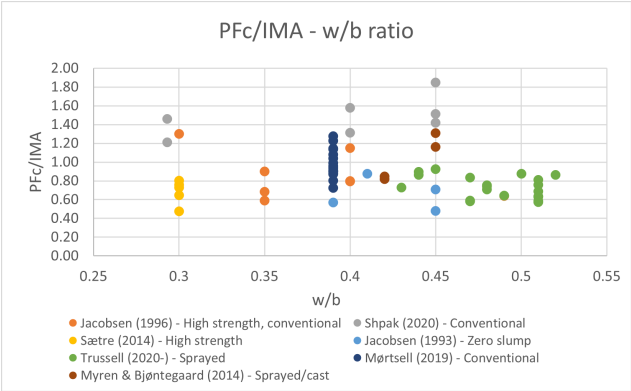

(a) w/b ratio vs PFc/IMA ratio.

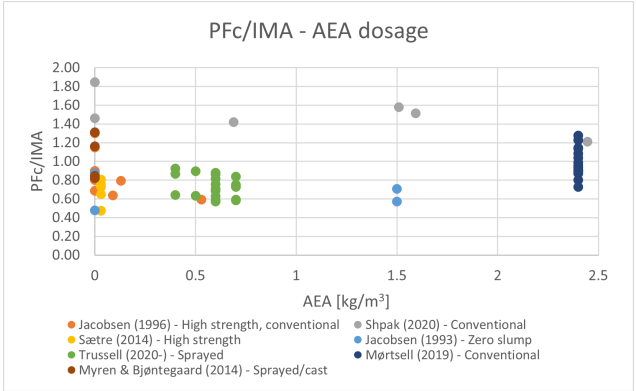

(b) AEA content vs PFc/IMA ratio.

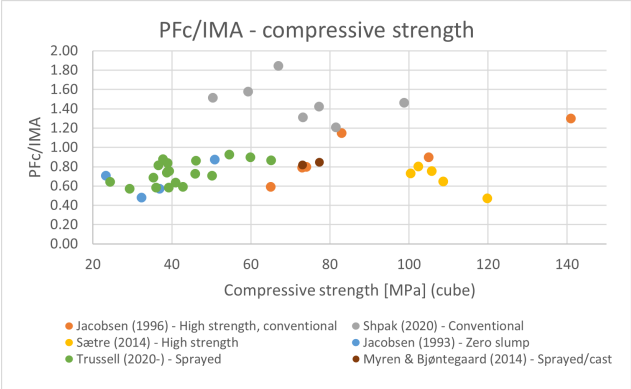

(c) Compressive strength vs PFc/IMA ratio.

Figure 25: w/b-ratio, AEA content and compressive strength vs PFc/IMA ratio.

Open macroporosity is in this thesis defined as the water uptake during submersion, after one sided capillary suction (PFo). Figure 26 can be used to check whether the definition in this thesis is equivalent to the difference between closed macroporosity with the PF method and total macroporosity with IMA, i.e. whether PFo = IMA - PFc [vol-%]. According to Figure 26, the relation between the two definitions is not one to one. The open macroporosity defined as the difference between PFc and IMA is considerably higher than the open macroporosity measured by submersion after capillary suction. In Myren and Bjøntegaard's study, closed PF macroporosity was measured higher than the macroporosity measured by IMA for the sprayed concretes [32]. Consequently, IMA - PFc becomes negative.

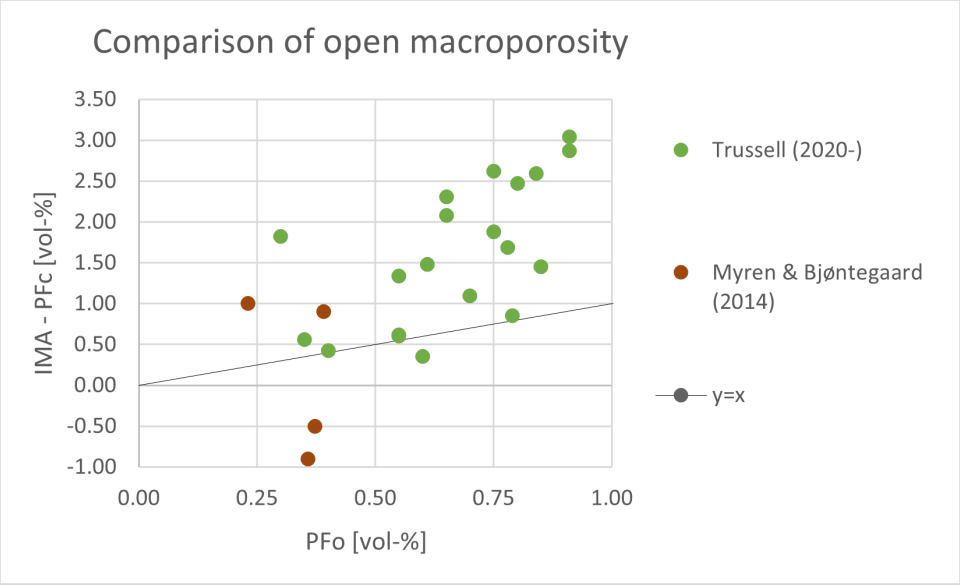

Figure 26: Open macroporosity as defined in this thesis vs open macroporosity defined as the difference between total macroporosity with IMA and closed macroporosity with the PF method. If the two definitions had included the same open macroporosity, the points would have followed the straight line.

4.3 Size distribution and air content measured with IMA

Figure 27 and 28 show the size distribution of macrovoids for mixes with varying set accelerator dosage. This was more thoroughly analyzed and discussed in the specialization project [12].

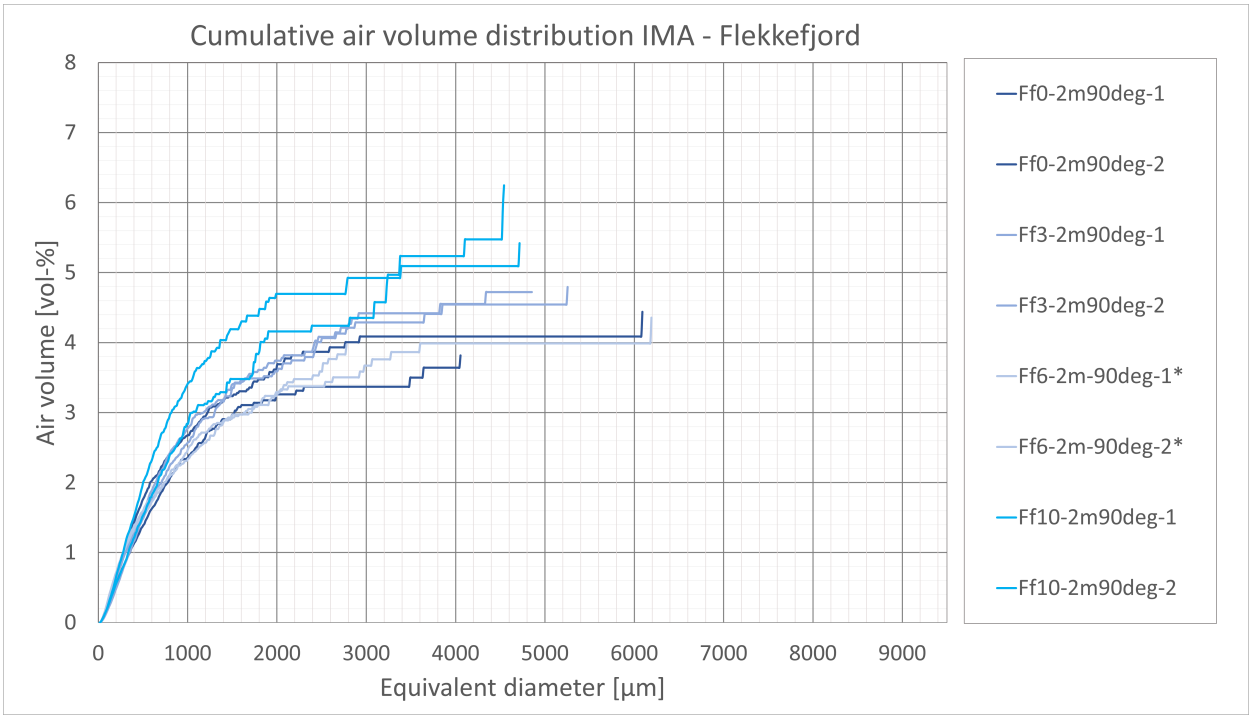

Figure 27: Size distributions for the samples from Flekkefjord. This figure was presented in the specialization project of Hårr and Kjeka [12]. *0% set accelerator.

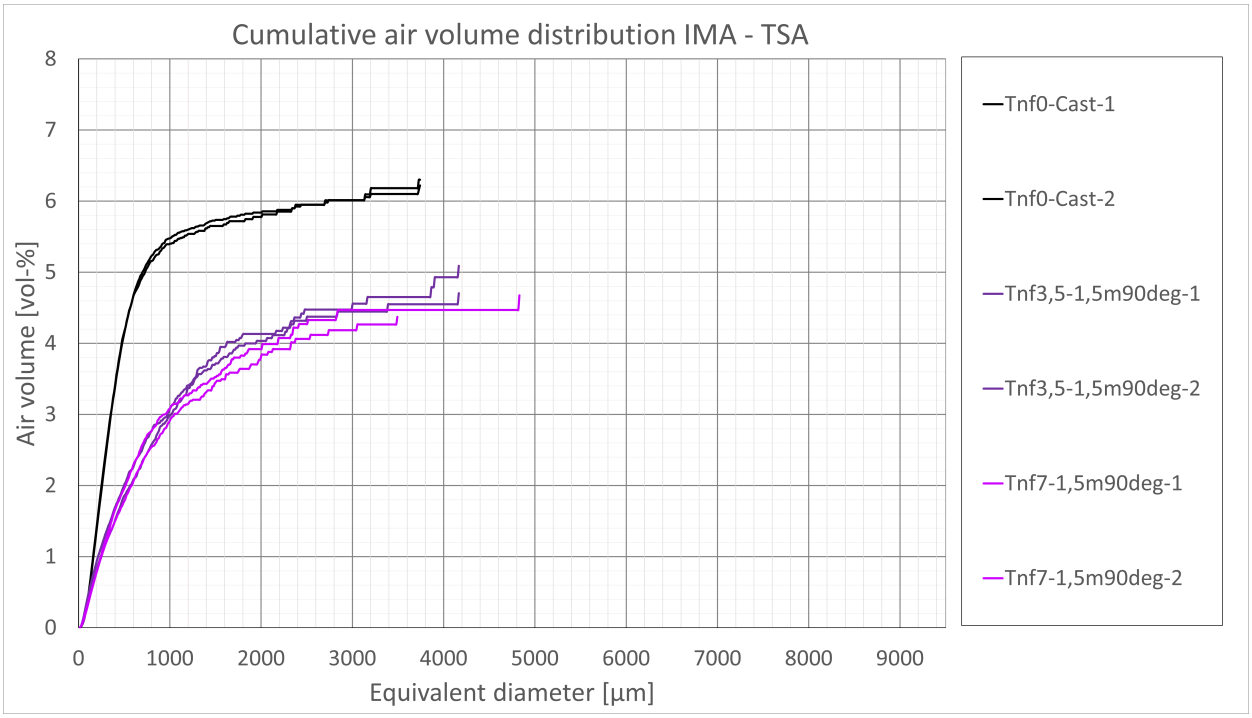

Figure 28: Size distributions for the samples from Trondheim set accelerator. This figure was presented in the specialization project of Hårr and Kjeka [12].

Figure 29 shows the cumulative air volume distributions from the Trondheim spraying mechanics series. The total air volume varies between 5.1% and 6.7%. The largest pore is of approximately 9.5 mm equivalent diameter. It is most likely formed due to minor lamination damage, and was not cropped away in the MATLAB analysis.

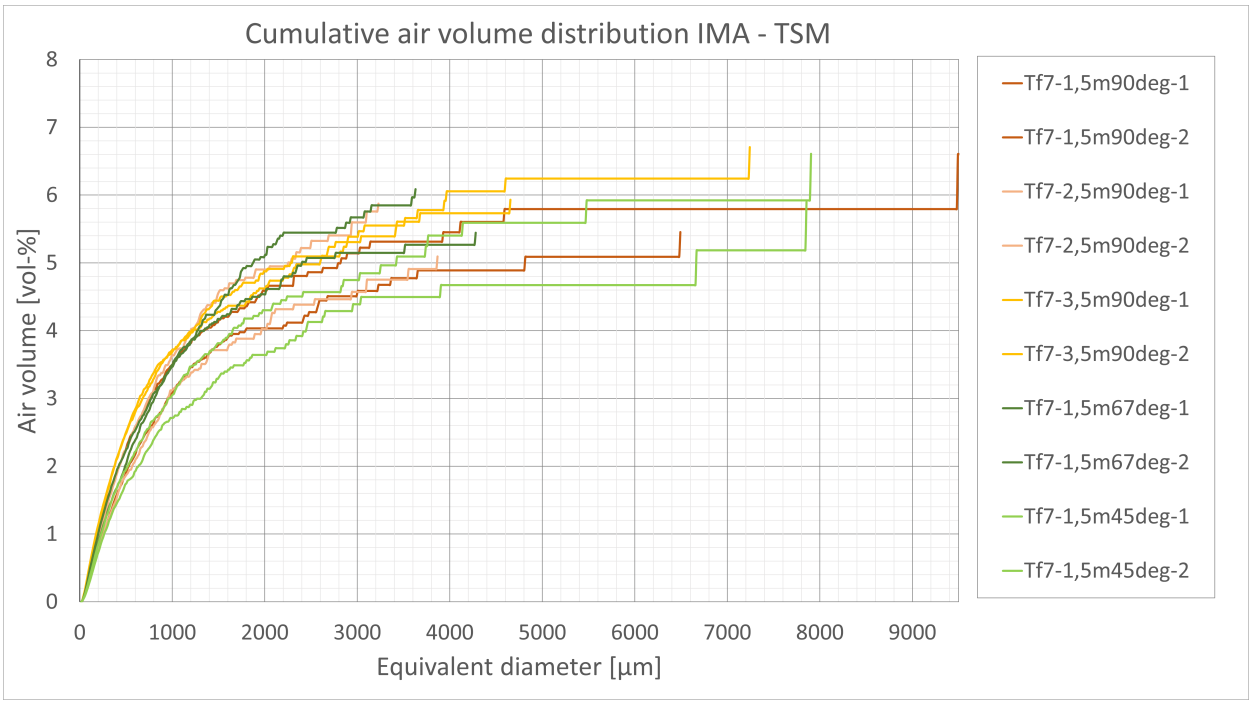

Figure 29: Size distributions for the samples from Trondheim spraying mechanics (TSM).

In TSM, the spraying distance and angle vary, and the reference mix has a spraying angle of 90 degrees and spraying distance of 1.5 m. Figure 30a and 30b show how different spraying distances and spraying angles deviate from the reference sample with regards to cumulative size distributions. Short versions of the mix names based on the spraying mechanics are used in this analysis. 2,5m is quite similar to 1,5m up to 1000 microns (entrained air), but has a higher porosity in the range of 1000 to 5000 microns. For pores with equivalent diameter of more than 5000 microns, the deviation is mainly controlled by individual large air voids. 3,5m deviates more from the reference in the entrained area, and has a further increase in cumulative air volume for the entrapped air as well. When spraying 45 degrees to the panel, a lower macroporosity was achieved both in the entrained area and entrapped area (up to 6000 microns). When spraying 67 degrees to the panel, there was an opposite effect.

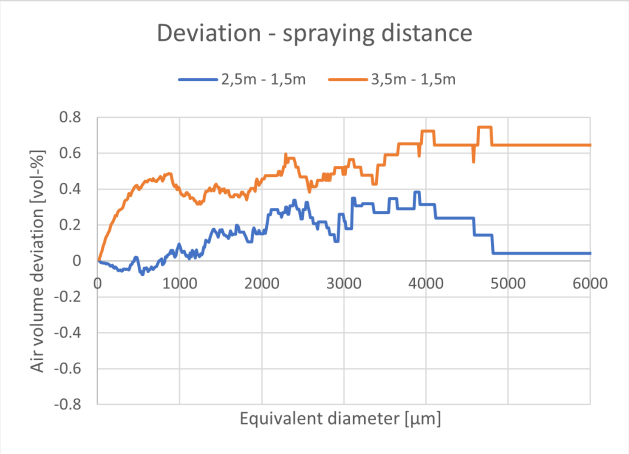

(a) Deviation of the Tf7-2,5m90deg and Tf7-3,5m90deg samples compared to Tf7-1,5m90deg.

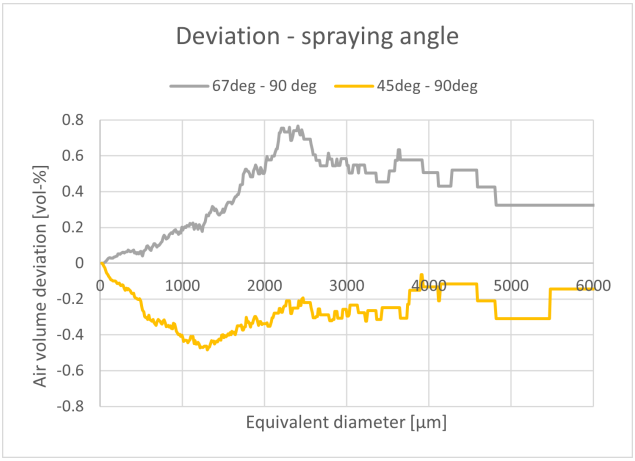

(b) Deviation of Tf7-1,5m67deg and Tf7-1,5m45deg compared to Tf7-1,5m90deg.

Figure 30: Deviation plots for the TSM test series that show the deviation between different spraying distances and spraying angles to the spraying mechanics of the reference (1.5m and 90 degrees).

The air void size distributions for the samples in Svorkmo are shown in Figure 31. The total air content varies between 5.1-7.5%. The largest air void has an equivalent diameter of approximately 9 mm in the Svorkmo test series.

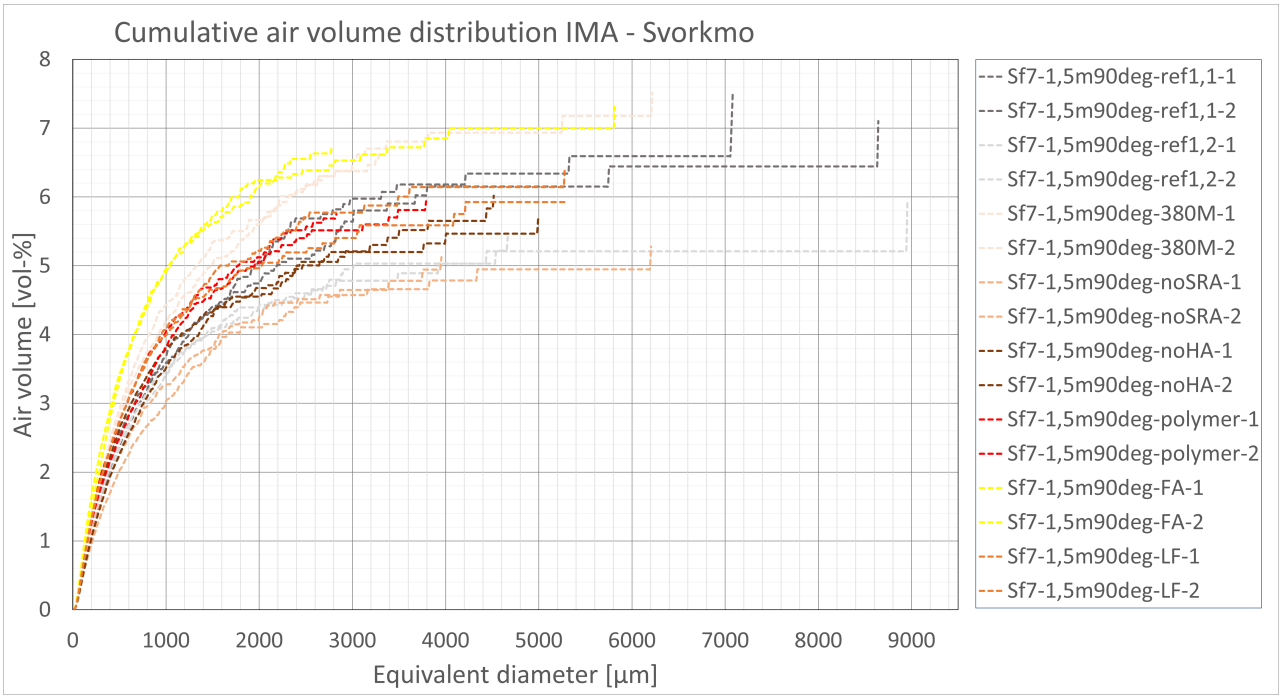

Figure 31: Size distributions for the samples from Svorkmo.

Table 18 and 19 show entrained air content, entrapped air content and total air content for every sample in the conducted project. Total air content varies between 3.8% and 7.5%.

Table 18: Different air void characteristics for Flekkefjord and Trondheim set accelerator. Entrained air includes all pores with a diameter less than 1 mm, while entrapped air includes all pores larger than 1 mm. *0% set accelerator. These air contents were also presented in the specialization project of Hårr and Kjeka [12]. Air contents are measured with IMA.

Sample	Entrained air < 1 mm pores $[vol-\%]$	Entrapped air > 1 mm pores $[vol-\%]$	Total air content $[vol-\%]$
Ff0-2m90deg-1	2.7	1.8	4.4
Ff0-2m90deg-2	2.4	1.5	3.8
Ff3-2m90deg-1	2.8	1.9	4.7
Ff3-2m90deg-2	2.6	2.2	4.8
Ff6-2m90deg-1	2.5	1.9	4.4
Ff6-2m90deg-2	2.3	1.6	4.0
Ff10-2m90deg-1	3.4	2.0	5.4
Ff10-2m90deg-2	2.8	3.4	6.2
Tnf0-1,5m90deg-1	5.4	0.9	6.3
Tnf0-1,5m90deg-2	5.6	0.6	6.1
Tnf3,5-1,5m90deg-1	3.0	2.1	5.1
Tnf3,5-1,5m90deg-2	3.1	1.6	4.7
Tnf7-1,5m90deg-1	2.9	1.4	4.4
Tnf7-1,5m90deg-2	3.1	1.6	4.7

Table 19: Different air void characteristics for Trondheim spraying mechanics and Svorkmo. Entrained air includes all pores with a diameter less than 1 mm, while entrapped air includes all pores larger than 1 mm. Air contents are measured with IMA.

Sample	Entrained air < 1 mm pores $[vol-\%]$	Entrapped air > 1 mm pores $[vol-\%]$	Total air content $[vol-\%]$
Tf7-1,5m90deg-1	3.1	2.4	5.5
Tf7-1,5m90deg-2	3.5	3.1	6.6
Tf7-2,5m90deg-1	3.1	2.0	5.1
Tf7-2,5m90deg-2	3.6	2.2	5.9
Tf7-3,5m90deg-1	3.7	2.2	5.9
Tf7-3,5m90deg-2	3.7	3.0	6.7
Tf7-1,5m67deg-1	3.5	1.9	5.4
Tf7-1,5m67deg-2	3.5	2.6	6.1
Tf7-1,5m45deg-1	3.1	3.6	6.6
Tf7-1,5m45deg-2	2.7	3.2	5.9
Sf7-1,5m90deg-ref1,1-1	3.6	3.9	7.5
Sf7-1,5m90deg-ref1,1-2	3.7	3.4	7.1
Sf7-1,5m90deg-ref1,2-1	3.4	2.5	5.9
Sf7-1,5m90deg-ref1,2-2	3.5	1.9	5.4
Sf7-1,5m90deg-380M-1	4.4	2.2	6.7
Sf7-1,5m90deg-380M-2	4.2	3.3	7.5
Sf7-1,5m90deg-noSRA-1	3.0	2.1	5.1
Sf7-1,5m90deg-noSRA-2	3.3	2.0	5.3
Sf7-1,5m90deg-noHA-1	3.5	2.5	6.0
Sf7-1,5m90deg-noHA-2	3.8	1.9	5.7
Sf7-1,5m90deg-polymer-1	3.8	2.1	5.9
Sf7-1,5m90deg-polymer-2	4.1	1.7	5.8
Sf7-1,5m90deg-FA-1	4.9	1.8	6.7
Sf7-1,5m90deg-FA-2	5.0	2.3	7.3
Sf7-1,5m90deg-LF-1	4.0	1.9	5.9
Sf7-1,5m90deg-LF-2	4.1	2.3	6.4

Table 18 and 19 show that cast SC (pumped), i.e the Tnf0 samples, have 5.4-5.6% entrained air and 0.6-0.9% entrapped air. The entrained air of SC with accelerator and AEA is 2.6-5.0%, and the entrapped air is 1.5-3.9%. For SC without accelerator (some of the Flekkefjord samples), the entrained air varies from 2.3-2.7%, whereas the entrapped air is 1.5-1.9%.

Figure 32 and 33 show the air contents from the literature and in Trussell's study. There is a complete overview of the values from the literature in Appendix C.1. The cast SC (not pumped) in Figure 32 has a considerably higher air content than concrete from the other SC categories. The air content in SC without accelerator is lower in Trussell's study than in literature, whereas the cast SC (pumped) of Trussell's study has higher air content than cast SC (pumped) in the

literature. For SC with accelerator, the Trussell mixes have a higher air content than in the studies from literature. Note that all the Trussell mixes contain AEA, whereas many of the mixes found in literature do not contain AEA.

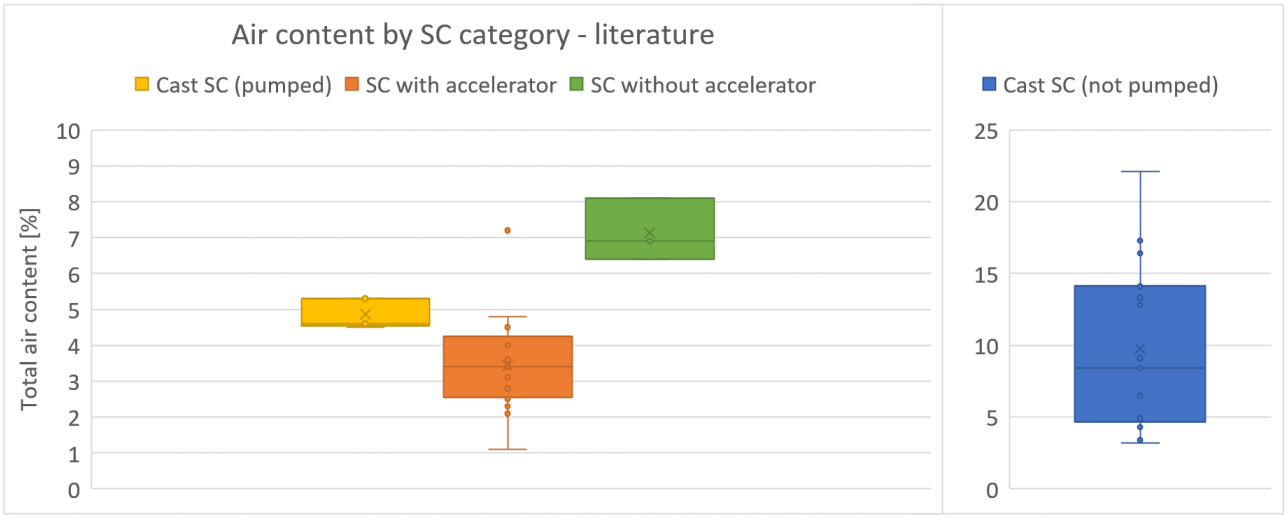

Figure 32: Air content by sprayed concrete category from studies in literature. Note that both axes show total air content [%]. The air contents where found in Yun et al. (2019) [48], Choi et al. [20], Yun et al. (2010) [19], Myren and Bjøntegaard [32] and Talukdar and Heere [47].

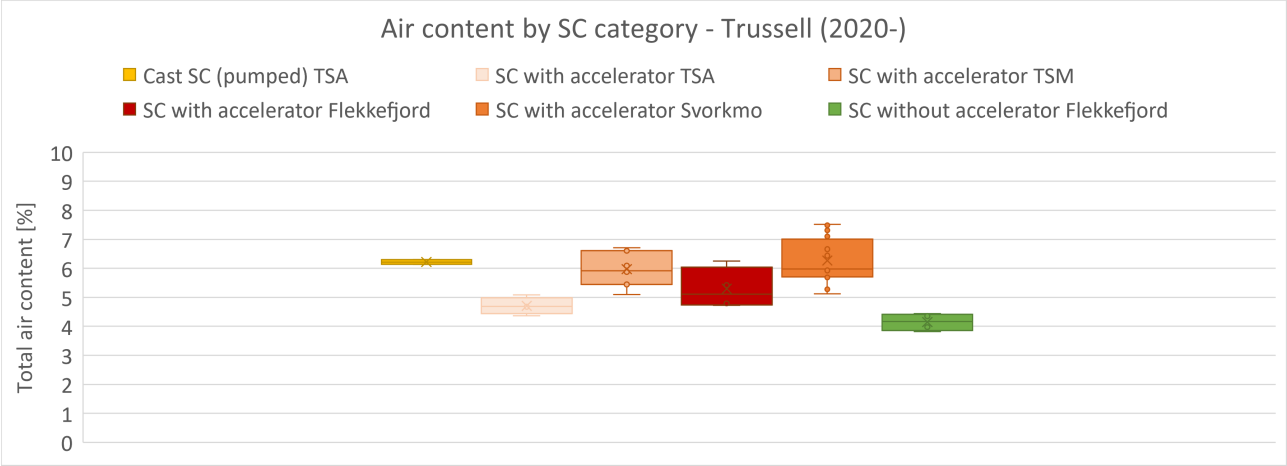

Figure 33: Air content by sprayed concrete category in Trussell's study.

Figure 34 shows that SC with accelerator generally has much higher air content if it contains AEA. SC with accelerator and AEA have air contents in the range 3.4%-7.5%, whereas SC with accelerator without AEA has air contents in the range 1.1%-3.6%. It should be noted that most of the samples included in Figure 34 are from Trussell's study, which were all air entrained. The other air entrained samples are 1 sample from Yun et al. (2019) [48] and 6 samples from Yun et al. (2010) [19] and Choi et al. [20].

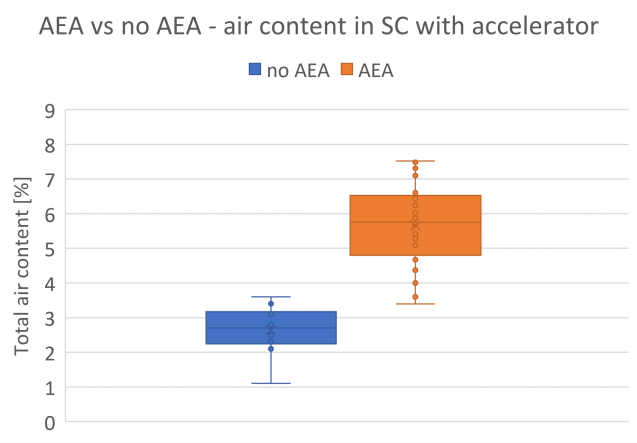

Figure 34: Effect of AEA on total air content in sprayed concrete with accelerator. The values were found in the Trussell study and in literature [19, 20, 32, 48].

4.4 Shape and orientation of macrovoids measured with IMA

Figure 35 and 36 show the cumulative shape distributions (L/W-ratios) for the Flekkefjord and TSA test series. These were analyzed and discussed in [12]. Note that air voids are considered spherical if L/W is 1.1 or lower.

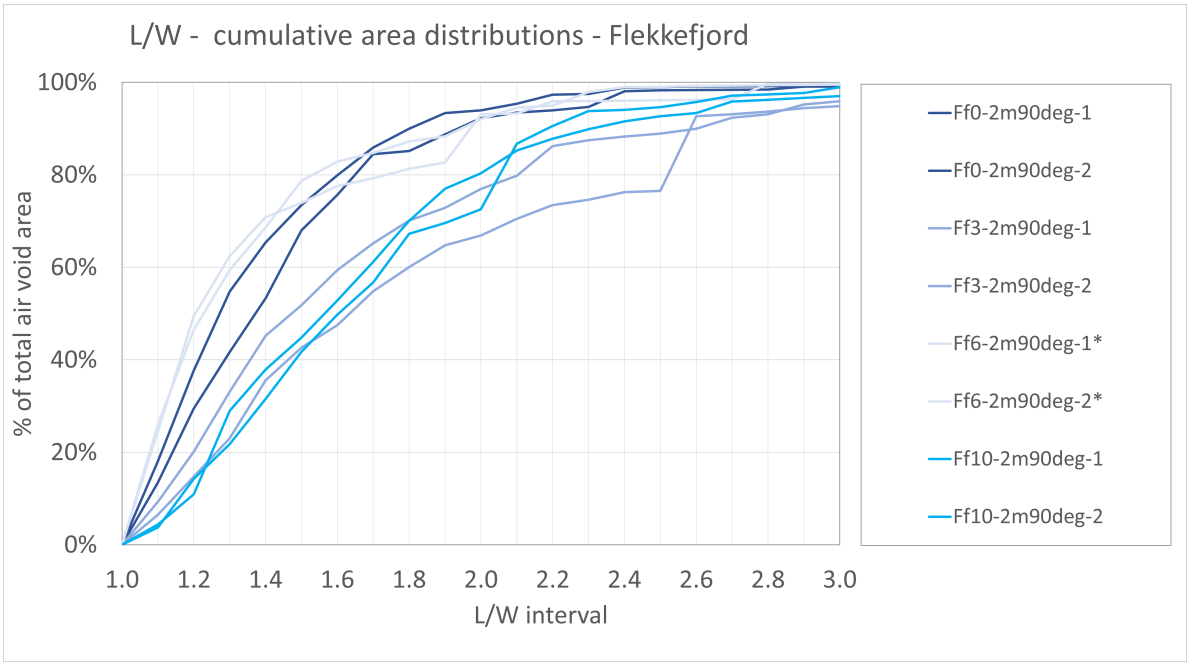

Figure 35: Length over width distributions for the samples from Flekkefjord. This figure was presented in the specialization project of Hårr and Kjeka [12]. *0% set accelerator.

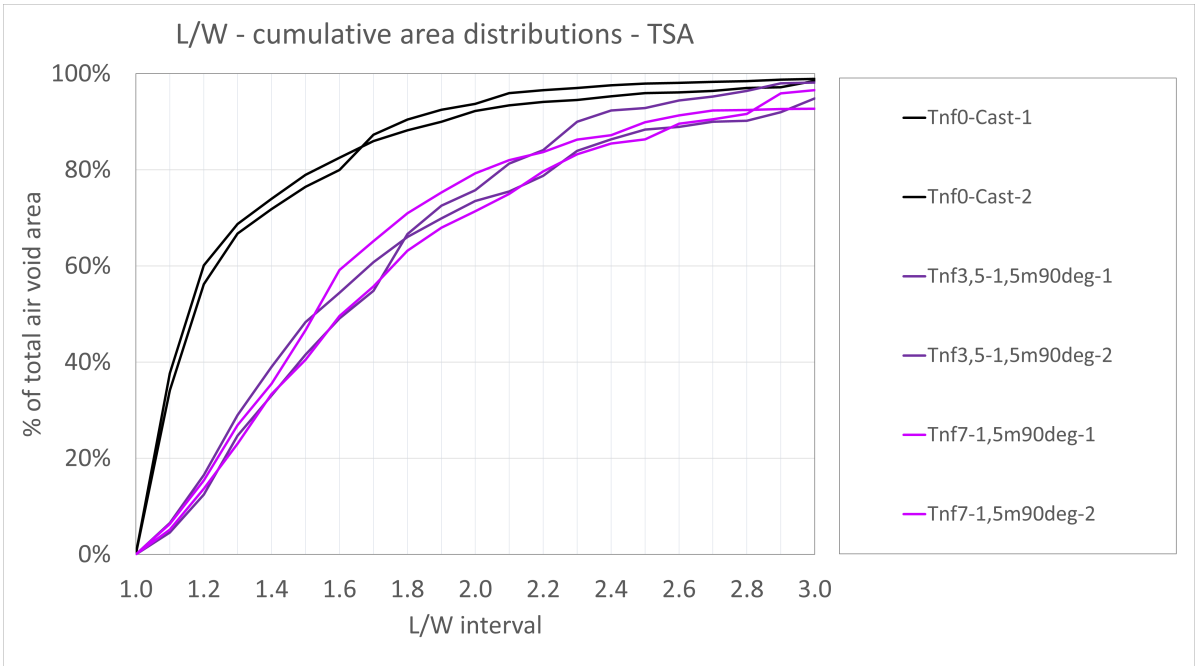

Figure 36: Length over width distributions for the samples from Trondheim set accelerator. This figure was presented in the specialization project of Hårr and Kjeka [12].

The length over width distributions in Trondheim spraying mechanics are shown in Figure 37. 2-8% of the air volume consists of spherical pores in the Trondheim spraying mechanics series. There is no relation between L/W distribution and different spraying distances and spraying angles.

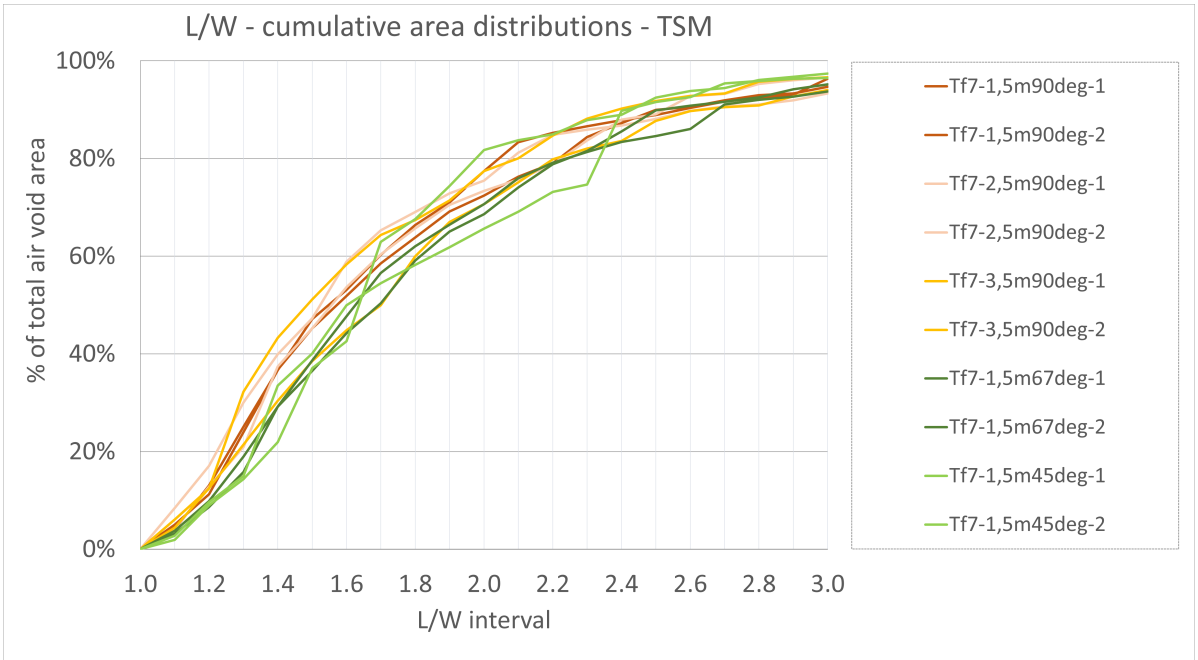

Figure 37: Length over width distributions for the samples from Trondheim spraying mechanics.

Figure 38 shows the length over width distributions in the Svorkmo series. 4-8% of the air volume consists of spherical pores in the Svorkmo samples. The distributions in Figure 38

resemble each other, and Svorkmo is the test series with the lowest scatter when it comes to length over width ratio.

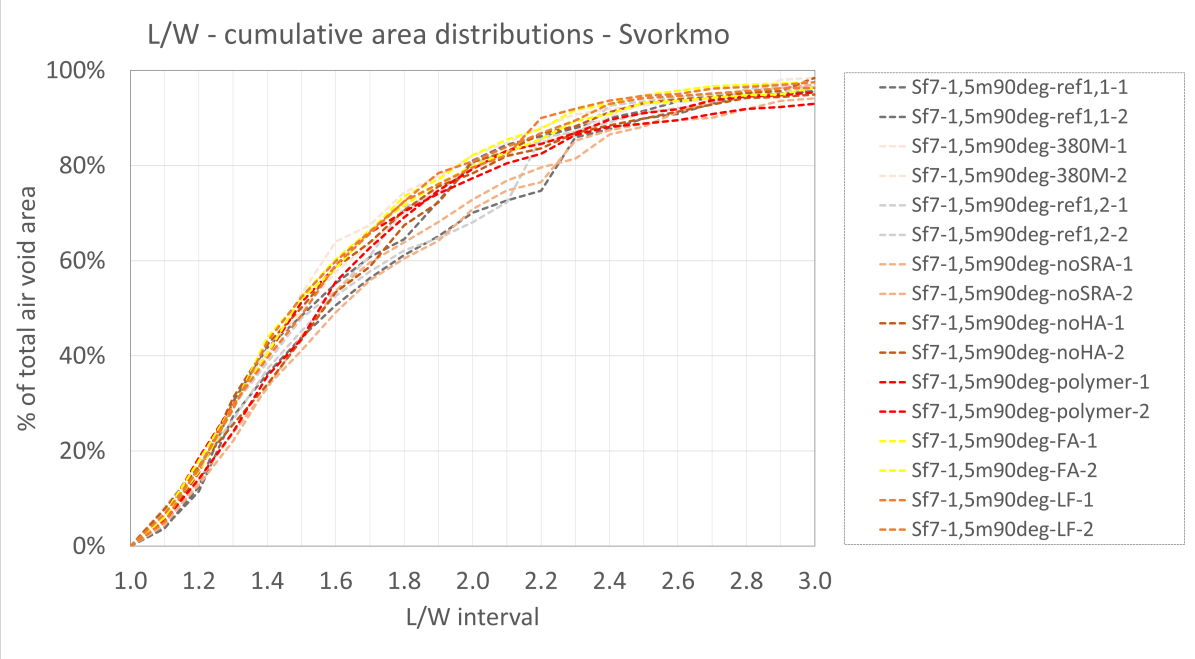

Figure 38: Length over width distributions for the samples from Svorkmo.

Figure 39 shows the L/W ratio of each air void in the Svorkmo series, plotted against the area of each air void. Most of the largest voids have a L/W ratio between 1 and 3. The most elongated void has a L/W ratio of 15.2, but is very small.

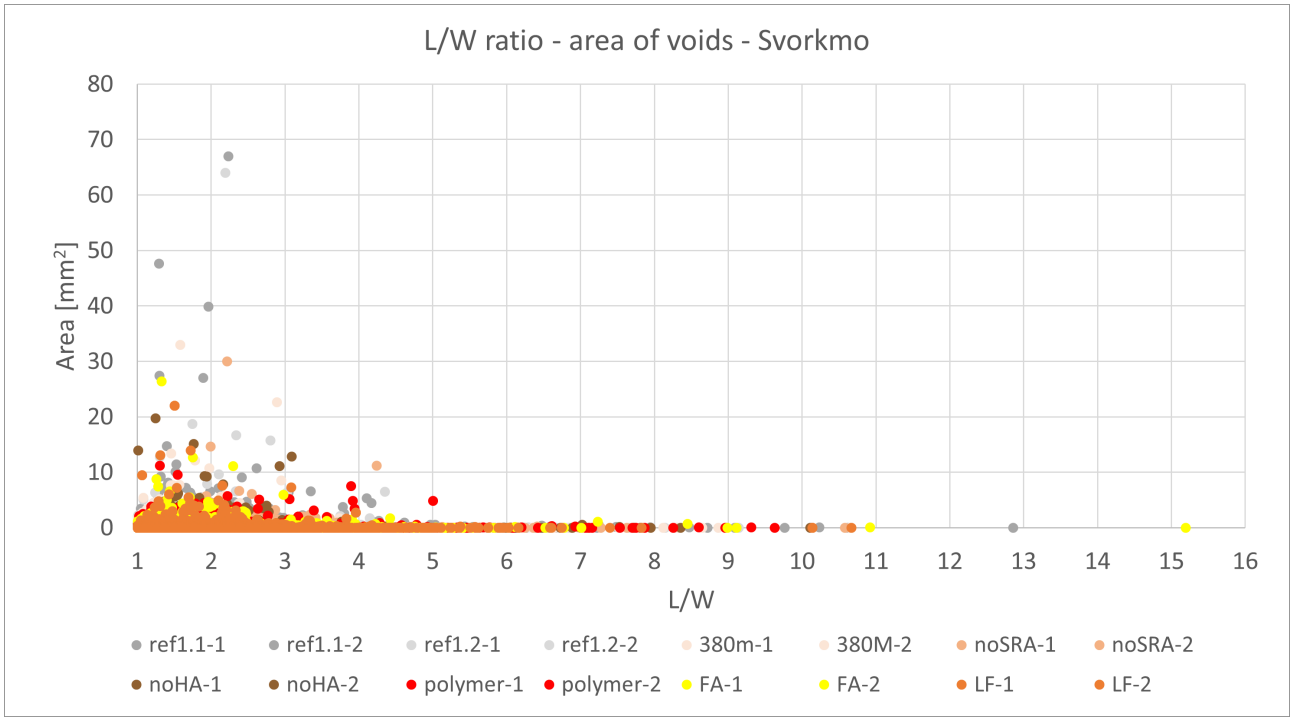

Figure 39: Length over width ratio for each void in the Svorkmo series plotted against the area of each void.

The orientation distributions in Flekkefjord are shown in Figure 40. Three of the mixes have more air volume with orientation normal to the spraying direction than parallel to the spraying direction. On average, there is more air volume oriented normal than parallel to the spraying direction in Flekkefjord. This is also the case in Trondheim set accelerator, see Figure 41. There is no unambiguous correlation between accelerator dosage and orientation of the air volume based on the mixes in Flekkfjord and TSA.

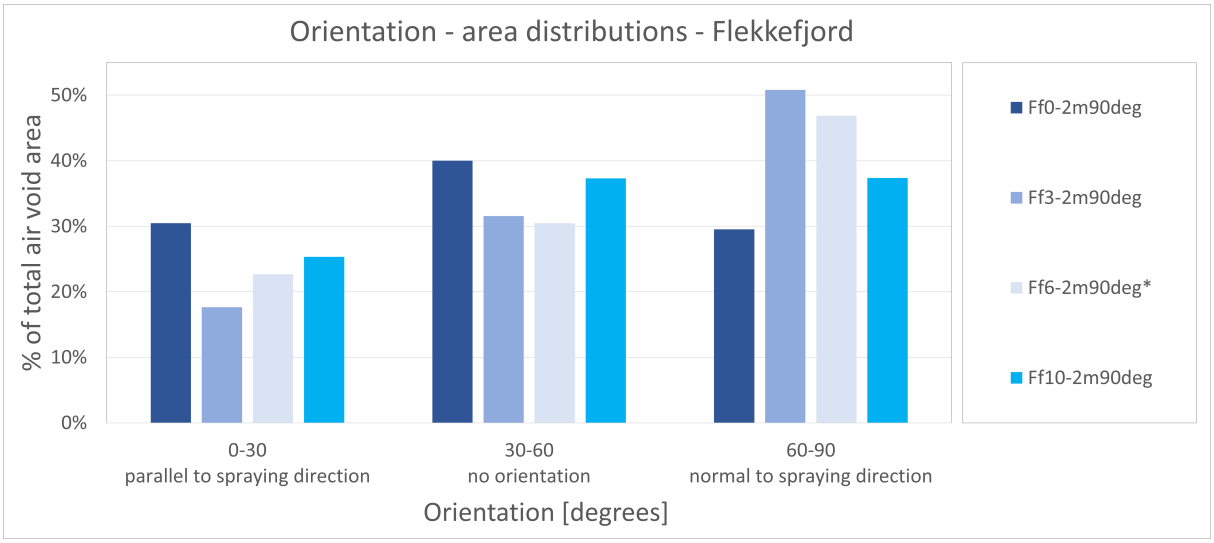

Figure 40: Orientation distributions for the samples from Flekkefjord.

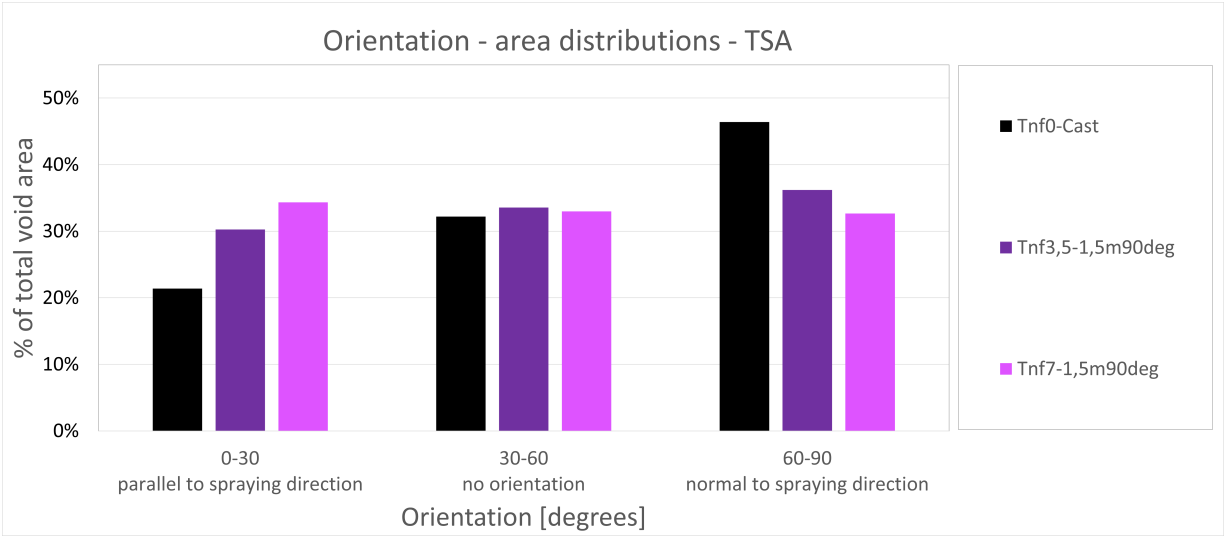

Figure 41: Orientation distributions for the samples from Trondheim set accelerator.

The orientation distributions for TSM and Svorkmo are shown in Figure 42 and 43. Two of the samples from TSM have more air volume normal to the spraying direction, whereas one sample has more air volume parallel to the spraying direction. Unlike the other test series, all the mixes in Svorkmo have more air volume normal to the spraying direction than parallel to the spraying direction.

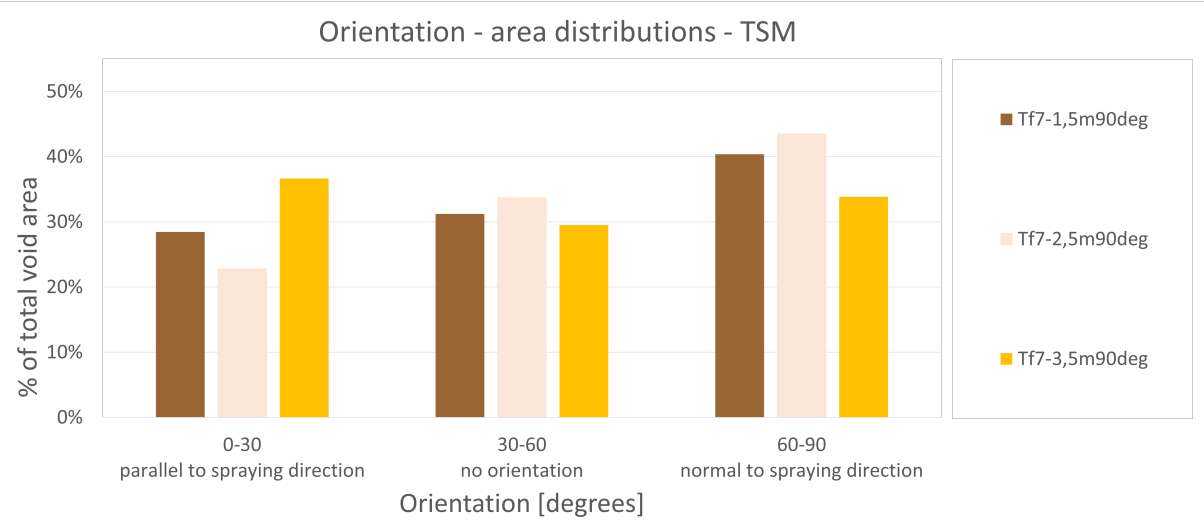

Figure 42: Orientation distributions for the samples from Trondheim spraying mechanics. Tf7-1,5m67deg and Tf7-1,5m45deg were not included in this plot due to different spraying angle. Hence, the orientations in these samples would not fit in the intervals in the figure.

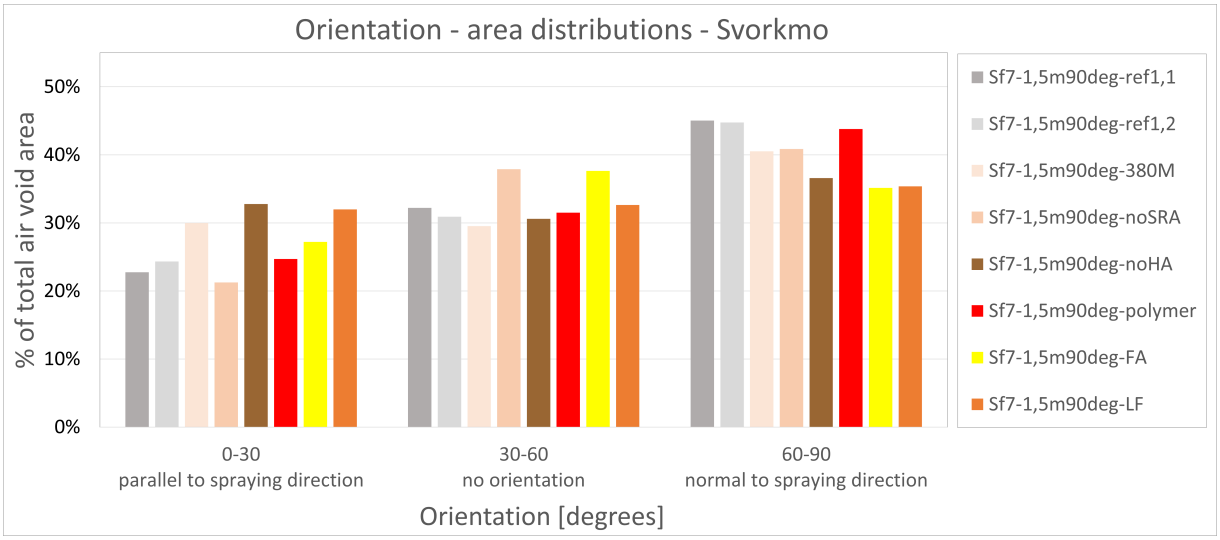

Figure 43: Orientation distributions for the samples from Svorkmo.

Figure 44 was made to investigate if there was any relation between the void sizes of each air void and orientation. The plot shows that there is no relation between orientation and the area of each air void in the mixes from Svorkmo.

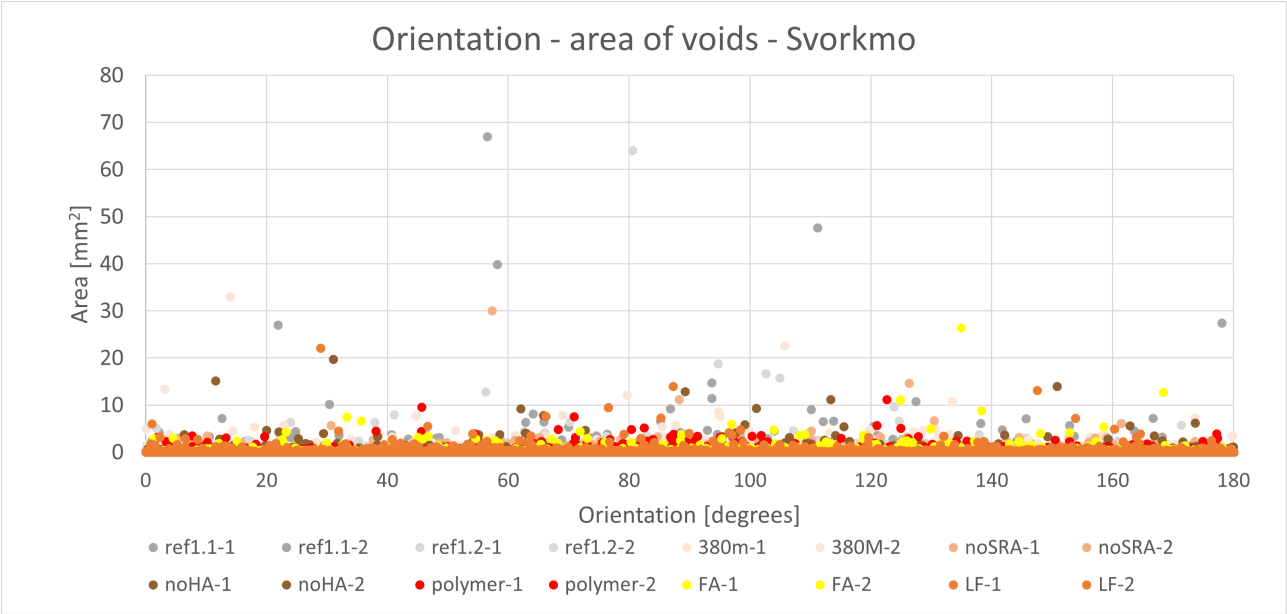

Figure 44: Orientation of each macrovoid plotted against the area of each macrovoid in the Svorkmo series.

4.5 Water penetration - effect of set accelerator and anisotropy

The water penetration results are presented in five tables in order to make it easier to compare the results. A complete overview of water penetration results, including pictures of penetration fronts, is given in Appendix D. The water penetration direction was normal to the spraying direction in N-cubes, and parallel to the spraying direction in P-cubes.

Table 21-25 show maximum penetration depths and calculated $K_{valenta}$ and $K_{vuorinen}$ (Equation 3 and 4) for the water penetration experiments. It was assumed that 3 mm is the lowest measurable penetration depth. Based on this minimum penetration depth and the given pressure and time, the minimum measurable Vuorinen coefficient was calculated ($K^{min}_{vuorinen}$). PFc values used for calculating $K_{valenta}$ are presented in Table 20.

Table 20: Open, closed and total macroporosities measured with the PF method for the samples tested for water penetration.

Mix name	PFo [%]	PFc [%]	PFt [%]
Ff3-2m90deg	1.0	4.4	5.4
Ff10-2m90deg	1.0	3.8	4.8
Sf7-1,5m90deg-ref1,2	1.1	4.2	5.3

Table 21 shows maximum penetration depths and calculated $K_{valenta}$ and $K_{vuorinen}$ for samples with 10% accelerator, tested normal and parallel to spraying direction. When applying water pressure normal to the spraying direction, the water entered clearly visible paths created by spitting/lamination damage. When applying water pressure parallel to the spraying direction, there was a big spread in the permeability. The 10%P3 sample had lamination damage near

the penetration surface and therefore some more penetration than the 10%P5 and 10%P6. The P-cubes were however much less permeable than the N-cubes.

Table 21: Water penetration - 10% accelerator N-cubes vs P-cubes.

Sample	Pressure $[MPa]$	Time $[h]$	Max penetration $[mm]$	$K_{valenta}$ $[m/s]$	$K_{vuorinen}$ $[m/s]$	$K^{min}_{vuorinen}$ $[m/s]$
10%P3	0.1	1.75	19	1.0E-10	8.7E-10	1.6E-12
10%P5	0.1	1.75	5	6.6E-12	7.6E-12	1.6E-12
10%P6	0.1	1.75	14	5.3E-11	2.7E-10	1.6E-12
10%N2	0.1	1.75	84	2.0E-09	1.4E-07	1.6E-12
10%N3	0.1	1.75	67	1.4E-09	7.1E-08	1.6E-12
10%N5	0.1	1.75	96	3.1E-09	2.9E-07	1.6E-12

In Table 22, 3% P-cubes and N-cubes are compared. It can be seen in this table that the penetration depth is higher for cubes tested normal to the spraying direction (N-cubes) than for cubes tested parallel to the spraying direction (P-cubes), just like for the 10%-cubes in Table 21. The 3% P-cubes experienced zero penetration, indicating a higher quality of concrete in this direction.

Table 22: Water penetration - 3% accelerator N-cubes vs P-cubes

Sample	Pressure $[MPa]$	Time $[h]$	Max penetration $[mm]$	$K_{valenta}$ $[m/s]$	$K_{vuorinen}$ $[m/s]$	$K^{min}_{vuorinen}$ $[m/s]$
3%P2	0.3	72	0	-	-	5.4E-16
3%P5	0.3	72	0	-	-	5.4E-16
3%P6	0.3	72	0	-	-	5.4E-16
3%N2	0.3	72	31	2.7E-12	1.6E-12	5.4E-16
3%N5	0.3	72	13	4.7E-13	8.2E-14	5.4E-16
3%N6	0.3	72	41	4.7E-12	4.2E-12	5.4E-16

Table 23 shows the results from tests at the 3% and 10% P-cubes. Generally, the pressure is higher and the durations are longer for the 3%-cubes than for the 10%-cubes. In spite of this, the penetration depths and the permeability coefficients are higher for the 10%-cubes. It seems clear that the 10% Flekkefjord concrete is more permeable and less watertight than the 3% Flekkefjord concrete. Note that the 3%P3 cube started leaking after a few hours due to poor concrete quality at the top of the cube.

Table 23: Comparison of 3% and 10% P-cubes. The K-values of 3%P1 and 3%P8 were based on a weighted average of the pressures. *The concrete quality at the top of 3%P3 was poor, and there was a leakage a few hours after the test had started.

Sample	Pressure $[MPa]$	Time $[h]$	Max penetration $[mm]$	$K_{valenta}$ $[m/s]$	$K_{vuorinen}$ $[m/s]$	$K^{min}_{vuorinen}$ $[m/s]$
3%P2	0.3	72	0	-	-	5.4E-16
3%P5	0.3	72	0	-	-	5.4E-16
3%P6	0.3	72	0	-	-	5.4E-16
3%P3*	0.5	3	23	2.1E-11	5.6E-11	5.2E-14
3%P7	0.5	70	6	6.1E-14	2.5E-15	2.3E-16
3%P1	0.5 (70h) & 0.7 (24h)	94	10	1.2E-13	7.4E-15	1.2E-16
3%P8	0.5 (70h) & 0.7 (24h)	94	11	1.4E-13	1.0E-14	1.2E-16
10%P1	0.3	6.33	70	1.3E-10	1.3E-09	2.7E-14
10%P2	0.3	6.33	80	1.7E-10	2.0E-09	2.7E-14
10%P3	0.1	1.75	19	1.0E-10	8.7E-10	1.6E-12
10%P5	0.1	1.75	5	6.6E-12	7.6E-12	1.6E-12
10%P6	0.1	1.75	14	1.7E-11	2.7E-10	1.6E-12
10%P4	0.1	24	26	1.4E-11	2.8E-11	1.8E-14

Table 24 illustrates the same tendencies as Table 23, because the penetration depth is higher for the 10%-cubes than the 3%-cubes. Here, the pressures and durations are equal for six of the cubes. The 3%N4 and 10%N4 cubes differ from the rest of the cubes, since they have high penetration depths, even though the pressure is lower and the duration is shorter than for the comparable cubes. The values for the 10%N4 cube are minimum values, since the penetration front had reached the bottom of the cube at the time of splitting.

Table 24: Comparison of 3% and 10% N-cubes. Note that the water penetrated the entire 10%N4 cube. Thus, the K-values for 10%N4 are minimum values.

Sample	Pressure $[MPa]$	Time $[h]$	Max penetration $[mm]$	$K_{valenta}$ $[m/s]$	$K_{vuorinen}$ $[m/s]$	$K^{min}_{vuorinen}$ $[m/s]$
3%N2	0.3	72	31	2.7E-12	1.6E-12	5.4E-16
3%N5	0.3	72	13	4.7E-13	8.2E-14	5.4E-16
3%N6	0.3	72	41	4.7E-12	4.2E-12	5.4E-16
3%N4	0.1	48	16	3.2E-12	2.2E-12	7.1E-15
10%N2	0.3	1.75	84	6.7E-10	1.4E-07	1.6E-12
10%N3	0.3	1.75	67	1.4E-09	7.1E-08	1.6E-12
10%N5	0.3	1.75	96	3.1E-09	2.9E-07	1.6E-12
10%N4	0.1	24	>100	>2.1E-10	>2.9E-09	1.8E-14

The 3% Flekkefjord mix is compared to one of the Svorkmo mixes, Sf7-1,5m90deg-ref1,2, in Table 25. The tests results from 3%P1, 3%P8 and S1-S4 are comparable with the criterion for watertightness in NS 3420-L5 (1986) [62], which was presented in subsection 2.9. Note that pressures and durations were not the same as suggested in the standard but the average pressure was higher, and the maximum pressure was the same as in the standard [62]. The

watertightness criterion is that the penetration depth should be less than 25 mm, which is the case for 3%P1, 3%P8 and S1-S4. The $K_{valenta}$ and $K_{vuorinen}$ for these samples are less than $1 \cdot 10^{-11}$, which is the criterion for the permeability coefficient. Note that the criterion for permeability coefficient is meant for a different test, and $K_{valenta}$ and $K_{vuorinen}$ are estimates of the permeability coefficient based on the water penetration test. Table 25 also shows that the Svorkmo samples have a lower penetration depth than the Flekkefjord samples.

Table 25: Comparison of 3% P-cubes and Svorkmo discs (S1-S4).

Sample	Pressure $[MPa]$	Time $[h]$	Max penetration $[mm]$	$K_{valenta}$ $[m/s]$	$K_{vuorinen}$ $[m/s]$	$K^{min}_{vuorinen}$ $[m/s]$
3%P2	0.3	72	0	-	-	5.4E-16
3%P5	0.3	72	0	-	-	5.4E-16
3%P6	0.3	72	0	-	-	5.4E-16
3%P3	0.5	3	23	2.1E-11	5.6E-11	5.2E-14
3%P7	0.5	70	6	6.1E-14	2.5E-15	2.3E-16
3%P1	0.5 (70h) & 0.7 (24h)	94	10	1.2E-13	7.4E-15	1.2E-16
3%P8	0.5 (70h) & 0.7 (24h)	94	11	1.4E-13	1.0E-14	1.2E-16
3%P4	0.1	48	14	2.4E-12	1.4E-12	7.1E-15
S1 (Ref1.2)	0.5	70	0	-	-	2.2E-16
S2 (Ref1.2)	0.5	70	6	5.9E-14	2.3E-15	2.2E-16
S3 (Ref1.2)	0.5 (70h) & 0.7 (24h)	94	5	2.7E-14	6.3E-16	1.1E-16
S4 (Ref1.2)	0.5 (70h) & 0.7 (24h)	94	11	1.3E-13	9.4E-15	1.1E-16

Table 21-25 show that some cubes deviate from the comparable cubes. In other words, there is a significant scatter. For example, 3%P3, 3%P4, 3%N4 and 10%N4 are less watertight than comparable cubes.

Figure 45-48 show four water penetration fronts (for 3%P6, 3%N6, 10%P5 and 10%N5) together with polished, coloured and binarized images of the same samples. In the cubes tested for water penetration, the polished sections were parallel to the split surface, and the distance between the split surface and the polished sections were a few cm. Lamination damages may be seen on both penetration front and binary images.

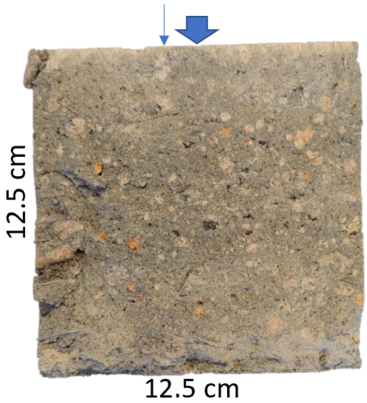

(a) Water penetration front of the 3%P6-cube.

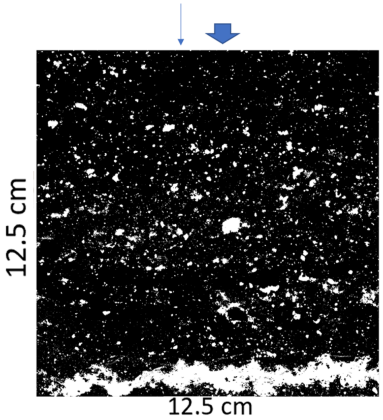

(b) Binary image of the 3%P6-cube.

Figure 45: Water penetration front and binary image of the 3%P6-cube. Thin and thick arrows show water penetration and spraying direction, respectively.

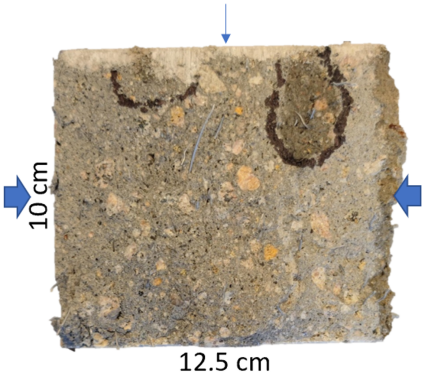

(a) Water penetration front of the 3%N6-cube.

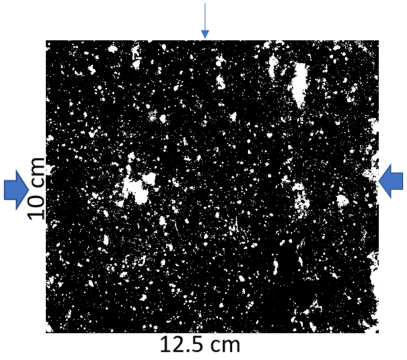

(b) Binary image of the 3%N6-cube.

Figure 46: Water penetration front and binary image of the 3%N6-cube. Thin and thick arrows show water penetration and spraying direction, respectively.

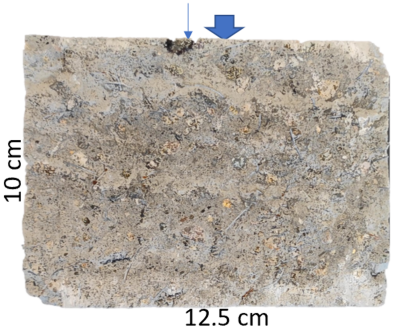

(a) Water penetration front of the 10%P5-cube.

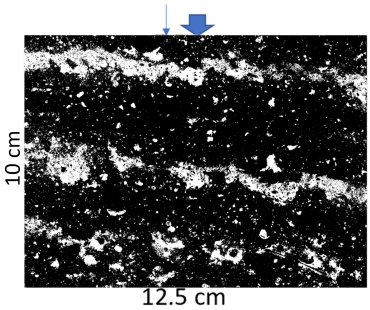

(b) Binary image of the 10%P5-cube.

Figure 47: Water penetration front and binary image of the 10%P5-cube. Thin and thick arrows show water penetration and spraying direction, respectively.

(a) Water penetration front of the 10%N5-cube.

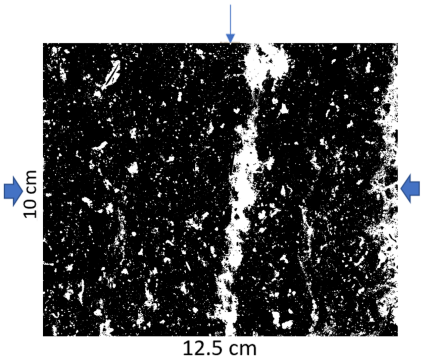

(b) Binary image of the 10%N5-cube.

Figure 48: Water penetration front and binary image of the 10%N5-cube. Thin and thick arrows show water penetration and spraying direction, respectively.

5 Discussion

5.1 Open macroporosity measured with the full PF method

Open macroporosity has been defined by SINTEF and in this thesis as the porosity which is not filled by four days of one sided capillary suction, but filled during submersion. However, Trussell's measurements indicate that different duration lengths for the capillary suction could be used. As Figure 15 and 16 show, the duration of the capillary suction has a large impact on the vol-% of open macroporosity. The knee point at a capillary suction curve, which is illustrated in Figure 2, is reached in less than 4 days of capillary suction. According to Hall and Hoff, trapped air pockets (not macropores) are filled after the knee point [28], whereas Sellevold suggests that small air voids (macropores) are filled by capillary suction [29]. The mechanism is important for the definition of open macroporosity. If Hall and Hoff's [28] suggested mechanism is correct, the capillary suction could go on for a long time to ensure that only macropores (and not air pockets) are filled during the subsequent immersion. If Sellevold's [29] proposed mechanism is correct, the capillary suction could be stopped at the knee point to ensure that all macropores are included in the open macroporosity. Another possibility is that both mechanisms act simultaneously, which makes it hard to propose a duration of the capillary suction test.

In the following, different factors affecting open macroporosity will be discussed. Salvador et al. [39] found that water accessible porosity increases with increasing accelerator dosage. However, it should be noted that Salvador et al. [39] examined water accessible porosity, and open macroporosity is a part of water accessible porosity. According to Figure 17, the same tendency can be seen in Myren and Bjøntegaard's [32] study and Trussell's study. For the steel fibre mixes in Myren and Bjøntegaard's [32] test series, the PFo/PFt ratio is higher in the sprayed concrete with accelerator than the cast. There is however no considerable increase in PFo/PFt ratio between the cast and sprayed macro pp fibre mixes. In this study (Trussell's study), the PFo/PFt ratio seems to increase with increasing accelerator dosage based on the samples from Flekkefjord and TSA. The reason for increased open macroporosity in sprayed concrete with high accelerator dosage is probably that the compaction is not complete when the set accelerator makes the concrete set. As the set accelerator dosage increases, the compaction may get poorer since the setting occurs earlier and quicker.

In Figure 18a and Figure 18b, each series ought to be considered separately. The studies by Rønnes [37], Myren and Bjøntegaard [32] and Justnes et al. [34] from the literature show that the PFo/PFt ratio may increase slightly when the w/b ratio increases. The same relation may be observed in Trussell's measurements. However, in Trussell's study, the changes in w/b ratio are caused by changes in accelerator dosages. Therefore, the increase in PFo/PFt ratio in sprayed concrete may be due to changes in accelerator dosage instead of changes in w/b ratio. Nevertheless, since the mixes in the studies by Rønnes [37] and Justnes et al. [34] do not contain accelerator, w/b ratio may affect PFo/PFt ratio.

Neither the studies from literature nor the Trussell study show a correlation between PFo/PFt

ratio and AEA dosage, see Figure 18c. For many of the studies in literature in Figure 18d, the PFo/PFt ratio is reduced as the compressive strength increases. These studies include Bjelland and Moi [36], Justnes et al. [34] and Myren and Bjøntegaard [32]. Moreover, the same relation seems to apply in Trussell's study. Air voids reduces compressive strength [24]. Hence, it seems reasonable that the PFo/PFt ratio is reduced as the strength increases. However, more measurements are required to verify or refute that there is a relation between w/b ratio, AEA dosage, and compressive strength on the one hand and PFo/PFt ratio on the other.

In Figure 14, it can be observed that several mixes have more than 0.5 vol-% open macroporosity. This applies to the studies by Trussell, Tandberg [33] and Bjelland and Moi [36]. According to SINTEF's procedure [31], larger values than 0.5 vol-% indicate continuous macropores, and is most common for sprayed concrete and dry compacted concretes. Consequently, there are most likely continuous macropores in Trussell's samples, and there could be continuous macropores in Tandberg's [33] samples as well. Image analysis (IMA) has shown that there is not percolation in macropores in most of the samples from Trussell's study [12]. The only exceptions are the Ff10-2m90deg samples, that had large lamination damages. However, image analysis can only be used to determine two-dimensional percolation, whereas the full PF measurements indicate that there could be partly three-dimensional percolation.

5.2 Comparison of air content measured with PF and IMA

As mentioned earlier, Jacobsen et al. (1993) [40] proposed that open macroporosity may explain differences in the PFc/IMA ratio. This could be the case for the sprayed concrete, zero slump concrete and cast "sprayed concrete" according to Figure 23. These types of concrete have PFc/IMA ratio less than 1, and Figure 19-21 show that this applies to all the mixes in Trussell's study. Since sprayed and zero slump concretes have high open macroporosity due to poor compaction [31], the IMA might measure all the pores whereas a large part of the macroporosity is not included in the PFc. This is because IMA does not take into consideration which mechanism fills which pore or whether pores are connected. However, when comparing the difference between IMA and PFc to PFo, the difference between IMA and PFc is in most cases considerably higher than the open macroporosity, PFo (see Figure 26). Hence, the deviation in air content measured by the two methods can not be solely explained by open macroporosity.

High strength concrete also has PFc/IMA ratios of less than 1 for most of the samples. A possible reason for high strength concrete to have low PFc/IMA ratio may be that high strength concrete is more compact than conventional concrete, and has low permeability and low porosity. Less water may enter the concrete in the PF method, and therefore IMA measures higher porosity. This explanation corresponds well with the findings in Sellevold and Farstad [7]. According to them, the suction porosity of high quality concrete (i. e. w/b = 0.35) increased by 0.4 vol-% when the duration of suction increased from 2 to 7 days. This increase in suction porosity reduces the open macroporosity with 0.4 vol-% as well. These observations indicate that the duration of capillary suction is important for the porosities measured by the full PF

method.

In conventional concrete, PFc is higher than IMA in most cases. A possible explanation for this could be that capillary pores may become macropores in the drying phase, as proposed by SINTEF [31]. This entails that the PF method measures higher macroporosity than IMA since samples are not dried before IMA. Therefore, it would be interesting to dry the concrete samples before IMA as well to compare the air contents in dried concrete. It is also difficult to distinguish accurately at which size pores become registered as macropores in the PF test. This is because the capillary driving force decreases as the size of capillary pores increase (Equation 1). The capillary suction for a pore of 10 microns is 0.03 MPa according to Equation 1. This is not much of a driving force [7]. IMA measures macropores as a minimum size detectable by the scanning device, for instance 10-30 microns. In other words, the smallest pores that may be registered as macroporosity in the PF method are not detectable by IMA. The consequence is that the PF method may measure higher macroporosity than IMA. Note that drying and unclear limit between capillary pores and macropores in the PF test influence the PFc/IMA ratio in all types of concrete, but in some types of concrete there are more influential effects that decrease PFc/IMA ratio to below 1.

From Figure 25a, 25b and 25c there is no clear relation between PFc/IMA ratio and w/b ratio, AEA content and compressive strength. These findings are important in order to exclude factors that may affect the ratio. The older studies, Sellevold (1986/2005) [7, 23], Jacobsen et al. (1993) [40] and Jacobsen et al. (1996) [44], used 10 MPa saturation pressure to fill the macrovoids with the PF method, while the others used 5 MPa. From Figure 24, it can be seen that the studies with 5 MPa have slightly lower PFc/IMA ratio, but because of a very big spread, there is no clear difference.

There are also some differences in how IMA has been performed. In the earlier studies, air voids were counted manually in a microscope (OA) [23, 40, 44] instead of automatically with an image analysis software. By making the process automated, more area is analyzed in shorter amount of time. However, when samples are analyzed with microscope, each air void is evaluated more carefully, and sources of error such as excessive powder, stroke marks and image noise are not present. There is no tendency that OA measures higher or lower PFc/IMA ratio than IMA.

Another factor that could affect the PFc/IMA ratio is the polishing procedure and preparation for IMA. Before performing image analysis, sections were ground and polished to make a smooth surface and sharp edges around air pores. In order for this test to be good, it is important to control the quality of the polishing. If the polishing is unsatisfactory, it will be difficult to apply barium sulphate to the pores only and not have it stick to the solid surface, which will give higher measured macroporosity than it really is (i.e. too low PFc/IMA ratio). Another source of error in Trussell's IMA procedure was that the barium sulphate powder could fall out of the pores when the samples were flipped onto the scanner. The powder fell more often out of the deeper pores. This powder could be registered as new pores. As a result, the IMA may measure

a too high macroporosity, and the PFc/IMA ratio would be reduced.

5.3 Size distribution and air content measured with IMA

In TSM, the total air content is quite similar in all the mixes, see Table 19, but the size distributions vary more, see Figure 29 and Figure 30. A comparison of the TSM and the Svorkmo test series indicates that changes in the mix have larger impact on air content than spraying mechanics (spraying distance and angle). In the Svorkmo test series, the "ref1,1" mix, the mix with FA and the mix with matrix volume of 380 $litres/m^3$ have the highest air content. Especially the FA and 380M mixes, also have large air volume with small equivalent diameter according to Figure 31. Based on the Flekkefjord and TSA series, total air content increases with addition of set accelerator. This could be because the concrete has less time to consolidate, since the accelerator makes it set immediately.

In the Trussell study, the total air content in SC with accelerator varies from 4.4-7.5%. This corresponds well with the findings of Yun et al. (2010) [19] and Yun et al. (2019) [48], where the air content is 3.4-7.2% SC with accelerator and AEA. In SC with accelerator and without AEA, the total air content is 1.1-3.6% [19, 32, 48], which is considerably lower than for air-entrained SC with accelerator. Talukdar and Heere [47] measured an air content of 6.4-8.1% in SC without accelerator, and Trussell found an air content of 3.8-4.4% in SC without accelerator (Ff0 and Ff6*).

Trussell's study shows that the total macroporosity increases with increasing flow rate for SC with set accelerator. This observation is based on the flow rates in Table 16 and the air contents in Table 18 and 19. The same tendency is found by Talukdar and Heere in SC without accelerator [47]. This could be because a higher flow rate will require a higher stroke rate in the pump, which may mix air into the fresh concrete.

In this project, there is only one cast SC (pumped) mix, Tnf0-cast. The air content for this mix was 6.1-6.3%. That is higher than the cast SC (pumped) mixes without AEA from Yun et al. (2019) [48], but in the same range as cast SC (not pumped) without AEA in Yun et al. (2010) [19] and Myren and Bjøntegaard [32]. Based on the measurements in the literature and in Trussell's study, pumping reduces the air content in cast SC.

The TSA mix with 7% accelerator and TSM test series were sprayed with the same equipment and the mixes are equal, but the TSA mix does not contain fiber. However, in Figure 28 and Figure 29 it can be seen that the TSM mixes have higher total air content and larger maximum pore sizes. Initially, it was assumed that the ref1,1 and ref1,2 mixes from Svorkmo would have similar air contents but they deviate from each other, see Figure 31. The only difference between the two reference mixes is the fiber type. Both these observations may indicate that fiber type affects the size distributions and total air content.

The sprayed concrete mixes (with AEA) in this study contain 2.6-5.0% entrained air and 1.5-3.9% entrapped air, whereas Choi et al. measured 2.9-4.2% entrained air and 0.5-0.8% entrapped

air in sprayed concrete with AEA [20]. The amount of entrained air is similar in these two studies, but there is a larger discrepancy between the values for entrapped air. Since Choi et al. [20] have measured pores with a maximum equivalent diameter of 6000 µm and Trussell have measured pores with a maximum equivalent diameter of 9500 µm, it is plausible that Trussell measured a higher content of entrapped air, i.e. large macropores. The maximum measurable size of the pores also impacts the total air content, but most of the samples had no pores with an equivalent diameter of more than 6000 µm. However, some of the samples from TSM and Svorkmo had pores with an equivalent diameter higher than 6000 µm.

5.4 Shape and orientation of macrovoids measured with IMA

From Figure 35, it is observed that the sprayed concrete with accelerator has a higher portion of elongated pores than the ones without accelerator. A possible reason for this may be that the pores become elongated when sprayed concrete is subjected to high energy after it hits the panel. Afterwards, the set accelerator probably ensures that shape of the pores do not change since the concrete sets instantly. There is little difference between 3% and 10% accelerator here, indicating that it is the addition of accelerator and not the dosage which is most important in this case. The same tendency is also seen in Figure 36, where there is little difference between 3.5% and 7% accelerator. From Figure 36, it is also observed a big difference in the shape of the pores from the sample which was cast and the ones which were sprayed. The cast sample had much more spherical pores than the sprayed ones (with accelerator). The cast sample (without accelerator) in TSA also had much more spherical pores than the sprayed concrete without accelerator in Flekkefjord. This indicates that both the addition of set accelerator and the process of spraying affects the shape of macropores.

The Svorkmo and TSM series have very similar L/W distributions, despite having different mix designs and spraying mechanics. There is also little spread between the samples in each of the series. All of these samples have 7% accelerator of total binder weight. These results indicate that different mix designs (except for set accelerator) and spraying mechanics have little influence on the air void elongation.

The shape distributions from Figure 35-38 may be compared to the numerical percolation thresholds from Garboczi et al. [52]. If the volume of air voids is equal to or higher than the percolation threshold, percolation is unavoidable, provided that the aspect ratio is equal for all air voids. Table 7 shows that the percolation thresholds from Garboczi et al. [52] is 22.4% for aspect ratio of 3 and 28.5% for aspect ratio of 1. The percolation thresholds are based on a three dimensional model with ellipsoids, whereas shape and air content in this shape analysis is two dimensional. Figure 39 shows that the most elongated pores in Trussell's study are very small and that most of the largest pores have a L/W ratio between 1 and 3. Moreover, in Trussell's study, all total macroporosities were far below 22.4%, and it is therefore not a high risk of having percolation through the entire samples, based on these thresholds. However, there are continuous macropores in Trussell's mixes according to Figure 14 and [31]. Because more

elongated air voids increase risk of percolation, the shape of the air voids may also explain the high open macroporosity and continuous macropores found with the PF method.

Figure 40-43 show that there are more voids oriented normal to the spraying direction than parallel to the spraying direction for 14 out of 17 mixes. This is another indication that macrovoids are squeezed in the spraying process. The combined effect of elongated voids and orientation perpendicular to the spraying direction may give the sprayed concrete anisotropic properties. Figure 44 shows that there is no relation between orientation and area of each void. Tnf0-Cast, which was pumped without accelerator, has also significantly more voids oriented normal to casting direction, which may indicate that casting direction is of high importance as well. Since many air voids are oriented normal to casting direction in Tnf0-Cast, other parameters than spraying direction may also affect orientation of air voids.

5.5 Water penetration - effect of set accelerator and anisotropy

The results in Table 21-25 show that penetration depth is higher for concrete tested normal to the spraying direction (N-cubes) than for concrete tested parallel to the spraying direction (P-cubes), both for 3% and 10% set accelerator. The penetration depth is however higher in the 10%-cubes than in the 3%-cubes. A possible explanation for different permeability normal and parallel to the spraying direction may be that the water flows through macropores that are elongated and that tend to orient parallel to the spraying direction, as discussed in the previous subsection. One other explanation for these observations is that water flows through lamination damages perpendicular to the spraying direction, caused by spitting. The lamination damages were most severe in the 10% samples.

Spitting is defined as the process where only accelerator comes out of the nozzle. In Figure 45b, 47b and 48b the lamination damages caused by spitting can be seen very clearly (white layer). Figure 48 shows that the water penetrates through the two lamination damages. It is evident that to make watertight and thus durable sprayed concrete, it is necessary to ensure satisfactory pumping and spraying of the concrete and avoid spitting.

There are different factors related to pumping and spraying that affect the risk of spitting, for instance the flow rate in the hose. The flow rate is controlled by the stroke rate. When the flow rate is high, the stroke rate must be high. A high stroke rate reduces spitting, because the concrete flow is then more continuous. In Table 16, the different pumps and flow rates are presented. The concrete flow rate for the Flekkefjord mixes is 10 m^3/h, whereas the flow rate for the Svorkmo mixes is 24 m^3/h. Since the flow rate was considerably higher in Svorkmo than in Flekkefjord, it seems reasonable that there are more lamination damages in the Flekkefjord mixes than in the Svorkmo mixes. Spitting is also more likely to occur if the viscosity is high since the concrete flows more easily with a low viscosity and high workability. Unfortunately, too low viscosity will give a lower early strength development. The time between batching and spraying is also significant because the workability of concrete is best right after it has been batched. To summarize, spitting can be reduced if the flow rate is high, the viscosity is low and

the time between batching and spraying is short. One other idea to reduce spitting could be to use a sensor at the end of the concrete hose or nozzle, that could detect if the flow of concrete stops. If the flow of concrete stops, the spraying of accelerator should stop as well.

The penetration depths in the 3% Flekkefjord samples and the Svorkmo samples are quite similar, although the Svorkmo mixes do not have visible lamination damages. Note that the Svorkmo mix has a set accelerator dosage of 7%. Nevertheless, the Svorkmo specimens (S1-S4) have lower penetration than the 3% Flekkefjord specimens, indicating that the accelerator dosage impacts the watertightness less than spitting and lamination damages. Table 20 shows that the closed macroporosities measured by the PF method is 4.4% in the 3% Flekkefjord mix and 4.2% in the Svorkmo ref1,2 mix. The open macroporosities were 1% for the 3% samples and 1.1% for the Svorkmo samples, which indicates continuous macropores according to [31]. Note that these air contents were measured on concrete specimens from a different panel of the same mix than the specimens that were tested in the water penetration test. Two of the 3% Flekkefjord P-cubes and two of the Svorkmo discs were tested for 0.5 MPa for 70 hours, followed by 24 hours of 0.7 MPa. These samples may therefore be evaluated with respect to the watertightness criterion in NS 3420-L5 [62]. Both the 3% P-cubes and the Svorkmo samples satisfy the criterion (i.e. penetration depth is lower than 25 mm), despite having a high open macroporosity. Hence, the permeability may still be satisfactory even though there is a high open macroporosity in sprayed concrete tunnel linings.

Some of the 3% Flekkefjord and one of the Svorkmo specimens had a penetration depth of zero, but in reality, the penetration depth could have been higher. The splitting technique may have influenced the results in cases where the specimens were split directly on the penetration surface. This could result in the sample becoming slightly ground. For most of the cubes, the front of the ground area was uneven, and in the worst cases the maximum depth of the ground area was 15 mm. Since the ground area could overlap the water penetration front, it could in some cases be difficult to read low penetration depths, see Figure 49b and 49c. Ground area may be seen at the top of the sample. All the samples but 3%P1, S3 and S4 were split on the penetration surface and the bottom of the sample (i.e. like in Figure 49b and 49c). Figure 49a shows a sample that was split from the side, but in the same plane. Areas with ground concrete may be seen on the sides in this case. If this sample had been split on the top, the ground area might have covered the penetration front. Consequently, all the samples should have been split like in Figure 49a.

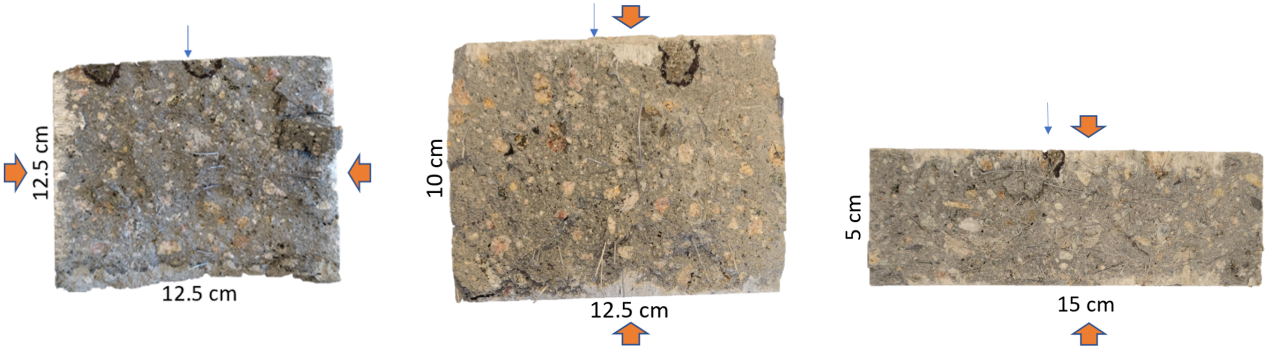

(a) A cube split with pressure applied perpendicular to water penetration direction. Ground area can be seen at the left side.

(b) A cube split with pressure applied parallel to the water penetration direction. Ground area can be seen at the top.

(c) A disc split with pressure applied parallel to the water penetration direction. Ground area can be seen at the top.

Figure 49: Example of two different splitting directions. Thin blue arrows show water penetration direction. Orange arrows show which sides pressure was applied to during splitting.

In conventional concrete, one would usually see a curved water penetration front with maximum penetration at the center of the penetration area, that decreases towards edges of the penetration area. In the sprayed concrete samples analyzed, the water penetrated through smaller weak points that may be at the edge of the penetration surface, and does not follow normal paths. This indicates that sprayed concrete is more in-homogeneous than conventional concrete when it comes to permeability, even when there is no visible lamination damage. For sprayed concrete with lamination damages, the water will penetrate weak points to reach lamination damages, and flow further down through the lamination damages.

To avoid that much water penetrates the sprayed concrete in tunnels, the sprayed concrete ought to be watertight, i.e. the permeability coefficient should be low. However, the permeability coefficient in permeability tests has a high coefficient of variation [57], for instance due to drying and re-saturation. The variation of the permeability coefficients may be high in this project due to different moisture history of the Flekkefjord samples and Svorkmo samples, but the permeability coefficients are still useful for comparing differences.

In this project, the permeability coefficient varied considerably, whereas the mass ratios of the mixes were almost equal. $K_{vuorinen}$ varied from 6.4E-16 to 2.9E-07, and the mass ratio varied from 0.43 to 0.47. Today, mass ratio is used as the main durability criterion in Norway. The comparison of mass ratios and $K_{vuorinen}$ in this thesis shows that water penetration and permeability measurements are supplements to the mass ratios when durability is evaluated. A low mass ratio will not necessarily guarantee sprayed concrete with low permeability.

6 Conclusions

Macroporosity and water penetration in sprayed concrete have been reviewed in literature and investigated in the laboratory. The conclusions from the literature review and the experimental tests are closely related and thus presented together.

Open and closed macroporosity were measured on sprayed concrete according to SINTEF's full PF procedure, and the findings were:

- Sprayed concrete has high open macroporosity, and the open macroporosity increases for increasing set accelerator dosage. In Trussell's study, open macroporosity in sprayed concrete with accelerator was in the range 0.8-1.6 vol-%.
- Duration of one sided capillary suction is important for amount of open macroporosity. Longer durations of one sided capillary suction decreases open macroporosity considerably. On average, open macroporosity decreased with 38% from 4 to 7 days and 36% from 4 to 6 days of one sided suction.
- Based on the analyzed data, it can not be verified or refuted that AEA dosage, w/b ratio and compressive strength affect open macroporosity.

Total air contents in different types of concrete measured by both the PF method and IMA were compared. The comparison showed the following:

- IMA measures higher air content than the PF method in sprayed concrete, zero-slump concrete, high strength concrete and cast "sprayed concrete", whereas the PF method measures highest air content in conventional concrete.
- Saturation pressure in the PF method, w/b ratio, AEA content and compressive strength do not seem to influence which method that measures the highest air content.
- Open macroporosity can not solely explain the deviation in air content measured by the PF method and IMA.

Total air content and size of macrovoids were measured with IMA in sprayed concrete and investigated with respect to various parameters. It was found that:

- Total macroporosity is higher in cast concrete than in sprayed concrete with the same mix design. Total air content of sprayed concrete with AEA and accelerator was measured to 4.7%, whereas cast "sprayed concrete" with the same mix design had 6.2% air content.
- The total macroporosity in sprayed concrete increases with addition of set accelerator and increased flow rate in the hose.
- Total air content seems to be more affected by mix design than spraying mechanics.
- Fiber type may affect size distributions and total air content.

Shape and orientation of macrovoids were measured with IMA in Trussell's study. The results showed that:

- The macropores become more elongated by the spraying process and addition of set accelerator. However, it seems like the most elongated pores are very small and most of the largest pores have a L/W ratio between 1 and 3.
- Shape of air voids is unaffected by spraying mechanics and different mix designs (except for set accelerator).
- Air voids tend to orient perpendicular to the spraying direction. There is however no relation between orientation and area of each air void.

Water penetration tests were carried out to examine the effect of set accelerator and anisotropy, and the findings were the following:

- Water penetrated the sprayed concrete more easily normal to the spraying direction than parallel to the spraying direction.
- Sprayed concrete with lamination damages caused by pure spray of accelerator ("spitting") has very high penetration depths, and "spitting" ought to be reduced to improve durability of sprayed concrete.
- Sprayed concrete was more permeable with 10% set accelerator than 3% set accelerator. However, pure spray of set accelerator ("spitting") and lamination damages seem to influence permeability more than set accelerator dosage.

Further work is recommended to:

- Examine water uptake in concrete during submersion compared to one sided capillary suction to get a better understanding of the open macroporosity.
- Measure shape and orientation on both cast and sprayed concrete in different planes to get a better 3D understanding.
- Investigate whether spitting could be avoided, for instance with a sensor at the end of the hose or nozzle that stops spraying accelerator when flow of concrete stops.

References

1. Maage M. B8 - Spesielle betongtyper. *Betong - Regelverk, teknologi og utførelse*. Ed. by Maage M. Fagbokforlaget, 2015 :176–91
2. Norsk Betongforening. Publikasjon nr 7. Sprøytebetong til bergsikring. Tech. rep. Oslo, Norway, 2011 Aug
3. Bane NOR. Endringsartikkel 1266. `https://trv.banenor.no/wiki/521_2015_Endringsartikkel_1266`. Accessed: 2022-06-03. 2015 Dec
4. Statens Vegvesen. Vegtunneler - normal, Håndbok 021. Standard. Norway, 2006 Nov
5. Statens Vegvesen. Vegtunneler - normal, Håndbok N500. Standard. Norway, 2014 Jun
6. Neville A. M. Properties of concrete. Essex, England: Longman Group Limited, 1995
7. Sellevold E. J. and Farstad T. The PF-method – A simple way to estimate the w/c-ratio and air content of hardened concrete. Proceedings of ConMat'05 and Mindess Symposium 2005; 3:10 p.
8. Opsahl O. A. A study of a wet-process shotcreting method. PhD thesis. Trondheim, Norway: The University of Trondheim, 1985 Nov
9. Holter K.G., Smeplass S., and Jacobsen S. Freeze-thaw resistance of sprayed concrete in tunnel linings. Materials and Structures 2015; 8:3075–93
10. Segura-Castillo L., Cavalaro S. H. P., Goodier C., Aguado A., and Austin S. Fibre distribution and tensile response anisotropy in sprayed fibre reinforced concrete. Materials and Structures 2018; 51:1–12
11. SINTEF. Facts about SUPERCON. `https://www.sintef.no/projectweb/supercon/new-page/`. Accessed: 2022-06-03
12. Hårr M. S. and Kjeka G. Macroporosity in sprayed concrete - Size, shape and percolation analysis. Report. Trondheim, Norway: Norwegian University of Science and Technology, 2021
13. Mørstell E. Modellering av delmaterialenes betydning for betongens konsistens. PhD thesis. Trondheim, Norway: Norwegian University of Science and Technology, 1996
14. Smeplass S. B6 - Proporsjonering. *Betong - Regelverk, teknologi og utførelse*. Ed. by Maage M. Fagbokforlaget, 2015 :154–75
15. Trussell N. and Jacobsen S. Review of sprayability of wet sprayed concrete. Nordic Concrete Research 2020; 63:21–42
16. Banthia N. Advances in sprayed concrete (shotcrete). *Developments in the formulation and reinforcement of concrete*. Ed. by Mindess S. Duxford, UK: Elsevier, 2019 :289–306
17. Smeplass S. B1 - Betongens struktur og egenskaper. *Betong - Regelverk, teknologi og utførelse*. Ed. by Maage M. Fagbokforlaget, 2015 :56–78

18. Herholdt A.D., Justesen C .F. P., Nepper-Christensen P., and Nielsen A. Beton-Bogen. Aalborg Portland. Cementfabrikkernes oplysningskontor, 1985

19. Yun K.-K., Choi S.-Y., Seo J.-Y., Jung B.-S., and Jeon C.-K. Air void structures in blended-cement wet-mix shotcrete. *The Third International Conference on Engineering Developments in Shotcrete*. Ed. by Bernard S. Boca Raton, Florida: CRC Press, 2010 :291–8

20. Choi P., Yeon J. H., and Yun K.-K. Air-void structure, strength, and permeability of wet-mix shotcrete before and after shotcreting operation: The influences of silica fume and air-entraining agent. Cement & Concrete Composites 2016; 70:69–77

21. Beaupré D. Rheology of high performance shotcrete. PhD thesis. Vancouver, Canada: University of British Columbia, 1994 Feb

22. Smeplass S. B7 - Betongens støpelighet. *Betong - Regelverk, teknologi og utførelse*. Ed. by Maage M. Fagbokforlaget, 2015 :176–91

23. Sellevold E. J. Herdnet betong: Bestemmelse av luft/makro og gel/kapillær porøsitet samt relativt bindemiddelinnhold. Tech. rep. O1731. Trondheim, Norway: Norges byggforskningsinstitutt, 1986 Sep

24. American Concrete Institute. Chemical admixtures for concrete. Standard. 2013 Jan

25. Smeplass S. B3 - Tilsetningsstoff. *Betong - Regelverk, teknologi og utførelse*. Ed. by Maage M. Fagbokforlaget, 2015 :108–16

26. Mehta P. K. and Monteiro P. J. M. Concrete: Microstructure, properties, and materials. McGraw Hill Professional, 2013

27. Collins F.G. and Sanjayan J.G. Capillary shape: Influence on water transport within unsaturated alkali activated slag concrete. Journal of Materials in Civil Engineering 2010; 22:260–6

28. Hall C. and Hoff W. D. Water transport in brick, stone and concrete. New York, United States: Spon Press, 2002

29. Sellevold E. J. Chapter 14 - Permeability, moisture condition. *Concrete technology*. Ed. by Jacobsen S. Norwegian University of Science and Technology, 2022 :1–21

30. Smeplass S. Kapillærabsorpsjon som kvalitetskriterium. Tech. rep. Trondheim, Norway: SINTEF, 1988

31. SINTEF. In-situ vanninnhold kapillær sugeevne og porøsitet. Standard. 2021 Feb

32. Myren S. A. and Bjøntegaard Ø. Fibre reinforced sprayed concrete (FRSC): Mechanical properties and pore structure characteristics. *Seventh international symposium on sprayed concrete – Modern use of wet mix sprayed concrete for underground support*. Vol. 7. Sandefjord, Norway: Seventh international symposium on sprayed concrete, 2014 :305–13

33. Tandberg M. K. Utvikling av prøvingsmetodikk, og prøving av frostbestandighet for sprøytebetong til vanntett permanent tunnelkledning i moderne veg- og jernbanetunneler. MA thesis. Trondheim, Norway: Norwegian University of Science and Technology, 2014 Jun

34. Justnes H., Dahl P.A., Ronin V., Jonasson J.-E., and Elfgren L. Microstructure and performance of energetically modified cement (EMC) with high filler content. Cement & Concrete Composites 2007; 29:533–41

35. Hermansen F. A. Betong med høy flyveaskedosering. MA thesis. Trondheim, Norway: Norwegian University of Science and Technology, 2018 Jan

36. Bjelland H. and Moi P. K. Alternative bindemidlers effekt på betong. BA thesis. Stavanger, Norway: University of Stavanger, 2021 May

37. Rønnes T. J. Fuktforhold i kjellervegger av betong under grunnvannstand. MA thesis. Trondheim, Norway: Norwegian University of Science and Technology, 2015 Jun

38. Holter K. G. A study of EVA-based sprayed membranes for waterproofing of rail and road tunnels in hard rock and cold climate. PhD thesis. Trondheim, Norway: Norwegian University of Science and Technology, 2015 Dec

39. Salvador R. P., Cavalaro S. H. P., Monte R., and Figuereido A. D. Relation between chemical processes and mechanical properties of sprayed cementitious matrices containing accelerators. Cement & Concrete Composites 2017; 79:117–32

40. Jacobsen S., Farstad T., Gran H. C., and Sellevold E. J. Frost/salt scaling of no-slump concrete: Effect of strength, air entraining agent and condensed silica fume. Nordic Concrete Research 1993; 12:51–71

41. Shpak A. Production and documentation of frost durable high-volume fly ash concrete: Air entrainment, cracking and scaling in performance testing. PhD thesis. Trondheim, Norway: Norwegian University of Science and Technology, 2020 Nov

42. Sætre K. Ice abrasion on fiber reinforced concrete - A study on the effects of various types of fiber and the reliability of the laboratory measurements. MA thesis. Trondheim, Norway: Norwegian University of Science and Technology, 2014 Jun

43. Mørtsell E. Banedekke av betong på Ørlandet Kampflyplass 2009–2019 - Sammenstilling av resultater fra målinger av porestruktur i betong. Tech. rep. Norway: SINTEF, 2019 Nov

44. Jacobsen S., Hammer T. A., and Sellevold E. J. Frost testing of high strength concrete: internal cracking vs. scaling of OPC and silica fume concretes. *Frost Resistance of Building Materials : Proceedings of the 2nd Nordic Research Seminar in Lund 1996*. Vol. 2. Lund, Sweden: Lund University, 1996 :49–68

45. Standard Norge. NS-EN 480-11 Admixtures for concrete, mortar and grout - Test methods - Part 11: Determination of air void characteristics in hardened concrete. Standard. Norway, 2006 Jan

46. Fonseca P. C. and Scherer G. W. An image analysis procedure to quantify the air void system of mortar and concrete. Materials and Structures 2015; 48:3087–98

47. Talukdar S. and Heere R. The effects of pumping on the air content and void structure of air-entrained, wet mix fibre reinforced shotcrete. Case Studies in Construction Materials 2019; 11:6 p.

48. Yun K.-K., Choi P., and Yeon J.H. Microscopic investigations on the air-void characteristics of wet-mix shotcrete. Journal of Materials Research and Technology 2019; 8:1674–83

49. ASTM International. ASTM C457/C457M:16 - Standard test method for microscopical determination of parameters of the air-void system in hardened concrete. Standard. 2016 Dec

50. Create a box and whisker Excel 2016. `https://www.myexcelonline.com/blog/create-box-whisker-chart-excel-2016/`. Accessed: 2022-02-28

51. Hsu W. Y and Wu S. Percolation behavior in morphology and modulus of polymer blends. Polymer Engineering and Science 1993; 33:293–302

52. Garboczi E. J., Snyder K. A., and Douglas J. F. Geometrical percolation threshold of overlapping ellipsoids. Physical Review 1995; 52:819–28

53. Kaufmann J., Frech K., Schuetz P., and Münch B. Rebound and orientation of fibers in wet sprayed concrete applications. Construction and Building Materials 2013; 49:15–22

54. Cáceres A.R.E., Cavalaro S.H.P., Monte R., and Figueiredo A.D. de. Alternative small-scale tests to characterize the structural behaviour of steel fibre-reinforced sprayed concrete. Construction and Building Materials 2021; 296:1–13

55. Manca M., Karrech A., Dight P., and Ciancio D. Image processing and machine learning to investigate fibre distribution on fibre-reinforced shotcrete round determinate panels. Construction and Building Materials 2018; 190:870–80

56. Galobardes I., Silva C.L., Figueiredo A., Cavalaro S.H.P., and Goodier C.I. Alternative quality control of steel fibre reinforced sprayed concrete (SFRSC). Construction and Building Materials 2019; 223:1008–15

57. Hooton R. D. Concrete permeability and the search for the holy grail. *The first Canadian symposium on cement and concrete*. Vol. 1. Université Laval: Université Laval, 1989 :1–10

58. Ibrahim M. and Issa M. Evaluation of chloride and water penetration in concrete with cement containing limestone and IPA. Construction and Building Materials 2016; 129:278–88

59. Sjölander A. and Ansell A. In-situ and laboratory investigation on leaching and effects of early curing of shotcrete. Nordic Concrete Research 2019; 61:23–37

60. Vuorinen J. Applications of diffusion theory to permeability tests on concrete Part I: Depth of water penetration into concrete and coefficient of permeability. Magazine of Concrete Research 1985; 37:145–52

61. Skutnik Z., Sobolewski M., and Koda E. An experimental assessment of the water permeability of concrete with a superplasticizer and admixtures. Materials 2020; 13:1–16

62. Norges Byggstandardiseringsråd. Beskrivelsestekster for bygg og anlegg - NS 3420 - Tekniske bestemmelser - Særtrykk betongkonstruksjoner. Standard. 1986 Nov

63. Standard Norge. NS-EN 206:2013+A2:2021+NA:2021 Concrete - specification, performance, production and conformity. Standard. Norway, 2021 Apr

64. Otsu N. A threshold selection method from gray-level histograms. IEEE Transactions on Systems, Man, and Cybernetics 1979; 9:62–6

65. Brun M. B. Thickness measurements of scaled fly ash concrete particles from frost testing methods ASTM c666 and CEN-TS 12390-9: Critical thickness in pure water and 3% salt solution. MA thesis. Trondheim, Norway: Norwegian University of Science and Technology, 2020 Jun

66. Standard Norge. NS-EN 12390-8 Testing hardened concrete - Part 8: Depth of penetration of water under pressure. Standard. Norway, 2019 Nov

67. Statens Vegvesen. Laboratorieundersøkelser - Håndbok R210. Standard. Norway, 2014 Jun

68. CEN. Testing concrete - Determination of the depth of penetration of water under pressure. Standard. European Committee for Standardization, 1994 May

69. RILEM. Concrete test methods - CPC 13.1. Test for the penetration of water under pressure on hardened concrete. Standard. 1979

70. Farstad T. Bestemmelse av betongs vanntetthet - NORDTEST Prosjekt 1219 95: Prosjektrapport 292 - 2000. Tech. rep. Oslo, Norway: Norges byggforskningsinstitutt, 2000

Appendix A Product data sheets for the constituents

Table 26: Overview of the constituents in the different test series.

Constituent	Flekkefjord	Trondheim	Svorkmo
Cement	Norcem Std FA	Norcem Std FA	Norcem Std FA
Super plasticiser	Dynamon SX-23	MasterEase 1020	MasterEase 1020
AEA	Mapeair 25 1:15	Amex 11 1:9	Amex 11 1:7
Steel fiber	Steelfibre DE 35/0,55 N	Dramix 4D 65/35BG	Dramix 4D 65/35BG
Steel fiber	-	-	Dramix 3D 80/30BGP
Set accelerator	MasterRoc SA 188	MasterRoc SA 168	MasterRoc SA 188
Retarder	-	MasterRoc HCA 20	MasterRoc HCA 20
Hardening accelerator	-	-	Master X-seed 100
Fly ash	-	-	FA Norcem
Polymer	-	-	Etonis 3500 W

PRODUKTDATABLAD

STANDARDSEMENT FA

CEM II/B-M

SIST REVIDERT MARS 2021

Sementen tilfredsstiller kravene i NS-EN 197-1:2011 til Portland blandingssement CEM II/B-M 42,5 R.

Egenskap		Deklarerte data	Krav ifølge NS-EN 197-1:2011
Finhet (Blaine m^2/kg)		450	
Spesifikk vekt (kg/dm^3)		3,00 (B) / 2,99 (K)	
Volumbestandighet (mm)		1	≤ 10
Begynnende størkning (min)		140	≥ 60
Trykkfasthet (MPa)	1 døgn	20	
	2 døgn	31	≥ 20
	7 døgn	42	
	28 døgn	55	≥ 42,5 ≤ 62,5
Sulfat (% SO_3)		≤ 4,0	≤ 4,0
Klorid (% Cl^-)		≤ 0,085 (B) /≤ 0,05 (K)	≤ 0,10
Vannløselig krom (ppm Cr^{6+})		≤ 2	≤ 2 [1]
Alkalier (% Na_2O_{ekv})		1,4 (B) / 1,5 (K)	
Klinker (%)		78	65-79
Flygeaske (%)		18	21-35
Kalkmel (%)		4	

1. I henhold til EU forordning REACH Vedlegg XVII point 47 krom VI forbindelser.

B = Brevik og K = Kjøpsvik

NORCEM
HEIDELBERGCEMENT Group

Norcem AS, Postboks 142, Lilleaker, 0216 Oslo
Tlf. 22 87 84 00 firmapost@norcem.no www.norcem.no

MAPEI

Dynamon SX-23

CE
EN 934-2
T 3.1/3.2

Superplastiserende tilsetningsstoff til betong og mørtel

PRODUKTBESKRIVELSE
Dynamon SX-23 er et svært effektivt superplastifiserende tilsetningsstoff basert på modifiserte akrylpolymerer.
Produktet tilhører **Dynamon**-systemet som er basert på DPP-teknologi, Designed Performance Polymers, utviklet av Mapei, hvor tilsetningsstoffenes egenskaper skreddersys til forskjellige betongtyper.
Dynamon-systemet er utviklet på grunnlag av Mapeis egen sammensetning og produksjon av monomerer.

BRUKSOMRÅDE
Dynamon SX-23 er spesielt utviklet til ferdigbetongproduksjon og brukes i alle betongtyper for å gjøre betongen enklere å bearbeide og/eller redusere vannbehovet.

Noen spesielle bruksområder er:

- Vanntett betong med krav om høy eller svært høy styrke, og med strenge krav til betongens holdbarhet i aggressive miljøer.
- Betong med særlige krav til høy støpelighet.
- Selvkomprimerende betong med noe lengre åpentid. Om nødvendig kan denne betongtypen stabiliseres med et viskositetsøkende tilsetningsstoff av type **Viscofluid** eller **Viscostar**.
- Frostbestandig betong – ved kombinasjon med et luftinnførende tilsetningsstoff – type **Mapeair**. Typen av luftinnførende tilsetningsstoff gjøres ut fra tilgjengelig kunnskap om de andre delmaterialenes egenskaper.
- Gulvbetong for å oppnå en smidig betong med forbedret støpelighet. Høye doseringer og lave temperaturer kan medføre en viss retardering av betongen.

Dynamon SX-23 skiller seg vesentlig fra superplastiserende tilsetningsstoffer basert på sulfonerte melaminer og naftalener samt fra første generasjons akrylbaserte polymerer, ved en betydelig høyere vannreduserende effekt og økt åpentid. Nødvendig dosering for ønsket bearbeidingsevne/vannreduksjon vil være vesentlig lavere med **Dynamon SX-23** enn med eldre typer superplastiserende tilsetningsstoffer.

Doseringstidspunktet for **Dynamon SX-23** er ikke så viktig, men kortest blandetid oppnås ved tilsetning av **Dynamon SX-23** etter tilsetning av minst 80 % av blandevannet. Også her er det viktig å foreta en utprøving for optimal utnyttelse av aktuelt blandeutstyr.

EGENSKAPER
Dynamon SX-23 er en vannoppløsning av aktive akrylpolymerer som effektivt dispergerer sementen i blandingen.

Denne effekten kan utnyttes på tre måter:

Dynamon SX-23

1. Reduksjon av betongens vannbehov og med samme bearbeidingsevne.
   Derved oppnås en betong med lavere vann/sement-forhold, en mer holdbar betong.

2. Økt bearbeidingsevne sammenlignet med en betong med samme vann/sement-forhold uten tilsetningsstoffer.
   Derved oppnås samme styrke, men utstøpningen blir mye lettere.

3. Reduksjon av både vann og sement uten endring av betongens bearbeidingsevne og styrke. Dermed kan betongens kostpris reduseres, mindre sement, reduksjon av svinnpotensial, mindre vann samt redusere faren for skadelige temperaturgradienter pga. lavere hydratiseringsvarme.
   Spesielt denne effekten er viktig ved betonger med høyere sementinnhold samt ved store, massive betongkonstruksjoner.

KOMPATIBILITET MED ANDRE PRODUKTER
Dynamon SX-23 kan kombineres med Mapeis andre betongtilsetningsstoffer som for eksempel størkningsakselererende tilsetningsstoffer som **Mapefast** og størkningsretarderende tilsetningsstoffer som **Mapetard**.

Produktet kan også kombineres med luftinnførende tilsetningsstoffer for produksjon av frostbestandig betong, **Mapeair**. Valg av type skjer ut fra tilgjengelig kunnskap om de andre delmaterialenes egenskaper.

Ved kombinasjoner anbefales alltid forsøksblandinger for å oppnå den ønskede effekten. Kontakt eventuelt vår tekniske avdeling.

DOSERING
Dynamon SX-23 tilsettes for å oppnå den ønskede effekten – styrke, holdbarhet, bearbeidingsevne, sementreduksjon – ved å variere doseringen mellom 0,3 og 2,0% av mengden av sement + flyveaske + mikrosilika.

Ved høyere dosering økes betongens åpentid, dvs. den tiden betongen lar seg bearbeide. Større dosering og lavere betongtemperatur vil forårsake en viss retardering.

Prøveblandinger anbefales alltid med aktuelle parametere.

EMBALLASJE
Dynamon SX-23 leveres i 25 liters kanner, 200 liters fat, 1000 liter IBC-tanker og i tank.

LAGRING
Produktet må oppbevares ved temperaturer mellom +8°C og +35°C. I lukket emballasje bevarer produktet sine egenskaper i minst 12 måneder. Hvis produktet utsettes for direkte sollys, kan det føre til variasjoner i fargetonen uten at dette påvirker egenskapene til produktet.

SIKKERHETSINSTRUKSJONER FOR KLARGJØRING OG BRUK
For instruksjon vedrørende sikker håndtering av våre produkter, vennligst se siste utgave av sikkerhetsdatablad på vår nettside www.mapei.no

PRODUKT FOR PROFESJONELL BRUK

MERK
De tekniske anbefalinger og detaljer som fremkommer i denne produktbeskrivelse representerer vår nåværende kunnskap og erfaring om produktene.
All overstående informasjon må likevel betraktes som retningsgivende og gjenstand for vurdering. Enhver som benytter produktet må på forhånd forsikre seg om at produktet er egnet for tilsiktet anvendelse. Brukeren står selv ansvarlig dersom produktet blir benyttet til andre formål enn anbefalt eller ved feilaktig utførelse.

Vennligst referer til siste oppdaterte versjon av teknisk datablad som finnes tilgjengelig på vår webside www.mapei.no

Alle relevante referanser for produktet er tilgjengelige på forespørsel og fra www.mapei.no

Dynamon SX-23

TEKNISKE DATA (typiske verdier)	
PRODUKTBESKRIVELSE	
Form:	væske
Farge:	gulbrun
Viskositet:	lettflytende; <30 mPa·s
Tørrstoffinnhold (%):	23,0 ± 1,1
Densitet (g/cm³):	1,05 ± 0,02
pH:	6 ± 1
Kloridinnhold (%):	< 0,05
Alkaliinnhold (Na_2O-ekvivalenter) (%):	< 2,0

6874-07-2017(NO)

MAPEI®
BUILDING THE FUTURE

MasterEase 1020

Aug. 2019 erst. April 2019

Superplastiserende tilsetningsstoff – for betong med lav viskositet og optimal reologi

PRODUKTBESKRIVELSE

MasterEase 1020 er et tilsetningsstoff for ferdigbetong som reduserer viskositeten og flytespenningen i fersk betong og gir enestående reologiske egenskaper.
Den nye teknologien er spesielt egnet til produksjon av optimaliserte betongblandinger med avanserte tekniske egenskaper og redusert karbonavtrykk.

INNOVASJON

MasterEase 1020 er basert på innovativ og patentert polymerteknologi utviklet av Master Builders Solutions Norway AS. MasterEase muliggjør fleksibel adsorpsjon av sementpartikler og reduserer betongens viskositet umiddelbart etter blanding.

BRUKSOMRÅDE

MasterEase 1020 anbefales til:

- Veggstøping
- Gulv
- Fundamenter
- Selvkomprimerende betong
- Sprøytebetong
- Lavkarbon-betong

EGENSKAPER OG FORDELER

- Kortere blandetid
- Lettere pumping
- Redusert pumpetrykk ved horisontal og vertikal bruk
- God åpentid
- Lettere utlegging
- Mindre etterbehandling
- Bedre utstøping
- Pene overflater
- Mulighet for å redusere innhold av CO_2 i betongblandingen

Tekniske data	
Produkt	Superplastifiserende tilsetningsstoff
Aktiv komponent	Polykarboksylater
Tørrstoffinnhold	21,0 ± 1,0 %
Kloridinnhold	< 0,01 %
Ekvivalent Na_2O	< 1,0 %
Densitet	1,05 ± 0,02 kg/l
pH-verdi	6,3 ± 1,5
Farge og form	Gullig væske

BRUKSANVISNING

MasterEase 1020 er et bruksklart, flytende tilsetningsstoff, som tilsettes betongen underveis i blandeprosessen. Produktet tilsettes sammen med eller etter tilsetning av minst 80 % av blandevannet.

Skal ikke tilsettes tørre materialer.

DOSERING

Minimum: 0,1 vekt% av sement + puzzolan
Maksimum: 2,0 vekt% av sement + puzzolan

Andre doseringer kan være relevante i spesielle tilfeller og under spesielle forhold i forbindelse med byggingen. Ta kontakt med Master Builders Solutions Norway A/S.

KOMPATIBILITET

MasterEase 1020 er kompatibelt med alle Master Builders Solutions-produkter.

OPPBEVARING

MasterEase 1020 skal oppbevares ved minst + 5 °C og ikke over + 30 °C. Omrøring anbefales.

Ved oppgitt temperatur i tett, lukket beholder er holdbarheten 12 måneder.

MasterEase 1020

Aug. 2019 erst. April 2019

Superplastiserende tilsetningsstoff – for betong med lav viskositet og optimal reologi

EMBALLASJE
200 kg fat, palletank, bulk.

ARBEIDSMILJØ
Se særskilt sikkerhetsdatablad/bruksanvisning.

YTTERLIGERE OPPLYSNINGER
Master Builders Solutions Norway AS har en landsdekkende konsulentservice som står til rådighet i forbindelse med spørsmål og konkret veiledning til våre produkter og løsninger. For ytterligere informasjon, kontakt vårt hovedkontor på tlf.: +47 62 97 00 20.

Forbehold om endringer og trykkfeil.

Master Builders Solutions Norway AS
Gullfotdalen 4
NO-2120 Sagstua
T +47 62 97 00 20
www.master-builders-solutions.com

CE

19

Master Builders Solutions Noreway AS
Gullfotdalen 4,
NO-2120 Sagstua

Ytelseseklæring
MasterEase 1020

NS-EN 934-2: 2009+A1:2012: T3.1/3.2

1111

Vannreduserende/superplastiserende tilsetningsstoff

Maksimum kloridinnhold:	<0,01%
Maksimum alkalieinnhold:	<1,0%
Korrosjon	Inneholder kun komponenter fra EN 934-1:2008, Annex A.1.
Trykkfasthet:	Oppfylt
Vannreduktion	Oppfylt
Luftinnhold:	Oppfylt
Konsistens	Oppfylt
Helseskadelige bestanddeler:	Ingen
www.master-builders-solutions.com	

MAPEI

Mapeair 25

Luftporedannende tilsetningsstoff

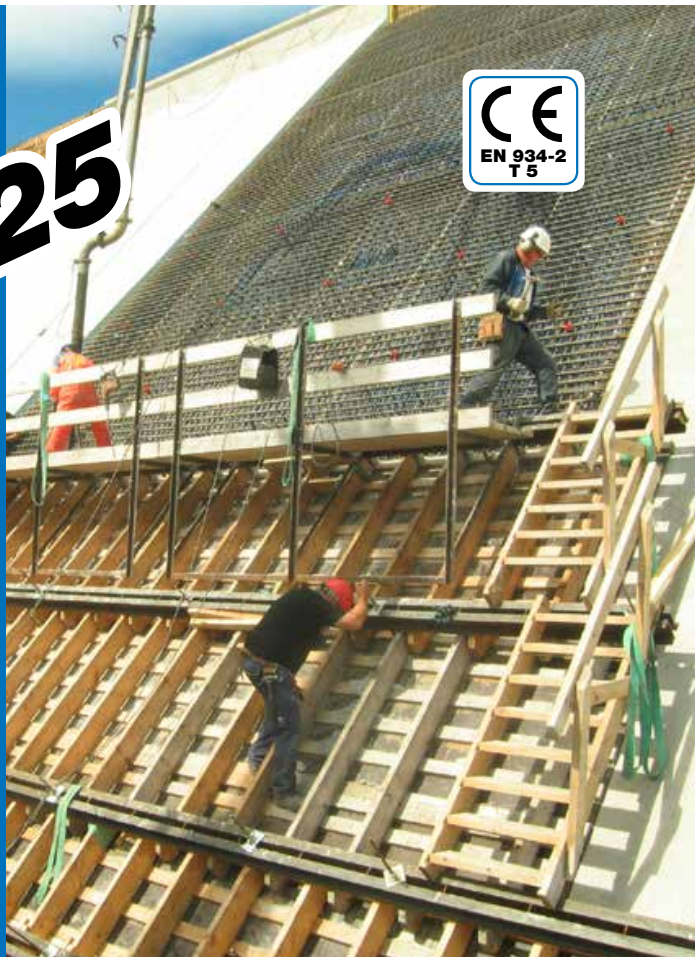

BRUKSOMRÅDE
Mapeair® 25 er et luftporedannende tilsetningsstoff som benyttes til å øke frostbestandigheten til betong og mørtel.
Mapeair® 25 virker også støpelighetsforbedrende og reduserer separasjonsfaren for betong. Produktet benyttes som regel i kombinasjon med Mapeis plastiserende eller superplastiserende tilsetningsstoffer.
Mapeair® 25 er formulert på basis av syntetiske tensider og talloljederivater.

EGENSKAPER
Betong inneholder alltid noe luft (1 - 3 %). For å oppnå det kravet som vanligvis stilles, 4 - 6 % luft i den ferske betongen, tilsettes **Mapeair® 25**, som gir mindre, bedre og fint fordelte porer, noe som øker betongens bestandighet mot fryse-tine påkjenninger.

Mapeair® 25 har den egenskap at den under blandingen omdanner den innpiskede luften til små, jevnt fordelte luftporer. Målt luftporevolum og avstandsfaktor i herdnet betong for **Mapeair® 25** er vist under tekniske spesifikasjoner. Disse porene gir også betongen en bedret støpelighet og redusert vannbehov.

Økt luftinnhold medfører generelt en reduksjon i trykkfastheten. En tommelfingerregel er at 1 % luft reduserer trykkfastheten med 5 %. Dette kompenseres delvis med betongens reduserte vannbehov og ved tilsetning av plastiserende og/eller høyplastiserende tilsetningsstoff.
Mapeair® 25 vil i tillegg forbedre transportstabiliteten ved å redusere separasjonsfaren for betong med lite finstoffer og aktivt motvirke betongs “bleeding” (vanntransport opp til overflaten av den ferske betongen).

UTFØRELSE
Mapeair® 25 leveres ferdig til bruk og skal tilsettes direkte i blanderen. For å oppnå jevn luftinnføring fra blanding til blanding er det viktig at **Mapeair® 25** tilsettes på samme tid hver gang.

Doseringen for å oppnå ønsket luftinnhold varierer med tilslag, sementtype og mengde. Andre tilsetningsstoffer kan også ha innvirkning. Det er viktig at tilsatsen av **Mapeair® 25** bestemmes ut fra prøveblandinger og at luftinnholdet i den ferske betongen kontrolleres jevnlig.

DOSERING
0,05 - 0,5 % av sementvekt.

Siden doseringsmengden for **Mapeair® 25** normalt er liten, vil en uttynning med vann være en fordel.
Bruk 1 del **Mapeair® 25** til 9 eller 19 deler vann.
Slik kan en oppnå sikrere dosering. Produktet lar seg lett blande med vann. Sørg likevel for omrøring før bruk for å sikre et homogent produkt.

Mapeair 25

VÆR OPPMERKSOM PÅ
Variasjoner i de øvrige delmaterialene i betongen kan sterkt påvirke dannelsen av luftporer i betong. I noen tilfeller kan også transportlengde og transportutstyr gi variasjoner i luftmengde. Dersom blandetiden har vært for kort, vil en kunne oppleve at den totale målte luftmengde øker fra produksjon til levering, mens det i de fleste tilfeller registreres en reduksjon i luftmengde. Som regel betyr denne reduksjonen ikke annet enn at større, uønskede luftbobler slipper ut. Betongprodusenten må derfor opparbeide egne erfaringstall med sine aktuelle delmaterialer.

EMBALLASJE
Mapeair® 25 leveres i 25 liters kanner, 200 liters fat, 1000 liter IBC-tanker og i tank.

LAGRING
Produktet må oppbevares ved temperaturer mellom +8°C og +35°C. I lukket emballasje bevarer produktet sine egenskaper i minst 12 måneder. Hvis produktet utsettes for direkte sollys, kan det føre til variasjoner i fargetonen uten at dette påvirker egenskapene til produktet.

SIKKERHETSINSTRUKSJONER FOR KLARGJØRING OG BRUK
For instruksjon vedrørende sikker håndtering av våre produkter, vennligst se siste utgave av sikkerhetsdatablad på vår nettside www.mapei.no

PRODUKT FOR PROFESJONELL BRUK

ADVARSEL
Selv om tekniske detaljer og anbefalinger i dette produktdatabladet er i henhold til vår beste kunnskap og erfaring, må all informasjon ovenfor i hvert tilfelle anses som kun indikerende og underlagt bekreftelse etter langvarig praktisk bruk. Derfor må alle som skal bruke dette produktet, på forhånd sørge for at det er egnet til tiltenkt bruksområde. I hvert enkelt tilfelle er brukeren alene ansvarlig for eventuelle konsekvenser som følge av bruk av produktet.

Se den aktuelle versjonen av det tekniske databladet som er tilgjengelig på vårt nettsted www.mapei.no

JURIDISK MERKNAD
Innholdet i dette tekniske databladet kan kopieres til andre prosjektrelaterte dokumenter, men det endelige dokumentet må ikke suppleres eller erstatte betingelsene i det tekniske datablad, som er gjeldende, når MAPEI-produktet benyttes. Det seneste oppdaterte datablad er tilgjengelig på vår hjemmeside www.mapei.no
ENHVER ENDRING AV ORDLYDEN ELLER BETINGELSER, SOM ER GITT ELLER AVLEDET FRA DETTE TEKNISKE DATABLADET, MEDFØRER AT MAPEI SITT ANSVAR OPPHØRER.

Alle relevante referanser for produktet fås på forespørsel og fra www.mapei.no

Mapeair 25

TEKNISKE DATA (typiske verdier)	
PRODUKTBESKRIVELSE	
Form:	væske
Farge:	lys gulbrun
Viskositet:	lettflytende; < 10 mPa·S
Tørrstoffinnhold, %:	6
Tyngdetetthet, g/cm³:	1,00 ± 0,02
pH:	9,0 ± 1
Kloridinnhold, %:	≤ 0,05
Alkaliinnhold (Na_2O-ekvivalent):	≤ 1,0
BRUKSEGENSKAPER I BETONG:	
Luftporevolum i betongmasse EN 12350-7:	6 % ved dosering 0,05 % av sementvekt (referanse 2,2 %)
Avstandsfaktor i herdnet betong, EN 480-11, (mm):	0,190 (krav < 0,200)
Spesifikk overflate, EN 480-11, (mm²/mm³):	25,2 (krav > 25)
Frostbestandighet (avskalling) – EN 12390-9, (kg/m²):	0,05 (beste klassifisering < 0,1 : excellent)

6908-09-2017 (NO)

MAPEI®
BUILDING THE FUTURE

BASF

The Chemical Company

AMEX 11

Januar 2012

LUFTINNFØRENDE TILSETNINGSSTOFF FOR BETONG.

Tekniske data:

Konsistens:	Lettflytende.	**Ekvivalent Na_2O:**	< 2,5%
Farge:	Gulaktig væske.	**Kloridinnhold:**	< 1,5%.
Tørrstoff:	11 ± 1,0%.	**Aktiv komponent:**	Tensider.
Densitet:	1,02 ± 0,03kg/l.		
pH- verdi:	7 ± 1,5		

Produktbeskrivelse.

AMEX 11 er luft innførende tilsetningsstoff som danner porer i betongen slik at vannet i kapillær poresystemet ikke sprenger betongen ved kulde.
Ved bruk av AMEX 11 får man et meget stabilt system med små luftporer i betongen. Det er meget viktig å være klar over at tilsetning av luft i betongen reduserer fastheten i betongen.

Bruksområder.

AMEX 11 kan anvendes i all betong med krav til frostbestandighet, dvs. all betong som utsettes for fukt og gjentatte fryse/tine vekslinger.
Hvis betongen er plassert i marint miljø, eller om det er tine salter tilstede, kreves høyere innhold av luftporer enn for normale betonger.
Kan også benyttes som støpeforbedrende tilsetning.

Egenskaper.

Ved bruk av AMEX 11 oppnår man følgende:

- Økt frostbestandighet.
- Minsket permeabilitet.
- Minsket separasjon og bleeding.
- Forbedret bearbeidbarhet.
- Klarer fryse / tine vekslinger bedre enn betong uten AMEX 11.
- Stabilt luftporesystem.

Andre anbefalte kombinasjoner.

AMEX 11 kan benyttes sammen med de aller fleste typer tilsetningsstoffer til betong.

Dosering.

Dosering av AMEX 11 for og få et bra luftpore system varierer fra 0,02 - 0,1 % av sementvekten. Grunnen til denne store variasjonen beror på forskjellige tilslag, sement- typer og tilvirknings prosesser. Det bør derfor alltid påregnes prøve-blandinger av betong med Amex 11. Det anbefales å tynne ut Amex 11 med vann i en løsning 1:9, eller 1:19.

Vanlig krav i Norge er et luftinnhold i fersk betong på 5 % ± 1,5 %. Som tommel-fingerregel får en, en fasthetsreduksjon på 5 % for hver prosentenhet luftinnholdet i betongen øker.

Bruksanvisning.

AMEX 11 bør tilsettes sammen med blandevannet.

BASF Construction Chemicals Norway
Granerud Industriområde
NO-2120 Sagstua
T +47 62 97 00 20
F +47 62 97 18 85

Adding Value to Concrete

Det er viktig at doseringstidspunktet ikke endres vesentlig, da dette kan påvirke luftinnholdet i den ferske betongen.

Forpakning.

- Kanner.
- 210 liters Fat.
- 1000 liters containere.
- Bulk.

Lagring.

AMEX 11 oppbevares frostfritt.
Lagringstid 12 mnd.

Sikkerhetstiltak.

Se produktets sikkerhetsdatablad.

CE

0615

BASF AS
Granerud industriområde
2120 Sagstua

0615-CPD-9803/25
NS-EN 934-2:2009

AMEX 11
Luftinnførende tilsetningsstoff

NS-EN 934-2; T5

Maksimum klorid innhold < 1,5%
Maksimum alkalie innhold < 2,5%

Adding Value to Concrete

MAPEI

Steelfibre DE 35/0,55 N

PRODUKTBESKRIVELSE
Steelfibre DE 35/0,55 N er en høypresterende stålfiber til intern armering av betong. Fiberlengden er 35 mm og er derfor meget godt egnet for tynnere betongskikt og sprøytebetong.**Steelfibre DE 35/0,55 N** leveres magnetisk orientert i 20 kg pappesker. Magnetisk orientering sikrer effektiv innblanding i betong.
Fiberen er laget av kaldstrukket karbonståltråd og har endeforankring i begge ender.
Steelfibre DE 35/0,55 N har strekkfasthet på 1250 (±15 %) MPa.

FUNKSJON OG FORDELER
Ved korrekt bruk fordeler **Steelfibre DE 35/0,55 N** seg jevnt i betong og sørger for å gi armeringseffekt i alle skikt av betongen. Stålfiber virker positivt inn på overflater av støpedekker og fungerer effektivt mot overflateriss og sprekkdannelse under herding.
Steelfibre DE 35/0,55 N kan også erstatte tradisjonell armering som nett og kamjern.
Steelfibre DE 35/0,55 N kan dermed redusere kostnader forbundet med innkjøp og installasjon av armering.

Kontakt Mapei for mer informasjon om dosering.

ANBEFALINGER
Det anbefales alltid å tilsette fiber på betongfabrikk.

I betongblander:
- Tilsett aldri fiber som første komponent. Tilsett fiber under omrøring i tilslag eller i ferdig blandet betong.
- Bland betongen til fibrene er homogent fordelt

I betongbil:
- Tilsett fiber under maksimal omdreining på trommel (12 - 18 rpm)
- Betongens synk skal være minst 120 mm
- Ikke tilsett mer enn 60 kg/min
- Etter endt tilsats, la trommel gå på maksimal hastighet i 5 min.

EMBALLASJE
Steelfibre DE 35/0,55 N leveres i 20 kg esker og 500 kg big-bag.

LAGRING OG HOLDBARHET
Ved tørr lagring i uåpnet original emballasje, beskyttet mot fukt, er holdbarheten minst ett år. Fuktskadet produkt med begynnende korrosjon kan ikke lenger påregnes å oppfylle de tekniske spesifikasjonene.

Steelfibre DE 35/0,55 N

TEKNISKE DATA	
PRODUKTBESKRIVELSE	
Lengde:	35 mm (±10 %)
Diameter:	0,55 mm (±10 %)
Strekkfasthet:	1350 MPa (±15 %)
Slankhetstall (l/d):	63,5

MERK
De tekniske anbefalinger og detaljer som fremkommer i denne produktbeskrivelse representerer vår nåværende kunnskap og erfaring om produktene.
All overstående informasjon må likevel betraktes som retningsgivende og gjenstand for vurdering. Enhver som benytter produktet må på forhånd forsikre seg om at produktet er egnet for tilsiktet anvendelse.
Brukeren står selv ansvarlig dersom produktet blir benyttet til andre formål enn anbefalt eller ved feilaktig utførelse.

Vennligst referer til siste oppdaterte versjon av teknisk datablad som finnes tilgjengelig på vår webside www.mapei.no

Alle relevante referanser for produktet er tilgjengelige på forespørsel og fra www.mapei.no eller www.mapei.com

03.09.2015 NO

MAPEI®
BUILDING THE FUTURE

BEKAERT
better together

Dramix®

4D Dramix® 65/35 BG

Aspect ratio | Length | Bright | Glued

DATASHEET

Characteristics

Material properties

Nom. tensile strength:	268 ksi (1,850 MPa)
Young's modulus:	29,000 ksi (200,000 MPa)
Strain at ultimate strength:	0.8 %

Geometry

Fiber family: 4D

Length (l): 1.4 in. (35 mm)

Diameter (d): 0.02 in. (0.55 mm)

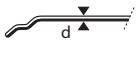

Aspect ratio (l/d): 65

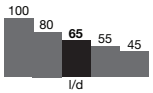

Minimum EN 14889-1 dosage

25 lb/yd³ (15 kg/m³)

Fiber network

20,146 ft/yd³ at 25 lb/yd³ (8,032) m/m³ at 15 kg/m³)
6,455 fibers/lb (14,232 fibers/kg)

Dramix® family

3D Typical SFRC applications
4D Supreme serviceability control
5D Advanced structural applications

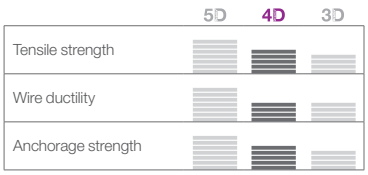

Product certificates *

CE

IAPMO ES

* Product certificates are plant specific.

Product conformity

Dramix® conforms to ASTM A820, EN 14889-1 and ISO 13270 Class A.

System certificates

TÜV NORD ISO 9001 TÜV NORD ISO 14001

All Dramix® plants are ISO 9001 and ISO 14001 certified.

Packaging

BAGS
44 lb
(20 kg)

BIG BAG
1,760 -2,420 lb
(800 - 1,100 kg)

Handling

DRAMIX® 4D 65/35BG

Optimized anchorage

Dramix® 4D provides optimal crack control for standard statically indeterminate concrete structures that are submitted to regular static, fatigue and dynamic loadings with high serviceability requirements.

Glue technology for three-dimensional reinforcement
Dramix® steel fibers are bundled with water-soluble glue. The glue helps avoiding fiber balling during mixing and ensures a homogeneous distribution of fibers throughout the concrete mix.

Bekaert construction support
You can count on our support for each step of your project, from concept design to on-site quality support. Our services include recommendations on slab design, construction detailing, concrete optimization and automatic total quality control procedures. We are also happy to share our knowledge with you and your team.
Feel free to ask us for a workshop or training on the topic of steel fiber reinforcement in your offices.

For recommendations on handling, dosing and mixing visit www.bekaert.com/dosingdramix.
Any other specific document or certificate can be found on www.bekaert.com/dramix/downloads.

Datasheet_Dramix 4D 6535BG_EN-US_20191015

BEKAERT
better together

Dramix®

3D Dramix® 80/30BGP

Aspect ratio | Length | Bright | Glued | Premium

DATASHEET

Characteristics

Material properties

Nom. tensile strength:	445.265856 ksi (3070 MPa)
Young's modulus:	29000 ksi (200000 MPa)
Strain at ultimate strength:	0.8 %

Geometry

Fiber family: 3D

Length (l): 1.1811 in. (30 mm)

Diameter (d): 0.014961 in. (0.38 mm)

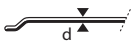

Aspect ratio (l/d): 80

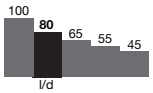

Minimum EN 14889-1 dosage

42 lb/yd³ (25 kg/m³)

Fiber network

#REF! ft/yd³ at 42 lb/yd³ (28045) m/m³ at 25 kg/m³)
16205 fibers/lb (35726 fibers/kg)

Dramix® family

3D Typical SFRC applications
4D Supreme serviceability control
5D Advanced structural applications

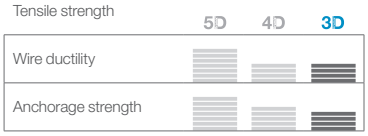

Product certificates *

CE

* Product certificates are plant specific.

Product conformity

Dramix® conforms to ASTM A820, EN 14889-1 and ISO 13270 Class A.

System certificates

TÜV NORD ISO 9001 TÜV NORD ISO 14001

All Dramix® plants are ISO 9001 and ISO 14001 certified.

Packaging

BAGS
44 lb
(20 kg)

BIG BAG
2,420 lb
(1,100 kg)

Handling

DRAMIX® 3D 80/30BGP

The original anchorage
Dramix® 3D is the cost-efficient fiber for standard statically indeterminate concrete structures that are submitted to regular static, fatigue and dynamic loadings.

Glue technology for three-dimensional reinforcement
Dramix® steel fibers are bundled with water-soluble glue. The glue helps avoiding fiber balling during mixing and ensures a homogeneous distribution of fibers throughout the concrete mix.

The high performant strength
Dramix® 3D Premium is a high performant fiber to create optimal ductility in high strength concrete.

Bekaert Bekaert construction support
You can count on our support for each step of your project, from concept design to on-site quality support. Our services include recommendations on slab design, construction detailing, concrete optimization and automatic total quality control procedures. We are also happy to share our knowledge with you and your team.
Feel free to ask us for a workshop or training on the topic of steel fiber reinforcement in your offices.

For recommendations on handling, dosing and mixing visit www.bekaert.com/dosingdramix.
Any other specific document or certificate can be found on www.bekaert.com/dramix/downloads.

Datasheet_Dramix 3D 80/30BGP_EN-US_20210927

MasterRoc® SA 188

Des. erst. okt. 2019

Alkalifri høyytelses størkningsakselerator i væskeform for sprøytebetong

PRODUKTBESKRIVELSE

MasterRoc SA 188 er en høyytelses alkalifri størkningsakselerator for sprøytebetong der doseringen kan varieres til ønskede størknings- og herdetider.

BRUKSOMRÅDER

- Midlertidig og permanent grunnforholdsstøtte i forbindelse med tunneldriving og gruvedrift.
- Egner seg også for akselerering av sementholdige sementblandinger som for eksempel støping av annulus i TBM-tunneler, sement injisering og skumbetong.

EMBALLASJER

MasterRoc SA 188 leveres i 210 liters tønner, 1000 liters containere eller i bulk.

PRODUKTEGENSKAPER

MasterRoc SA 188 egner seg meget godt for våtblandet sprøytebetong.

- De raske størkningsegenskapene gir muligheten til å legge på tykke betonglag ved hjelp av påføring i flere lag under en sprøytesyklus.
- Den unike oppskriften gir hurtig størkning, høy tidlig-fasthet, god langtidsstabilitet.
- Svært lav støvutvikling under påføring og dermed gode arbeidsforhold.
- Muligheten for lavt prelletap når korrekt dysevinkel og avstand overholdes.
- Ikke-aggressive egenskaper gir bedre arbeidssikkerhet, redusert miljøpåvirkning og lavere håndteringskostnader.

Tekniske data	
Form	Suspenjon
Farge	Beige til hvit
Densitet (+ 20 °C, Gamm-Ball)	1,44 ± 0,02 g/ml
pH-verdi (1:1 vannløsning)	3,0 ± 0,5
Viskositet*	350 ± 250 mPa.s
Varmestabilitet	+ 5 °C til + 35 °C
Tørrstoffinnhold	50-58 %
Kloridinnhold	< 0,1 %
[Na_2O] EQV. (%bw)	< 1 %

*Brookfield, + 20 ℃. Viskositeten er avhengig av hvor godt produktet har vært blandet samt temperaturen.

PÅFØRINGSPROSEDYRE

Underlaget må være rent og fritt for løse partikler og fortrinnsvis fuktig etter forhåndsfukting. Det anbefales å bruke bare fersk sement etter som alder på sementen kan ha negative påvirkning på størkningskarakteristikkene til blandingen.
MasterRoc SA 188 kan være sensitiv overfor ulike typer sement. Det kan med noen sementtyper, være nødvendig å tilsette økte doseringer av MasterRoc SA 188 for hurtig størkning. Vi anbefaler bruk av Portland-sementtyper (PC/HPC) som normalt gir hurtigere størkning enn blandede eller sulfatmotstandsdyktige sementtyper. Men MasterRoc SA 188 fungerer også godt med kompositttsementtyper (blandede sementtyper, flygeaske/slagg). Uansett anbefaler vi sterkt å utføre tester på forhånd for å kontrollere størkningen og 1 døgnfastheten på sement som planlegges brukt i et prosjekt.
Evalueringen av størkningen og 1 døgnfastheten bør utføres på en testmørtel i samsvar med EFNARC European Specification for Sprayed Concrete (Spesifikasjoner for sprøytebetong) (1996), Vedlegg 1, avsnitt 6.3.

Følgende resultater bør bare ses på som indikative for resultatet:

Initial herding	Endelig herding	24-timers-styrke	Vurdering
2 min.	6-8 min.	18-20 N/mm^2	God
5 min.	8-12 min.	12-15 N/mm^2	OK
> 10 min.	> 15 min.	< 10 N/mm^2	Dårlig

BETONBLANDING

Når MasterRoc SA 188 brukes i våtsprøytebetong bør vann/sementforholdet være under 0,5 og fortrinnsvis <0,45. Når en har som mål å få ekstremt høy tidlig størkning, bør forholdet være 0,40 eller lavere. Jo lavere vann/sementforhold, desto hurtigere størkning, høyere tidlig styrke, bedre holdbarhet, lavere akseleratordosering og tykkere lag kan legges på i taket.

MasterRoc® SA 188

Des. erst. okt. 2019

Alkalifri høyytelses størkningsakselerator i væskeform for sprøytebetong

DOSERINGSSYSTEM

MasterRoc SA 188 tilsettes i munnstykket. Det er meget viktig å ha konstant og nøyaktig dosering av akseleratoren inn i betongstrømmen. For å sikre sprøytebetong av høy kvalitet må du følge retningslinjene for valg av pumpe som er gjengitt under:

Fungerer godt med:
- Monopumper (stator- & rotorpumper)
- Peristaltiske pumper (Bredel)

Bør ikke brukes sammen med:
- Stempelpumper
- Alle pumper med kule- og seteventiler
- Trykktanker
- Girpumper

Ikke bruk filter i sugeslangen da dette fører til tilstopping. Materialet bør fortrinnsvis trekkes fra bunnen av trommelen/beholderen.

KOMPATIBILITET MED ANDRE AKSELERATORER

MasterRoc SA 188 kan byttes ut med de fleste av Master Builders Solutions alkalifrie akseleratorer. For mer informasjon bes du ta kon- takt med din lokale – Master Builders Solutions-representant.

Ikke bland eller bytt ut MasterRoc SA 188 med en akselerator som er produsert av en annen produsent da dette kan føre til tilstopping av doseringspumpen og slangene.

FORBRUK

Forbruket av MasterRoc SA 188 avhenger også av vann/sementforholdet, temperaturforholdene (betong og omgivelser), sementreaktiviteten til den sementen som brukes og ønsket lagtykkelse, størkningstid og utviklingen av tidlig styrke. Forbruket av MasterRoc SA 188 er vanligvis innenfor et område mellom 3 og 10 % av vekten av bindemiddelet.

Overdosering (>10 %) kan føre til redusert endelig styrke.

RENGJØRING AV DOSERINGSPUMPEN

Etter bruk av MasterRoc SA 188 må doseringspumpen og de andre delene av systemet **rengjøres grundig** med mye vann. Hvis du unnlater å gjøre dette vil det føre til tilstopping av doseringssystemet. Pass på at alle operatører som er involvert i testing og påføring er fullstendig informert.

OPPBEVARING

- Må oppbevares ved minimum +5 °C og maksimum +35 °C (optimal temperatur for lagring og resultat +20 °C).
- Må oppbevares i lukkede beholdere laget av plast, glassfiber eller rustfritt stål.
- **Må ikke** oppbevares i vanlige stålbeholdere.
- Oppbevaring i bulktanker **krever** bruk av agitering og/eller sirkulasjonssystemer.
- Etter lengre oppbevaring eller transport anbefaler vi fullstendig agitering av produktet før bruk ved hjelp av mekanisk røring eller resirkulasjonspumping.
- Hvis produktet oppbevares i tett lukkede originalbeholdere og under de forholdene som er nevnt over kan det lagres i minst 6 måneder. Periodisk blanding kan forlenge lagringstiden ytterligere.
- Ta kontakt med din lokale Master Builders Solutions-representant før du bruker noen produkter som har vært frosset.
- Etter langvarig lagring bør det alltid foretas ytelsestesting før bruk.

SIKKERHETSTILTAK

De samme forholdsreglene som ved håndtering og bruk av sementholdige produkter bør overholdes.
Unngå øye- og hudkontakt og bruk gummihansker og vernebriller. Hvis slik kontakt oppstår må området skylles med mye vann. I tilfelle øyenkontakt, søk legehjelp med en gang.

Informasjonen som er oppgitt her er korrekt, representerer vår beste kunnskap og er basert på både laboratoriearbeid og praktisk erfaring. Ettersom flere faktorer påvirker resultatene tilbyr vi denne informasjonen uten garanti og uten patentansvar. Kontakt din lokale representant for ytterligere informasjon eller spørsmål.

MasterRoc® SA 188

Des. erst. okt. 2019

Alkalifri høyytelses størkningsakselerator i væskeform for sprøytebetong

CE

19

Master Builders Solutions Norway AS
Gullfotdalen 4
NO-2120 Sagstua

Ytelseserklæring:
MasterRoc SA 188

NS-EN 934-5: 2007: T2

1111

Alkalifri størkningsakselerator for sprøytebetong

Maksimum kloridinnhold	< 0,1 %
Maksimum alkalieinnhold	< 1,0 %
Korrosjonsatferd:	Oppfylt
Trykkfasthet:	Oppfylt
Størkningstid:	Oppfylt
Helseskadelige bestanddeler:	Ingen

www.master-builders-solutions.com

Master Builders Solutions Norway AS
Gullfotdalen 4
NO-2120 Sagstua
T +47 62 97 00 20
F +47 62 97 18 85
www.master.builders-solutions.com

MasterRoc SA 168

Mai 2021 ers. sep. 2019

Alkaliefri, flytende højeffektiv akselerator for sprøytebetong

BESKRIVELSE AV PRODUKTET
MasterRoc SA 168 er en alkaliefri, høyeffektiv akselerator for sprøytebetong. Doseringen kan justeres til ønsket avbindings- og herdnetid.

BRUKSOMRÅDER
- Midlertidig og permanent fjellsikring i tunneler og gruver.
- Stabilisering av skråninger.
- Kan også brukes til å akselerere sementbaserte mørtler, som benyttes for eksempel ved støping av annulus i TBM-tunneler, sementinjeksjon i bakken og skumbetong.

EMBALLASJE
MasterRoc SA 168 leveres i 210 liters tromler, 1000 liters containere eller bulk.

PRODUKTEGENSKAPER
MasterRoc SA 168 er spesielt godt egnet til våtsprøyting av betong ved fjellsikring:

- Raskere avbinding gir raskere fremdrift og mulighet til å lage tykkere konstruksjoner gjennom lagvis oppbygning i én arbeidsgang.
- Den unike formuleringen gir rask avbinding, kontinuerlig økning av tidligfastheten, god bestandighet og sluttfasthet.
- Lav støvproduksjon under bruk gir godt arbeidsmiljø.
- Muliggjør påføring med mindre tilbakeslag ved korrekt avstand og vinkel på munnstykket.
- Ikke-aggressive egenskaper gir forbedret arbeidssikkerhet, redusert miljøpåvirkning og lavere håndteringskostnader.

Tekniske Data	
Form	Suspensjon
Farge	Beige til hvit
Tørstof	57,5±7,5
Densitet (+ 20 °C)	1,45 ± 0,02 g/ml
pH-verdi	3,0 ± 0,5
Viskositet [1)]	300 ± 150 mPa.s
Varmestabilitet	+ 5 til + 35 °C
Kloridinnhold	< 0,1 %
[Na_2O]-ekv. (vektprosent)	< 1 %

[1)] Brookfield, + 20 °C. Viskositeten avhenger av grad av omrøring av produktet samt produktets temperatur.

BEARBEIDING
Underlaget skal være rent og fritt for løse partikler og helst være fritt for fukt.

Det anbefales å bruke kun fersk sement fordi alderen på sementen kan påvirke blandingens bindingsegenskaper.

MasterRoc SA 168 er lite påvirket av sementtypen. Ved enkelte typer sement kan det imidlertid være nødvendig med høyere dosering for å få en rask avbinding. Vi anbefaler bruk av Portlandsement (PC/HPC), som ofte gir raskere avbinding enn blandings- eller sulfatresistente sementtyper. MasterRoc SA 168 virker imidlertid også bra med kompositttsementer (blandingssementer, flyveaske/slagg). Under alle omstendigheter er forberedende tester sterkt å anbefale for å kontrollere avbindingstid og fasthet etter 24 timer hos sementtypene som skal brukes i et prosjekt.

Avbindingstid og fasthet etter 24 timer bør testes ut i en mørtel i henhold til EFNARC Europeisk spesifikasjon for sprøytebetong (European Specification for Sprayed Concrete) (1996), Vedlegg 1, punkt 6.3.

MasterRoc SA 168

Mai 2021 ers. sep. 2019

Alkaliefri, flytende højeffektiv akselerator for sprøytebetong

Følgende resultater er kun veiledende:

Avbinding start	Avbinding slutt	Klassifisering	Fasthet
2 min.	6 - 8 min.	18 - 20 N/mm^2	God
5 min.	8 - 12 min.	12 - 15 N/mm^2	OK
> 10 min.	> 15 min.	< 10 N/mm^2	Dårlig

BETONGBLANDING

Når MasterRoc SA 168 brukes til våtsprøyting, skal v/c+b-tallet ligge under 0,5 og helst under 0,45. Når målet er ekstremt høy tidligfasthet, anbefales det å ligge på 0,40 eller lavere. Lavere tall gir raskere avbinding, høyere tidligfasthet, forbedret bestandighet, og tykkere lag kan legges "over hodet".

For å maksimere effekten (og dermed også ytelsen) tilsettes alkaliefrie akseleratorer (AFA) i den våte betongstrømmen i munnstykket ved hjelp av doble trykkluft-/AFA-rør til sprøytemunnstykket.

DOSERINGSSYSTEM

MasterRoc SA 168 tilsettes i munnstykket For å sikre en konstant og nøyaktig dosering av akseleratoren til betongstrømmen og få en høykvalitetsbetong, er det avgjørende å følge retningslinjene for pumper under:

Fungerer godt med:
- Monopumper (stator- og rotorpumper)
- Slangepumper (Bredel)

Bør ikke brukes med:
- Stempelpumper
- Alle pumper med kuleventiler
- Trykktanker
- Tannhjulspumper

Bruk ikke filter i sugeslangen siden dette forårsaker tilstoppinger. Helst skal materialet suges opp fra bunnen av fatet/beholderen.

KOMPATIBILITET MED ANDRE AKSELERATORER

MasterRoc SA 168 kan byttes ut med de fleste av Master Builders Solutions alkaliefrie akseleratorer. Kontakt din lokale Master Builders Solutions-representant for rådgivning.

MasterRoc SA 168 skal ikke blandes med andre typer alkaliefrie akseleratorer. Dette kan føre til umiddelbar tilstopping av doseringspumper og slanger.

FORBRUK

Forbruket av MasterRoc SA 168 avhenger også av v/c-tallet, temperaturforhold (betong og omgivelser), sementens reaktivitet og kravene til tykkelse på lagene, avbindingstid og tidligfasthet. Forbruket av MasterRoc SA 168 ligger normalt innenfor intervallet 3 til 10 % av bindemiddelsvekten.

Overdosering (> 10 %) kan resultere i redusert sluttfasthet.

RENGJØRING AV DOSERINGSPUMPE

Etter bruk av MasterRoc SA 168 må doseringspumpe og andre deler av doseringssystemet **rengjøres grundig** med store mengder vann. Manglende rengjøring gjør at doseringssystemet blir tett til neste gangs bruk. Sørg for at alle operatører som er involvert i testing og bruk er grundig informert om dette.

OPPBEVARING

- Oppbevares ved min. + 5 °C og maks. + 35 °C (optimal temperatur for lagring og ytelse er + 20 °C).
- Oppbevares i lukkede beholdere av plast, glassfiber eller rustfritt stål.
- **Skal ikke** lagres i vanlige stålbeholdere.
- Oppbevaring i bulkbeholdere **krever** bruk av omrørings- og/eller sirkulasjonssystemer.
- Etter langvarig lagring anbefaler vi fullstendig omrøring, enten mekanisk eller med sirkulasjonspumpe.

MasterRoc SA 168

Mai 2021 ers. sep. 2019

Alkaliefri, flytende højeffektiv akselerator for sprøytebetong

- Dersom produktet oppbevares i tett lukkede beholdere under forhold som anbefalt over, kan det lagres i opp til 6 måneder. Regelmessig omrøring kan forlenge holdbarheten ytterligere.
- Kontakt din lokale Master Builders Solutions-representant før bruk av et produkt som har vært utsatt for frost.
- Etter langvarig lagring bør produktet testes før bruk.

sMaster Builders Solutions Norway AS
Gullfotdalen 4
NO-2120 Sagstua
T +47 62 97 00 20
F +47 62 97 18 85
www.master-builders-solutions.com

CE

11

Master Builders Solutions Norway AS
Gullfotdalen 4
NO-2120 Sagstua

Ytelseserklæring:
MasterRoc SA 168

NS-EN 934-5: 2007: T2

1111

Alkalifri størkningsakselerator for sprøytebetong

Maksimum kloridinnhold	< 0,1 %
Maksimum alkalieinnhold	< 1,0 %
Korrosjonsatferd:	Oppfylt
Trykkfasthet:	Oppfylt
Størkningstid:	Oppfylt
Helseskadelige bestanddeler:	Ingen

www.master-builders-solutions.com

MasterRoc HCA 20

Des. 2019 erst. April 2010

Sement hydratiseringskontroll for våt- og tørrsprøyting av betong, fyllmørtel og injektionsmørtel

Tekniske data:			
MasterRoc HCA 20		**Løselighet i vann:**	Fullstendig.
Form:	Væske.	**Termisk stabilitet:**	+1°C.
Farge:	Rød.	**Tørrstoffinnhold:**	19 ± 1%.
Densitet (20°C):	1,10 ± 0,02.	**Kloridinnhold:**	<0,1%.
PH-verdi:	<2.	**Fysiologisk effekt:**	Kaustisk

PRODUKTBESKRIVELSE

MasterRoc HCA 20 er et unikt ikke-kloridholdig kjemisk produkt for fullstendig avbrudd av den normale hydratiseringen av sement innenfor timer eller dager etter ønske, med mulighet for aktivering på et hvilket som helst tidspunkt, uten tap av kvalitet for den herdnede betongen.

MasterRoc HCA 20 er et flytende tilsetningsstoff. Når det tilsettes betongen på blanderiet, enten våt-, eller tørrblanding, vil det fullstendig avbryte hydratiseringen, ved å danne en beskyttende barriere rundt alle sementpartikler. Barrieren er aktiv overfor alle typer sementmineraler (C3S, C3A, C2S, C4AF og gips).

BRUKSOMRÅDE

MasterRoc HCA 20 er egnet for alle anvendelser innen våt- og tørr- sprøyting av betong:

Tunnel og gruvedrift.
- Midlertidig sikring
- Permanent sikring

Midlertidig og permanent stabilisering av skråninger.

Reparasjoner av betongkonstruksjoner og i tillegg:
- I suspensjoner for trykkinjeksjon.
- Bakfyllingsmørtler for betongelementer.

EGENSKAPER OG FORDELER

MasterRoc HCA 20 for våt- og tørrsprøyting kan betongblandingen holdes fersk over en hvilken som helst periode opp til 3 dager.

Dette gir meget gode fordeler med hensyn til blandingen og bruk av sprøytebetong:

- Full fleksibilitet med hensyn til leveringsmåte for blandet sprøytebetong.
- Unødvendig å rengjøre pumper og betong-ledninger hvis det er pauser i arbeidet.
- Ingen fare for at deler av blandingen blir for gammel til å tillates sprøytet.
- Mindre betongavfall til dumping.
- Enklere planlegging av fremdrift og mindre risiko for forsinkelser.
- Dyre alternative betongmaterialer i sekk eller big bag kan erstattes med mer økonomisk ferdigbetong.
- Ofte store besparelser i totalkostnad.

I tillegg til de nevnte fordeler som et middel til å kontrollere hydratisering, har MasterRoc HCA 20 følgende fordeler.

- Betydelig reduksjon av støvproduksjon og av prelletap.
- Tydelig forbedret tidligfasthet. Sammenlignet med vanlig sprøytebetong (våt og tørr).

MasterRoc HCA 20

Des. 2019 erst. April 2010

Sement hydratiseringskontroll for våt- og tørrsprøyting av betong, fyllmørtel og injektionsmørtel

BRUKSANVISNING

MasterRoc HCA 20

Tørrsprøytebetong:

Utfør blanding av tilslag og sement, der fuktinnhold i tilslag bør være mellom 3 og 6 % regnet av vekt tilslag. Hvis fuktinnholdet er lavere enn 3 % må det tilsettes vann slik at riktig nivå kan etableres.

Nødvendig mengde MasterRoc HCA 10 tilsettes langsomt og kontrollert, manuelt eller med doseringsutstyr, under konstant omrøring i blanderen. Blanding fortsettes i minst 2-3 minutter etter avsluttet tilsetning. Det anbefales å bruke en sprøytedyse som kan finfordele tilsetningsstoffet under tørrblandingen.

Tilsetning av MasterRoc HCA 20 til den ferske blandingen er best, men forsinket tilsetning medfører ingen problemer, så lenge man holder seg innenfor 30 minutter etter blanding av sand og sement.

Våtsprøytebetong:

Bland sand og sement med ca. halvparten av tilsiktet vannmengde. Tilsett under konstant omrøring. MasterRoc HCA 20 og aktuelt vannreduserende tilsetningsstoff, enten forblandet i resten av blandevannet, eller etter at alt vann er tilsatt. Normal blandetid er tilstrekkelig. For å unngå slumptap, er minste anbefalte vannmengde 200 l/m³ betong.

I tilfeller der en forsinkelse går ut over planlagt stabilisert tid, kan en senere ekstra dosering av 0,6 – 1,0 % MasterRoc HCA 20 benyttes for å oppnå ytterligere noen timer stabilisering.

FORPAKNING

MasterRoc HCA 20 leveres i

- 25 l kanner.
- 210 l fat.
- 1000 l palletank

LAGRING

For å hindre tap av vann under lagring, er det viktig både for våt- og tørrblandinger å beskytte mot direkte sollys, frost og å bruke tett plastikk-membran over eventuelle åpne beholdere.
Det anbefales å kontakte lokal representant for Master Builders Solutions Norway AS, før eventuell bruk av produkt som har vært frosset.
Maksimal lagringstemperatur for produktet er +60 °C. Test av virkning bør alltid gjennomføres før bruk.

Hvis produktet lagres i lukket beholder under betingelser som angitt over, vil MasterRoc HCA 20 være lagerstabil i minst 6 måneder.

FORBRUK

Våtsprøyting "normal resept"

Norcem Standard FA:	450 -480 kg/m³.
Mikrosilika:	25-30 kg/ m³.

MasterRoc HCA 20

Des. 2019 erst. April 2010

Sement hydratiseringskontroll for våt- og tørrsprøyting av betong, fyllmørtel og injektionsmørtel

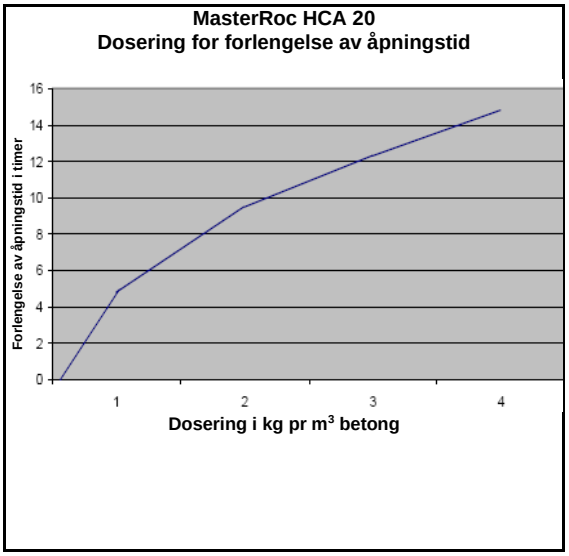

MasterRoc HCA 20

Des. 2019 erst. April 2010

Sement hydratiseringskontroll for våt- og tørrsprøyting av betong, fyllmørtel og injektionsmørtel

CE

15

Master Builders Solutions Norway AS
Gullfotdalen 4
NO-2120 Sagstua

Ytelseseklæring
MasterRoc HCA 20

NS-EN 934-2: 2009 + A1:2012 (T8)

1111

Retarderende tilsetningsstoff for sprøytebetong.
(Sement hydratiseringskontroll for våt- og tørrsprøyting av betong, fyllmørtel og injektionsmørtel).

Maksimum kloridinnhold:	<0,1%
Maksimum alkalieinnhold:	<0,25 %
Korrosjon	Inneholder kun komponenter fra EN 934-1:2008, Annex A.1.
Trykkfasthet:	Oppfylt
Størkningstid	Oppfylt
Luftinnhold:	Oppfylt
Helseskadelige bestanddeler:	Ingen
www.master-builders-solutions.com	

Master Builders Solutions Norway AS
Gullfotdalen 4
NO-2120 Sagstua
T +47 62 97 00 20
F +47 62 97 18 85
www.master-builders-solutions.com

Master X-Seed 100

Okt. 2019 erst. aug. 2019

Brukes som herdningsakselerator der det er behov for høy tidligfasthet

BRUK

MasterX-Seed 100 er et bruksklart, flytende tilsetningsstoff som tilsettes betongen under blandeprosessen. For å sikre homogen dispersjon skal man bruke tilstrekkelig blandetid.

PRODUKTBESKRIVELSE

MasterX-Seed 100 er en nyutviklet suspensjon av aktive nanopartikler designet til å fremme hydratiserings-prosessen i tidlig fase (6-12 timer).
Konseptet er basert på en enestående og innovativ krystalldannelsesteknologi, som gir kraftig akselerert dannelse av kalsiumsilikathydrater.

MasterX-Seed 100 fremmer betongherdingen ved både lave og høye herdingstemperaturer. I motsetning til tradisjonelle akselereringsmetoder og ved hjelp av en unik reaksjonsprosess - en virtuell, barrierefri krystalldannelse mellom sementkornene - akselereres den tidlige styrkeutviklingen samtidig med at den endelige mikrostrukturen oppnår tilsvarende eller forbedrede egenskaper.

CRYSTAL-SPEED HARDENING

MasterX-Seed 100 er den helt avgjørende komponenten i Master Builders Solutions konsept Crystal Speed Hardening.
Konseptet med Crystal Speed Hardening representerer den verdiøkning som tilbys i Master X-SEED's enestående krystalldannelsesteknologi:

- Effektive produksjonsprosesser
- Energireduksjon
- Materialoptimering
- Høye kvalitetskrav

Konseptet imøtekommer nøkkelkrav i byggebransjen og har styrke til å overgå alle andre nåværende løsninger. Konseptet er spesielt utviklet for å bidra til å imøtekomme byggebransjens krav til bærekraft.

BRUKSOMRÅDER:

MasterX-Seed 100 kan brukes til alle typer betong og er særdeles velegnet til produksjon av betongelementer, der høy tidlig styrkeutvikling er det avgjørende suksesskriteriet. MasterX-Seed 100 er et anvendelig alternativ til varmeherding, og den kraftige akselereringen av hydratiseringen understøtter bruk av mindre rene sementtyper som bindemiddel.
MasterX-Seed 100 kan brukes til alle typer betong og er meget velegnet til produksjon av ferdigbetong og betongelementer.

FORDELER OG EGENSKAPER:

Master X-SEED 100 tilbyr følgende fordeler:

- Tidlig styrkeutvikling ved lave, høye og stabile herdingstemperaturer
- Fleksibel tilpasning av produksjonskapasiteten
- Økt antall produksjonssykluser pr. dag (dobbelt eller tredobbelt rotasjon)
- Bedre utnyttelse av former ved tidligere avforming
- Reduksjon/eliminering av varmeherding
- Muliggjør reduksjon av sementinnholdet
- Optimering av bindemiddel gjennom bruk av mindre rene sementtyper eller økt bruk av supplerende sementlignende materialer (kalkstein, flygeaske, slagge, osv.)
- Lav risiko for forsinket ettringittdannelse
- Redusert vannabsorbering
- Forbedrede holdbarhetsegenskaper for betong
- Miljømessige forbedringer ved produksjon og av ferdige produkter gjennom reduserte CO_2-utslipp

DOSERING

Den anbefalte doseringsmengden er 2-4 % i forhold til sementmengden. Under spesielle forhold kan andre doseringsmengder brukes. Kontakt våre tekniske konsulenter for rådgivning.

Tekniske data	
Chloridindhold:	< 0,01 %
Ækvivalent Na_2O	<4,0%
Ph-værdi	11,0±1,0
Tørrstoff:	22,0 ±1,1%
Densitet:	1,14±0,03 kg/ltr.
Farge	Hvid

Master X-Seed 100

Aug. 2019 erst. juni 2010

Brukes som herdningsakselerator der det er behov for høy tidligfasthet

KOMPATIBILITET

Master X-SEED 100 er kompatibel med alle Master Builders -teknologier som f.eks. ZERO ENERGY SYSTEM™ OG SMART DYNAMIC CONCRETE™:

- MasterGlenium – høytytende superplastifiserings-midler til reodynamisk teknologi
- MasterMatrix viskositetsmodifiserende middel for robust, selvkompakterende betong
- MasterAir luftinnblandingsmiddel for forbedret frostbestandighet
- MasterFinish formoljer for enkel avforming og estetisk overflatefinish.

LEVERING

210 liter fat tank.

OPBEVARING

Master X-SEED 100 skal oppbevares ved minimum +5 °C. Må beskyttes mot frost! Hvis produktet har vært frosset, skal det varmes opp og røres opp igjen før bruk. Ved oppbevaring i uåpnet emballasje ved den foreskrevne temperaturen, er holdbarheten 12 måneder.

HÅNDTERING OG TRANSPORT:

Det er ingen spesielle krav som skal overholdes ved bruk av produktet. Det anbefales å bruke beskyttelseshansker og -briller. Unngå røyking og inntak av mat og drikkevarer når produktet brukes.

MasterX-SEED 100 er giftfri og verken lokalirriterende eller brennbar, og det er ingen spesielle krav til transport.

ARBEIDSMILJØ

Se særskilt sikkerhetsdatablad/bruksanvising.

CE

10

Master Builders Solutions Norway AS
Gullfotdalen 4,
NO-2120 Sagstua

Ytelseseklæring
Master X-Seed 100

NS-EN 934-2: 2009+A1:2012: T7

1111

Herdningsaksellererende tilsetningsstoff

Maksimum kloridinnhold:	<0,01%
Maksimum alkalieinnhold:	<4,0%
Korrosjon	Inneholder kun komponenter fra EN 934-1:2008, Annex A.1.
Trykkfasthet:	Oppfylt
Luftinnhold:	Oppfylt
Helseskadelige bestanddeler:	Ingen
www.master-builders-solutions.com	

Master X-Seed 100

Aug. 2019 erst. juni 2010

Brukes som herdningsakselerator der det er behov for høy tidligfasthet

Tildelt EFCA EQ miljøkvalitetsmærke.

Master Builders Solutions Norway AS
Gullfotdalen 4
NO-2120 Sagstua
T +47 62 97 00 20
www.master-builders-solutions.com

MasterLife SRA 150

Sep. 2021 erst. nov. 2019

Ekspanderende tilsetningsstoff til produksjon av svinnkompensert betong

BESKRIVELSE OG BRUKSOMRÅDER

MasterLife SRA 150 er et uorganisk produkt i pulverform som brukes i tillegg til andre betongkomponenter til produksjon av svinnkompensert betong. Det er et spesielt klinkermateriale som er brent ved høy temperatur, er rik på fri kalk, og der de mindre forbindelsene består av kalsiumsilikater, aluminater, jern-aluminater og sulfater.
Ved kontakt med blandevann forårsaker transformasjonen av oksidet til det korresponderende kalsiumhydroksidet en ekspansjon som kompenserer for påfølgende kryp i betongen.

Klinkermaterialets temperatur i MasterLife SRA 150, kornfordelingen og forekomsten av de mindre forbindelsene som dekker kalsiumoksidet, fremmer korrekt regulering av hydratiseringshastigheten og dermed også den ekspansive prosessen.

BRUKSANVISNING

MasterLife SRA 150 skal alltid brukes sammen med sement, tilsetningsstoffer og vann, ikke kun vann.
Produktet kan tilsettes betongblandingen samtidig med sementen, og er kompatibel med de fleste tilsetningsstoffer, spesielt med MasterEase, MasterGlenium, MasterSet, MasterPozzolith og MasterAir. Produktet bør alltid brukes sammen med MasterLife SRA 848, 900 eller 915 som eliminerer svinneffektene fullstendig. Kan også brukes sammen med herdemidlet MasterKure og betonggulvherdemidlene Master-Top 200.

MasterLife SRA 150 skal blandes nøye med andre betongkomponenter. Etter utlegging kreves egnet fuktherding.

DOSERING

Doseringen av MasterLife SRA 150 varierer fra 20 til 40 kg per m^3 betong avhengig av betongresepten.
Normal dosering er fra 20 til 30 kg per m^3 betong.

HERDING OG EKSPANSJON

En av de viktigste fordelene med MasterLife SRA 150 sammenlignet med andre ekspanderende tilsetningsstoffer som forårsaker ettringitt-dannelse er den korte herdetiden som kreves for å garantere ekspansjon. Ekspanderende tilsetningsstoffer kan kun gi volumøkning hvis betongen holdes i et fuktig miljø med tilstrekkelig mengde vann for at ekspansjonsreaksjonen skal kunne skje. Reaksjonen som fører til ettringitt-dannelse trenger omtrent 7 dager i fuktig atmosfære for å oppnå maksimal ekspansjon, mens det ved bruk av MasterLife SRA 150 er nok med en dags herding for å oppnå nesten fullstendig ekspansjon (Fig.1). Lenger betongen som inneholder MasterLife SRA 150 utsettes for fuktig herding, bedre vil betongen yte.

Likevel vil herding i kun 24 timer – i betong som inneholder MasterLife SRA 150 – ikke forhindre ekspansjon, som det vil dersom man bruker andre ekspanderende tilsetningsstoffer.

I varmt og tørt klima må fuktherding opprettholdes. Vi anbefaler bruk av membranherder MasterKure, og at man fukter og beskytter betongen med våte presenninger i minst syv dager.

Teknisk informasjon	
Form	Pulver, lys grå
Relativ densitet (kg/l)	0,900 – 1,200
Reell tetthet (kg/l)	3,000 – 3,400

MasterLife SRA 150

Sep. 2021 erst. nov. 2019

Ekspanderende tilsetningsstoff til produksjon av svinnkompensert betong

Bruk av MasterLife SRA 150 for svinnkompensert betong anbefales til følgende bruksområder;

- Demninger
- Tanker
- Reservoarer og svømmebassenger
- Renseanlegg
- Kaier og konstruksjoner utsatt for sjøvann
- Moloer og blokker til marine konstruksjoner
- Beholdere for væsker og/eller gass
- Runde konstruksjoner i spennarmert betong
- Avløp, tunneler og kanaler
- Forseglingsinjeksjoner

SPENNBETONG OG ARMERTE BETONG-KONSTRUKSJONER

- Lange konstruksjoner
- Tynne, massive konstruksjoner
- Spennbetongbjelker
- Ringformede bjelker til sportsanlegg
- Gulv i kjølelager
- Brodekker
- Fylling av hule konstruksjoner
- Industrigulv
- Gulv i sportssentre (skøytebaner, tennisbaner, stadion baner osv.)
- Hyperstatiske konstruksjoner med dårlig armering
- Båter i armert betong
- Skjold til atomanlegg
- Tunnelhvelv til vei og jernbane
- Undersjøiske- og undergrunnskonstruksjoner
- Fundamenter og underbygg
- Hyperstatiske buebroer
- Bankhvelv, kupler og tynne konstruksjoner i armert betong.
- Tak og dekker i arkitektonisk betong

PREFABRIKKERTE ELEMENTER

- Sviller, kantstein, fortau
- Spennbetongbjelker med stort spenn
- Prefabrikkerte paneler
- Betongmaster til el. ledninger, rør osv.

ARMERTE KONSTRUKSJONER

- Reparasjon av vertikale konstruksjoner og lastbærende søyle
- Ekstra elementer til bevaring av eksisterende konstruksjoner
- Stabilisering av grunn

SKAL IKKE BRUKES TIL

MasterLife SRA 150 skal ikke brukes der det kreves svært nøyaktig kontroll av dimensjonsvariasjoner i betong, mørtel eller fugemasser, ettersom kun små endringer i doseringen av et ekspanderende tilsetningsstoff kan forringe kvaliteten på arbeidet.

Typiske eksempler på slike bruksområder er: maskinstøping, reparasjon eller påstøp av gamle overflater. For alle disse bruksområdene anbefaler vi MasterEmaco-produktene. MasterLife SRA 150 bør kun brukes i armert betong. Bruk av MasterRoc FLC 150 anbefales til fylling av etterspente kabelhylser.

EMBALLASJE OG LAGRING

MasterLife SRA 150 leveres i 20 kg sekker. Produktet lagres på et tørt og beskyttet sted.
Produktet skal ikke brukes hvis posen er skadet. Bruk av vernehansker anbefales.

MasterLife SRA 150

Sep. 2021 erst. nov. 2019

Ekspanderende tilsetningsstoff til produksjon av svinnkompensert betong

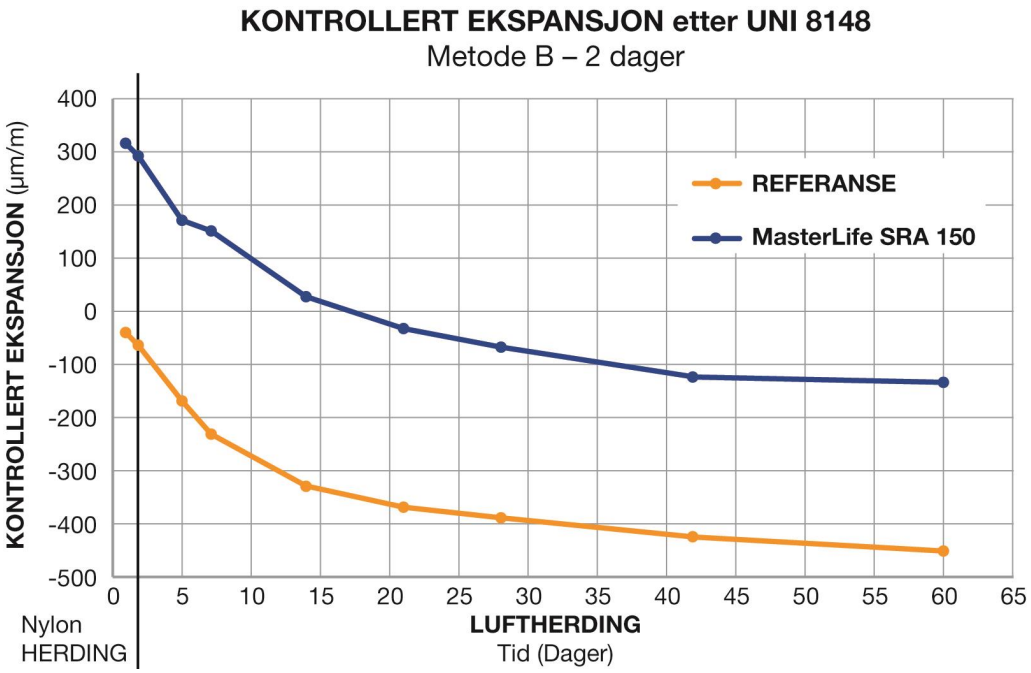

Fig. 1: Kontrollert ekspansjon etter UNI8148 med MasterLife SRA 150 (Sement CEM I 42,5 = 300 kg/m³, vann -180 l/m³ MasterLife SRA 150 = 20 kg/m³; tilslag = 1975 kg/m³).

Master Builders Solutions Norway AS
Gullfotdalen 4
NO-2120 Sagstua
T +47 62 97 00 20
F +47 62 97 18 85
www.master-builders-solutions.com

Norcem AS
Postboks 142, Lilleaker, 0216 Oslo
Tlf. 22 87 84 00
firmapost@norcem.no
www.norcem.no

TILLEGGSMATERIALE
FLYGEASKE

PRODUKTINFORMASJON - FEBRUAR 2019

Norcem AS ivaretar salg og distribusjon av flygeaske til sement- og betongproduksjon. Flygeasken er sertifisert i overensstemmelse med kravene i NS-EN 450-1, klasse A.

Flygeaske er et bearbeidet restprodukt fra kull brukt i kullkraftverk. Flygeaske er silikatholdig og er et pozzolan som sammen med sement og vann gir en tettere betong. Kombinert med sement har flygeaske vært brukt i Norge siden 80-tallet. Norcem FA-sementer inneholder flygeaske.

DEKLARERTE VERDIER

Flygeasken er sertifisert i overensstemmelse med kravene i NS-EN 450-1:2012, klasse A.

Egenskap	Deklarerte verdier	Krav i henhold til NS-EN 450-1
Glødetap (%)	≤ 5,0	Tilfredsstiller kravene gitt NS-EN 450-1
Klorid (% Cl^-)	≤ 0,10	Tilfredsstiller kravene gitt NS-EN 450-1
Sulfat (% SO_3)	≤ 3,0	Tilfredsstiller kravene gitt NS-EN 450-1
Fritt kalsiumoksid (% fri CaO)	≤ 1,5	Tilfredsstiller kravene gitt NS-EN 450-1
Reaktivt kalsiumoksid (% reaktiv CaO)	≤ 10	Tilfredsstiller kravene gitt NS-EN 450-1
Partikkeldensitet (kg/m$^{3)}$	2300	Dekl.verdi +/- 200 kg/m ^{3}
Øvrige kjemiske og fysiske parametere		Tilfredsstiller kravene gitt NS-EN 450-1

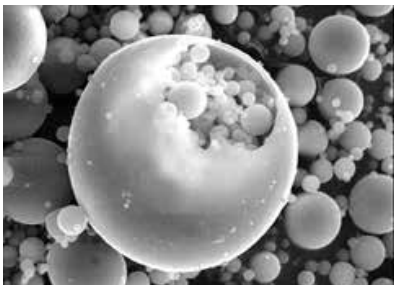

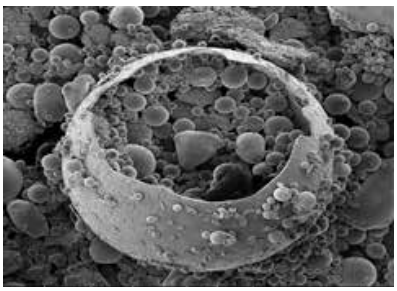

ETONIS® 3500 W (GER)

Dispersible Polymer Powders

ETONIS® 3500 W is suitable for modifying concrete, specialty mortar and cementitious coatings for infrastructure products, in particular for shotcrete applications in underground construction, tunneling and mining. ETONIS® 3500 W is a polymer powder with a low glass transition temperature (Tg). remains flexible down to temperatures below freezing and is suitable for end products with low emissions.

Properties

ETONIS® 3500 W makes fresh concrete easier to process and pump because it reduces the frictional forces between cement and aggregates.
It significantly reduces spray rebound while greatly improving adhesion to all substrates, particularly wet surfaces. Concrete modified with ETONIS® 3500 W produces very little dust, especially during dry spraying. The cohesive properties of ETONIS ® 3500 W increase the sedimentation stability of concrete and specialty mortars, reducing bleeding and segregation.
ETONIS® 3500 W has a plasticizing effect and reduces the water/cement ratio without compromising the concrete's workability.
In hardened concrete, ETONIS® 3500 W improves adhesion, enhances flexural strength, reduces the modulus of elasticity (imparting flexibility) and increases abrasion resistance. It does not impair the concrete's high ultimate strength. Concrete modified with ETONIS® 3500 W seals against pressing water, shows enhanced carbonation resistance and prevents the ingress of aggressive media into the mix. In combination with suitable foam-control agents, ETONIS® 3500 W also increases compressive and flexural strength.

Technical data

Specification

Property	Condition	Value	Method
Bulk density	-	400 - 550 kg/m³	DIN EN ISO 60
Ash content	-	max. 12 %	specific method
Solids content	-	min. 98 %	DIN EN ISO 3251

General Characteristics

Property	Condition	Value	Method
Appearance	-	white to light beige powder	Visual

These figures are only intended as a guide and should not be used in preparing specifications.

Protect against frost.

Applications

- Water Management and Tunneling

Packaging and storage

Packaging

25 kg paper bags.
Other sizes on request.

Storage

During storage, protect the product from contact with moisture. Prolonged storage at temperatures above 30 °C, especially in combination with pressure, humidity or exposure to sunlight, may result in blocking. Carefully seal any open containers and store them under suitable conditions. We recommend storing the product in a warehouse that provides cool and dry conditions. Do not store the product for more than six months, starting from the date at which it was received, unless the Certificate of Analysis contains a different date, which would take precedence. If the product is stored longer than recommended, it may still be used but users are advised to verify the properties required for the intended use.

Safety notes

Comprehensive instructions are given in the appropriate Material Safety Data Sheets. These are available on request from WACKER sales offices.

QR Code ETONIS® 3500 W (GER)

For technical, quality or product safety questions, please contact:

Wacker Chemie AG, Hanns-Seidel-Platz 4, 81737 Munich, Germany
info@wacker.com, www.wacker.com

Appendix B MATLAB scripts for IMA

B.1 Readimage.m

Listing 1: Readimage.m

```
% Read a grayscale image for image analysis.
% readimage(Filename) reads a grayscale image, where Filename is
% the name of the graphics file located in the current working directory.
% Example: readimage('ex1.tif') reads in an image located in
% the same directory as readimage.
%
% readimage(Filename,Folder) reads the image named Filename located in the
% specified Folder.
% Example: readimage('ex1.tif','Images') reads in the image
% "ex1.tif" located in the directory "Images."
%
% readimage(Filename,Folder,'cr') initiates the interactive Crop Image Tool
% that allows you to crop the image.
% Example: readimage('ex1.tif','Images','cr') allows you to crop the
% image 'ex1.tif.'  If you want to read and crop the image located in
% the current working directory, type
% "readimage('exlocal.tif','','cr')".
%
% Basic information about the image is processed and written to the
% base workspace.  The variables "grayimage", "pixsize", and "ppmm" are
% assigned to the base workspace for use by the function basicanalysis.
% "grayimage" is a matrix containing the graylevels of each pixel,
% "pixsize" is the size of each pixel in mm, and "ppmm" is the resolution
% in pixels per millimeter.
%
% The Image Processing Toolbox must be installed to use this function.
% Type "ver" at the command prompt to determine which toolboxes are
% installed.
%
% The resolution of the image will be automatically determined.  The
% function "readimage" assumes that the image resolution unit is in
% [pixels/inch]. If the image resolution unit is not in [pixels/inch],
% then the variable "ppmm" [pixels/mm] must be modified in this function.
%
% See also basicanalysis and reconstructspheres.


function readim_var = readimage(varargin)


% The user must pass the filename of the image
if nargin == 0
    error('A filename is a required input')
end
```

```
45
46 % If the optional Folder is not passed, then the path is the filename
47 if nargin == 1
48     fpath = varargin{1};
49 end
50
51 % If a folder is passed, concatenate the folder and filename into a path
52 if nargin > 1
53     fpath = strcat(varargin{2},'/',varargin{1});
54 end
55
56
57 % Determine the resolution of the image in pixels per inch (dpi).  The
58 % resolution in the vertical and horizontal directions should be the same.
59 finfo = imfinfo(fpath);
60 xR = finfo.XResolution;          % xR should be the image resolution in dpi
61 yR = finfo.YResolution;
62 if xR ~= yR
63     disp('The vertical and horizontal resolution does not match.')
64     disp('The analysis may not be valid.  Check the scanning resolution.')
65 end
66
67 mmpi = 25.4;                     % the number of mm per inch
68 ppmm = xR/mmpi;                  % ppmm is pixels per mm
69 assignin('base','ppmm',ppmm)     % write ppmm to the base workspace
70 psize = 25400/xR;                % psize is pixel size in microns
71 assignin('base','pixsize',psize)% write psize->pixsize to the workspace
72
73 fname = varargin{1};             % assign the filename to variable "fname"
74
75 % Display resolution infomation to the user
76 disp(' ')
77 str = ['The resolution of image "',fname, '" is ', num2str(xR), ' pixels/inch'];
78 disp(str)
79 str = ['or ', num2str(ppmm), ' pixels/mm.'];
80 disp(str)
81 str = ['The size of each pixel is ', num2str(psize), ' microns.'];
82 disp(' ')
83 disp(str)
84 disp(' ')
85
86
87 % Read image using function imread.
88 airnocrop = imread(fpath);
89
90 % Display the grayscale image
91 Im = figure;
92 imshow(airnocrop);
93 readim_var.grayimage = airnocrop;
```

```
94  readim_var.pixsize = psize;
95
96  % If a 3rd argument is passed, the user wants to crop the image
97  if nargin == 3
98      disp('You have chosen to crop your image.  Drag a rectangular ')
99      disp('region on the figure window and double click to crop image.')
100     disp(' ')
101     I = imcrop(airnocrop);
102     assignin('base','grayimage',I);
103     readim_var.cropped = I;
104     % Display the cropped grayscale image
105     figure;
106     imshow(I);
107 else
108
109 % Else the image is already ready to go
110 assignin('base','grayimage',airnocrop);
111
112
113
114 end
```

B.2 Basicanalysis.m

Listing 2: basicanalysis.m

```
% Basic image analysis to determine the air content, specific surface, and
% the Powers spacing factor of the air voids shown in a grayscale image.
% The output is written to the Matlab Command Window.
%
% basicanalysis(paste_solids) takes in the variable paste_solids, where
% paste_solids is the paste/solids ratio.
% Example: basicanalysis(0.8) specifies a paste/solids ratio of 0.8.
%
% basicanalysis(paste_solids,thresh) includes a user-defined
% input thresh, where thresh is the image threshold.  If thresh is not
% specified, then the threshold will be determined using Otsu's method.
% Type 'help graythresh' for more information on automatic thresholding.
%
% basicanalysis must be run after running the function readimage.
% The variables "grayimage", "pixsize", and "ppmm" are taken from the base
% workspace.
%
% See also readimage and reconstructspheres.

function Variables = basicanalysis(varargin)

% Get "grayimage" and "ppmm" from the base workspace
grayimage = evalin('base','grayimage');
ppmm = evalin('base','ppmm');


% The user must pass the paste/solids ratio as an argument
if nargin < 1
    error('basicanalysis requires a paste:solids ratio as input.')
end

% The first argument corresponds to paste_solids
paste_solids = varargin{1};

% If more than one argument is passed, the 2nd argument is the
% threshold
if nargin > 1
    thresh = varargin{2};
end


cropdim = size(grayimage)/ppmm;          % dimensions of the image in mm
assignin('base','cropdim',cropdim)


% If the user does not specify a threshold, compute the threshold using
```

```
47 % Otsu's method.  The user may want to first compute the automatic
48 % threshold and then adjust the binary image by matching the void
49 % diameters in the grayscale image with the diameters of the corresponding
50 % objects in the binary image.
51
52 if nargin < 2
53     thresh = graythresh(grayimage)*255;
54 end
55
56 assignin('base','threshold',thresh)
57
58 bw = im2bw(grayimage,thresh/255);
59
60 % Remove the smallest voids by selecting any cluster of white pixels that
61 % contain less than or equal to a specified number "tinyobjects."  If you do
62 % not want to remove any white pixels, set tinyobjects = 0.  A cluster is
63 % defined using nearest neighbors for each pixel.  In 2D, a square pixel
64 % has either 4 maximum neighbors or 8 maximum neighbors, depending on
65 % whether or not you want to include neighbors at a diagonal.  Therefore,
66 % neigh=4 or neigh=8.  Store the new binary image into a matrix called bw2.
67 % Note that if tinyobjects=0, then bw2=bw.
68 %
69 tinyobjects = 1;
70 neigh = 4;
71 bw2 = bwareaopen(bw,tinyobjects+1,neigh);
72 assignin('base','bw2',bw2)
73
74 figure;
75 imshow(bw2);
76
77 disp(' ')
78 str = ['The threshold is ', num2str(thresh), '.'];
79 disp(str)
80
81 % Find connected components in a binary image.  Set conn=4 or conn=8, which
82 % defines the number of maximum neighbors for a square pixel in 2D.
83 conn = 4;
84 cc = bwconncomp(bw2,conn);       % connectivity, image size, number of
85                                  % connected components, pixel index list
86 assignin('base','cc',cc)
87
88 % Measures a set of properties for each connected component in cc
89 stats = regionprops(cc,'Area','Perimeter');
90 assignin('base','stats',stats)
91 % stats = regionprops(cc,'EquivDiameter','PixelIdxList','PixelList');
92
93 areapix = [stats.Area];          % number of pixels per object (vector)
94 areamm2 = [stats.Area]/(ppmm*ppmm);% area of each profile in mm^2 (vector)
95 diameterpix = 2*sqrt(areapix/pi);     % equivalent diameter of each object (
```

```
    vector)
diametermic = 2*sqrt(areamm2/pi)*1000; %diameter of each profile in microns
radiimic = 1/2*diametermic;          %radius of each profile in microns

assignin('base','radiimic',radiimic)

% The fractional area content is the sum of the areas of each void divided
% by the area of the image
[m,n] = size(grayimage);
aircontent = sum(areapix)/(m*n)*100;
%aircontent = sum(areamm2)/(cropdim(1)*cropdim(2))*100;

disp(' ')
str = ['The air content is ', num2str(aircontent), ' percent.'];
disp(str)



%maxD = max(diameter);

Ptot = sum([stats.Perimeter]);      % perimeter in pixels
Atot = sum([stats.Area]);           % area in pixels^2
specsurfpix = Ptot/Atot*4/pi;       % specific surface in pixels^(-1)
specsurf = specsurfpix*ppmm;        % specific surface in mm^-1

disp(' ')
str = ['The specific surface is ', num2str(specsurf), ' mm^-1.'];
disp(str)

% spacing factor

p_A = paste_solids*(100-aircontent)/(aircontent); % paste:air ratio

disp(' ')
str = ['The paste/air ratio is ', num2str(p_A), '.'];
disp(str)

% Compute Powers spacing factor in mm
if p_A < 4.342
    Pspacef = p_A/specsurf;
else
    Pspacef = (3/specsurf)*(1.4*(1+p_A)^(1/3)-1);
end

disp(' ')
str = ['The Powers spacing factor is ', num2str(Pspacef), ' mm.'];
disp(str)
%Variables = [thresh,aircontent,specsurf,p_A,Pspacef,bw,bw2];
Variables.thresh = thresh;
```

```
144 Variables.aircontent = aircontent;
145 Variables.specsurf = specsurf;
146 Variables.p_A = p_A;
147 Variables.Pspacef = Pspacef;
148 Variables.bw = bw;
149 Variables.bw2 = bw2;
```

B.3 Reconstructspheres.m

Listing 3: reconstructspheres.m

```
% Saltykov sphere reconstruction method to estimate the 3D size distribution
% of air voids using the size distribution of 2D observed profile sizes as
% input.  The output includes the mean observed circle radius, computed
% sphere radius, and histograms of both the observed 2D and computed 3D radii.
%
% reconstructspheres plots the histograms using the Freedman-Diaconis
% rule is used to estimate a binwidth.  The computed binwidth is written
% to the Matlab Command Window.  This value may be a good starting point
% attempting to determine an appropriate binwidth.
%
% reconstructspheres(binwidth) takes in the variable binwidth and plots
% the distributions accordingly, where the units of binwidth is in microns.
% Example: reconstructspheres(4) produces histograms with binwidth = 4 microns.
%
% reconstructspheres(binwidth,xmax) specifies the maximum x-limit on the
% plotted distributions, where the unit of xmax is microns.
% Example: reconstructspheres(4,160) produces histograms with binwidth =
% 4 microns and a horizontal axis with range (0,160) microns.
%
% See also readimage and basicanalysis.
%
function variables = reconstructspheres(varargin)

% If a binwidth is passed
if nargin > 0
    binwidth = varargin{1};
end

% If an maximum x-limit is pssed
if nargin > 1
    XL2 = varargin{2};
end

% Get "grayimage", "stats", and "ppmm" from the base workspace
grayimage = evalin('base','grayimage');
stats = evalin('base','stats');
ppmm = evalin('base','ppmm');


%close all % to keep images

areapix = [stats.Area];          % number of pixels per object (vector)
areamm2 = areapix/(ppmm*ppmm);% area of each profile in mm^2 (vector)
diameterpix = 2*sqrt(areapix/pi);      % equivalent diameter of each object (
    vector)
diametermic = 2*sqrt(areamm2/pi)*1000; %diameter of each profile in microns
```

```
radiimic = 1/2*diametermic;          %radius of each profile in microns

averageradmic = sum(radiimic)/length(radiimic);  % mean observed radius
% averagediammic = 2*averageradmic                % mean observed diameter


% If no binwidth is specified, use Freedman-Diaconis rule to estimate a
% binwidth
if nargin == 0
    IQRradii = iqr(radiimic);        % interquartile range of radiimic
    binwidth = 2*IQRradii*length(radiimic)^(-1/3);
end


%binwidth = 5;                      % bin width in microns
r = min(radiimic):binwidth:max(radiimic);

% bin the elements of radiimic into 'r' equally spaced containers
[N,X] = hist(radiimic,r);
freqN = 1/(sum(N))*N;

% Get number density of void profiles on image
cropdim = 1/ppmm*size(grayimage);                % image dimensions [mm]
NA = length(radiimic)/(cropdim(1)*cropdim(2));  % number density of bubble
                                                 % profiles [mm^-2]


figure2 = figure;
set(figure2,'Position',[133 921 562 345]);
NAr = 1/binwidth*NA.*freqN;
bar(X,NAr);
ylabel('Number density per mm^2','FontSize',14);
xlabel('Observed profile radii [\mum]','FontSize',14);
%xlim([0 150])
title('Distribution of observed bubble profiles','FontSize',16);
XL = xlim; YL = ylim;
XL(1) = 0; YL(1) = 0;
if nargin > 1
    XL(2) = XL2;
end
xlim(XL); ylim(YL);


%Rm = ceil(max(radiimic));          % maximum radius
nbins = length(r);
Dr = binwidth;                      % width of each class of radii

NArorig = NAr;
```

```
95
96  rmod = [0  r];
97  r = rmod;
98  NARmod = [0  NAr];              % modify vector to include a bin with 0 radius
99
100 NAr = NARmod';
101
102
103 meanprofileradius = 1/sum(NAr)*sum(NAr.*r');  % mean observed radius in microns
104 disp(' ')
105 str = ['The mean observed profile radius is ', num2str(averageradmic), ' microns
        .'];
106 disp(str)
107
108
109
110 rm = max(r);                    % largest radius of the current working class
111
112 NArm = zeros(length(r),1);
113 NVR = zeros(length(r),1);
114
115 for k=1:length(NAr)-1
116
117     % compute the numerical density of the largest spheres NVm
118     NVm = NAr(length(NAr)-k+1)/(2*sqrt(2*(length(NAr)-k)-1)*Dr);
119     NVR(length(NAr)-k+1) = NVm;       % store into a vector NV
120
121     NArm = zeros(length(r),1);        % reset profile number density of rmax
122
123     % compute number of profiles per section area
124     for i=1:length(r)-k+1
125         NArm(i) = NVm*2*(sqrt(rm^2-(r(i)-Dr)^2)-sqrt(rm^2-r(i)^2));
126     end
127     rm = rm-Dr;                       % new maximum radius
128
129     NArm;
130     NAr = NAr - NArm;                 % get new profile number density
131
132 end
133
134
135 NV = sum(NVR);                      % sum under sphere histogram
136
137 maxfreq = max(NVR);
138 minfreq = min(NVR);
139 fR = 1/NV*NVR;                      % frequency of sphere radii
140
141
142
```

```
143 meansphereradius = 1/NV*sum(NVR.*r'); % mean radius of reconstructed bubbles
144 disp(' ')
145 str = ['The mean computed sphere radius is ', num2str(meansphereradius), '
      microns.'];
146 disp(str)
147
148 %get total volume and total profile area in microns^2 or microns^3
149 radius = r';
150 Abox = NARmod'.*pi.*radius.^2;
151 Aboxtotal = sum(Abox);
152
153 Vbox = 4/3*pi*NVR.*radius.^3;
154 Vboxtotal = sum(Vbox);
155
156 % delete negative bins in NVR
157 for i=1:length(NVR)
158     if NVR(i) < 0
159         NVR(i) = 0;
160     end
161 end
162
163 NV = sum(NVR);                          % sum under sphere histogram
164 meansphereradius = 1/NV*sum(NVR.*r');
165 meanspherediameter = 2*meansphereradius;
166
167
168
169 % Roughly estimate the median of the sphere radii.  The median will be used
170 % to estimate lognormal distribution parameters. If the binwidth is
171 % inappropriate, this estimate will be inaccurate.
172 cumsumNVR = cumsum(NVR);
173 midpt = cumsumNVR(end)/2;
174 for i=1:length(cumsumNVR)
175     if cumsumNVR(i) > midpt
176         idx = i;
177     break
178     end
179 end
180 medianestupper = r(idx);
181 medianestlower = r(idx-1);
182 %medianRest = (medianestupper+medianestlower)/2;
183 medianRest = medianestupper;
184 medianDest = 2*medianRest;
185
186 % compute mu and sigma from the estimated median of sphere radii
187 muest = log(medianRest);
188 sigmaest = sqrt(2*(log(meansphereradius)-muest));
189
190
```

```
% plot estimated air void size distribution
%figure;
%bar(r,NVR);
%set(gcf,'Position',[135 516 562 345]);
%ylabel('Number density per mm^3','FontSize',14);
%xlabel('Computed sphere radii [\mum]','FontSize',14);
%XL = xlim;
%XL(1) = 0;
if nargin > 1
    XL(2) = XL2;
end
xlim(XL);
%% Uncomment the following lines to plot estimated lognormal distribution
% hold on
% rsm = 0:0.1:XL(2);
% YsphereR=lognpdf(rsm,muest,sigmaest);
% p5=plot(rsm,binwidth*NV.*YsphereR);
% set(p5,'Color','red');
% title('Distribution of reconstructed bubbles','FontSize',16);
YL = ylim;
YL(1) = 0;
ylim(YL);

disp(' ')
str = ['The binwidth is ', num2str(binwidth), ' microns.'];
disp(str)
disp(' ')
variables = [averageradmic,meansphereradius,binwidth];
%% Uncomment the following lines to display lognormal parameters
% str = ['The estimated lognormal distribution parameters '];
% disp(str)
% str = ['for the sphere distrition are: '];
% disp(str)
% disp(' ')
% str = ['   MU = ', num2str(muest), ' microns and SIGMA = ' num2str(sigmaest) '
    microns.'];
% disp(str)
% disp(' ')
```

B.4 Fullanalysis.m

Listing 4: fullanalysis.m

```
function fullanalysis(filename,paste_solids,excelfile)

readimage_var = readimage(filename,'Images','cr')%Im, grayimage, pixsize
grayimage = readimage_var.grayimage;
pixsize = readimage_var.pixsize;
cropped = readimage_var.cropped;
dim_full = size(grayimage)*pixsize*0.001
dim_cropped = size(cropped)*pixsize*0.001
% saveas(figure, 'Cropped image','png')
% Can manually change folder here, and option not to crop.
% Variables = [thresh,aircontent,specsurf,p_A,Pspacef,bw,bw2];
% image([0 dim_cropped(2)],[],cropped)

variables_struct = basicanalysis(paste_solids)
variables(1) = variables_struct.thresh;
variables(2) = variables_struct.aircontent;
variables(3) = variables_struct.specsurf;
variables(4) = variables_struct.p_A;
variables(5) = variables_struct.Pspacef;
%variables(6) = variables_struct.bw;

variables_reconstr = reconstructspheres(6.25,1000)
% binwidths may be changed.
move2excel(excelfile,variables, variables_reconstr,paste_solids,dim_full(1)...
    ,dim_full(2),dim_cropped(1),dim_cropped(2));

bw2 = variables_struct.bw2;
figure()
imshow(bw2)
saveas(gcf, 'Binary image','png') % save binary figure as png.

imwrite(bw2,'Binary image.tiff','tiff');



end
```

B.5 move2excel.m

Listing 5: move2excel.m

```
function move2excel(filename,variables,variables2...
    ,paste_solids,dimoriginal1,dimoriginal2,dimcropped1,dimcropped2)

D = get(gca,'Children');
XData = get(D,'XData');
YData = get(D,'YData');
%Data = [XData',YData'];

xlswrite(filename,[XData(:),YData(:)],'IMA','C13');
xlswrite(filename,variables(2),'IMA','E2') % Air content
xlswrite(filename,variables(3),'IMA','E3') % Specific surface
xlswrite(filename,variables(5),'IMA','E4') % Power spacing factor
xlswrite(filename,variables2(1),'IMA','E5') % mean observed sphere radii
xlswrite(filename,variables2(2),'IMA','E6') % average computet sphere radii
xlswrite(filename,paste_solids,'IMA','V13') % paste/solids ratio
xlswrite(filename,dimoriginal1,'IMA','V14') %
xlswrite(filename,dimoriginal2,'IMA','W14') %
xlswrite(filename,dimcropped1,'IMA','V15') %
xlswrite(filename,dimcropped2,'IMA','W15') %
end
```

Appendix C IMA - total air content and binary images

C.1 Literature study - total air content

Table 27: Total air content for sprayed concrete in studies by Yun et al. (2010) [19] and Choi et al. (2016) [20]. SC means sprayed concrete.

Reference	Mix	Air content cast SC (not pumped) [%]	Air content SC with accelerator [%]
Yun (2010) Choi (2016) [19, 20]	SF0	9.1	2.6
	SF4.5	8.4	2.8
	SF9	6.5	2.5
	SF0 A	16.4	4.8
	SF4.5 A	14.2	4.5
	SF9 A	12.8	3.4
	SF9 A-F	17.3	3.6
	SF9 A-FP	22.1	4.5
	SF9 A-FPV	14.1	7.2

Table 28: Total air content for sprayed concrete in the study by Yun et al. (2019) [48]. Air content for cast SC (pumped) for AG3.AE04 was not given in the reference.

Reference	Mix	Air content cast SC (not pumped) [%]	Air content cast SC (pumped) [%]	Air content SC with accelerator [%]
Yun (2019) [48]	AG3	4.4	4.6	1.1
	AG3.AE04	13.3		4.0
	AG3.FA20	4.3	4.5	3.4
	AG3.SF10	3.4	5.3	3.6
	AG3.MK10	3.2	5.3	2.1
	AG3.GGBFS40	4.9	4.6	2.3

Table 29: Total air content for sprayed concrete in the study by Talukdar and Heere (2019) [47] and Myren and Bjøntegaard (2014) [32].

Reference	Mix	Air content [%]
Talukdar & Heere (2019) [47]	9 m^3/h	6.4
	11 m^3/h	6.9
	17 m^3/h	8.1
Myren & Bjøntegaard (2014) [32]	Steel fibre, cast	6.6
	Steel fibre, sprayed	2.9
	Macro pp-fibre, cast	5.0
	Macro pp-fibre, sprayed	3.1

C.2 Binary images

Ff0-2m90deg-1:

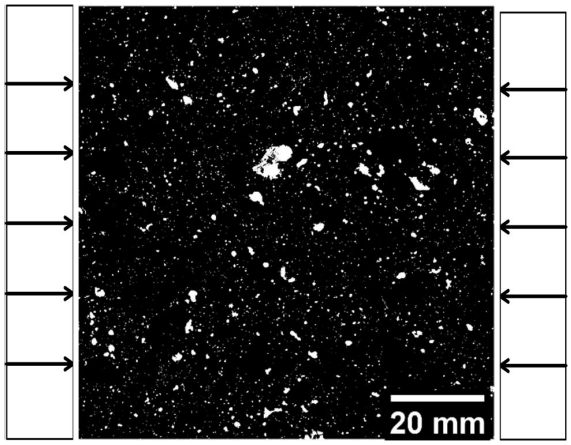

Ff0-2m90deg-2:

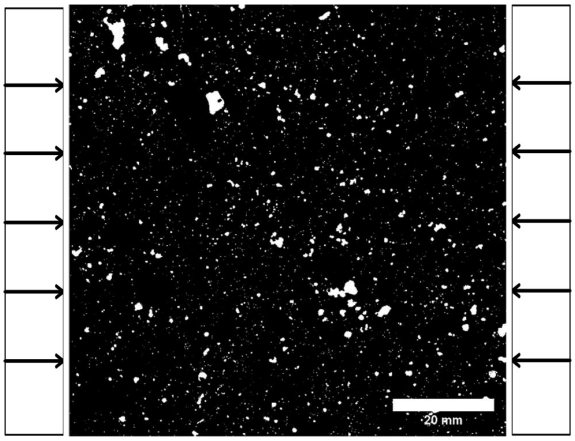

Ff3-2m90deg-1:

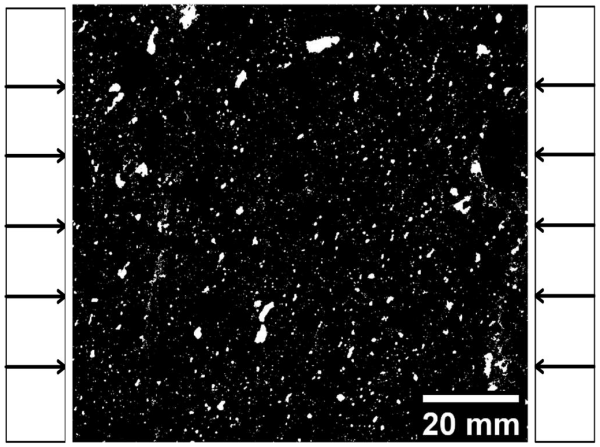

Ff3-2m90deg-2:

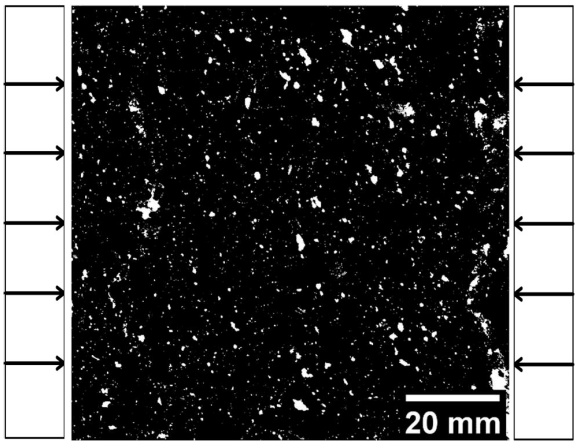

Ff6-2m90deg-1:

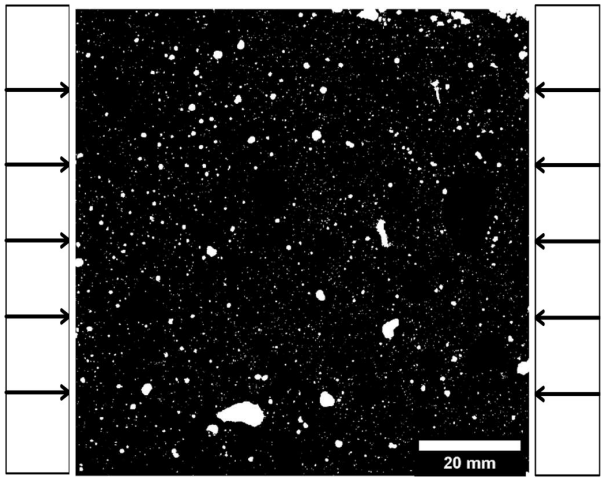

Ff6-2m90deg-2:

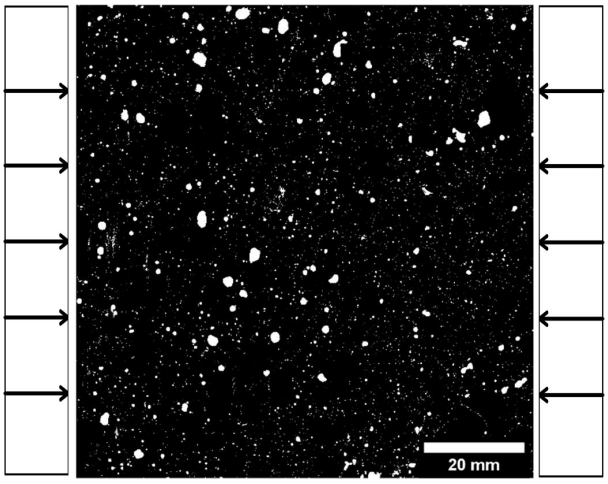

Ff10-2m90deg-1

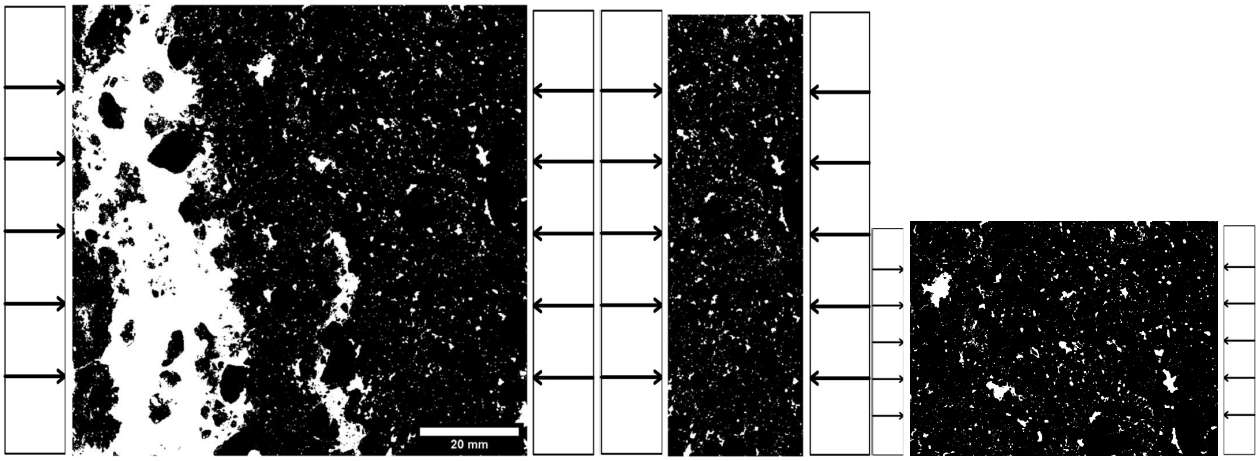

Ff10-2m90deg-2

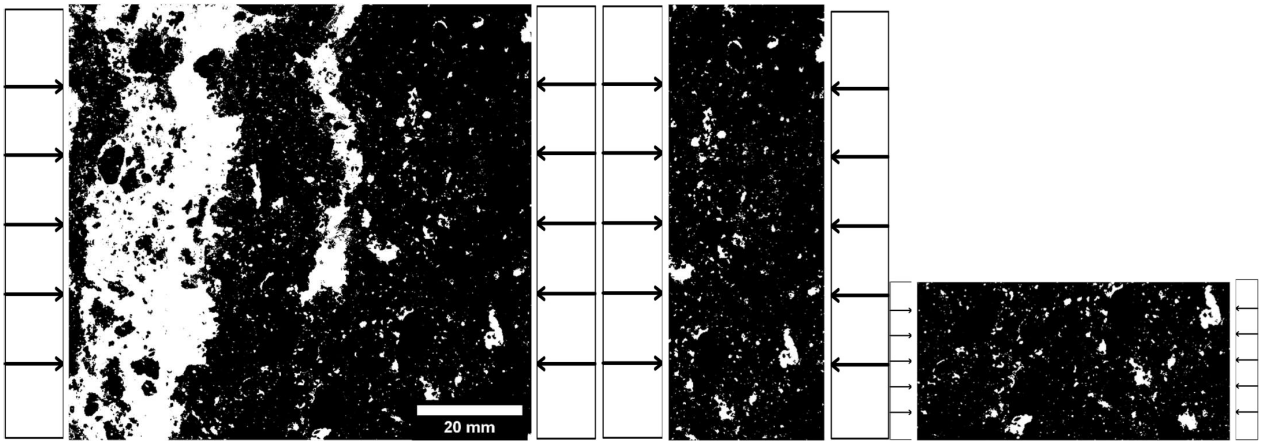

Tnf0-Cast

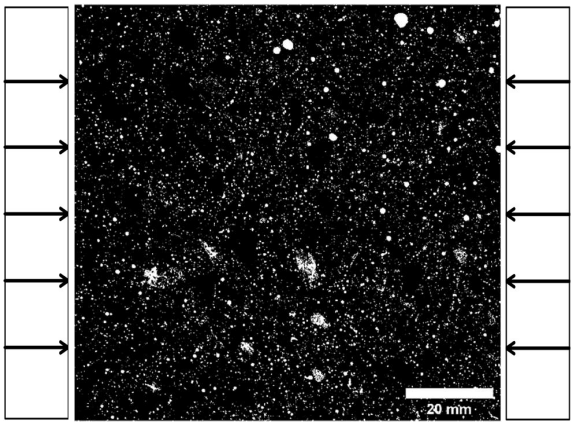

Tnf0-Cast

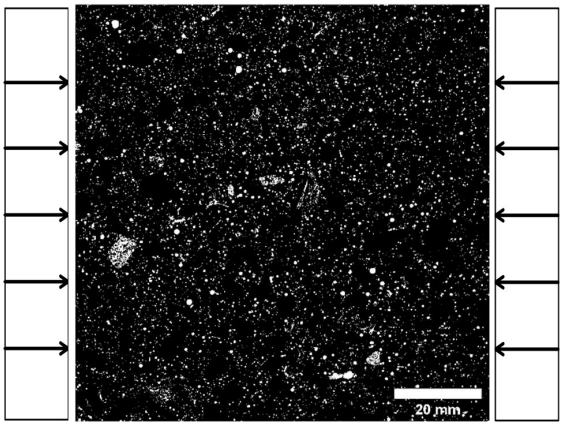

Tnf3,5-1,5m90deg-1:

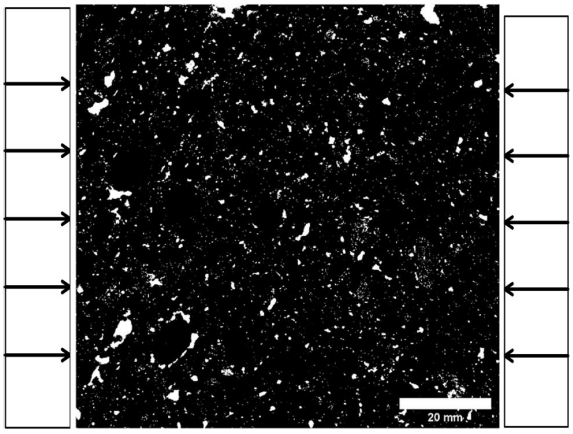

Tnf3,5-1,5m90deg-2:

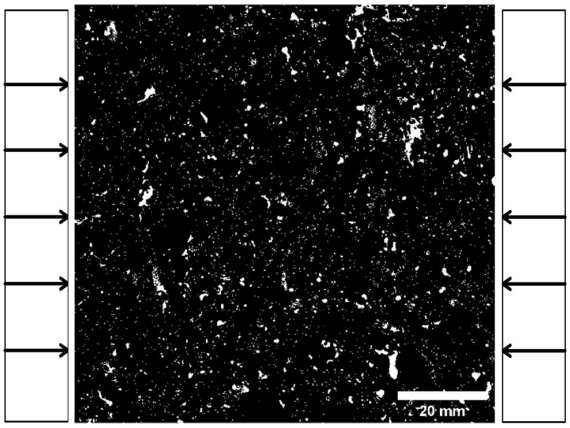

Tnf7-1,5m90deg-1:

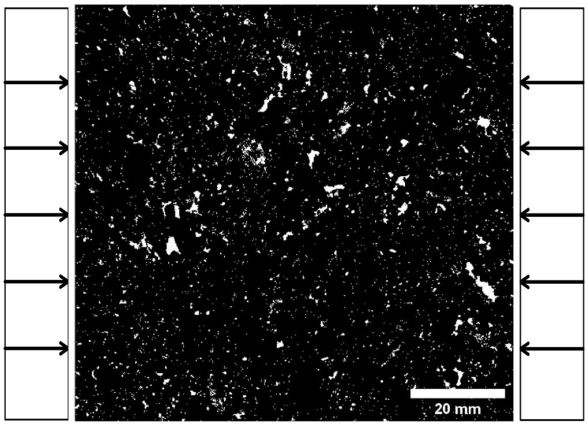

Tnf7-1,5m90deg-2:

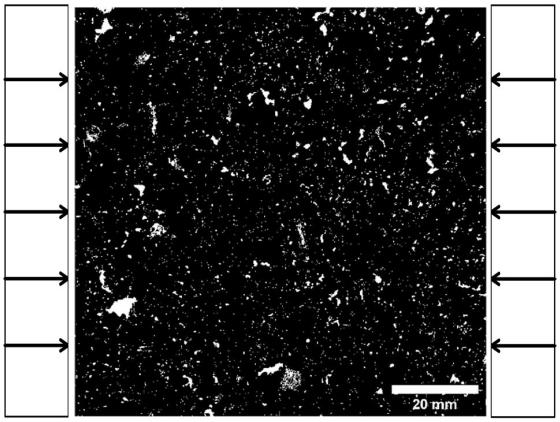

Tf7-1,5m90deg-1:

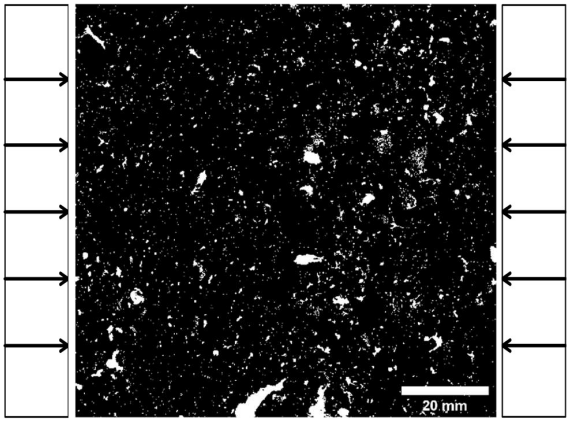

Tf7-1,5m90deg-2:

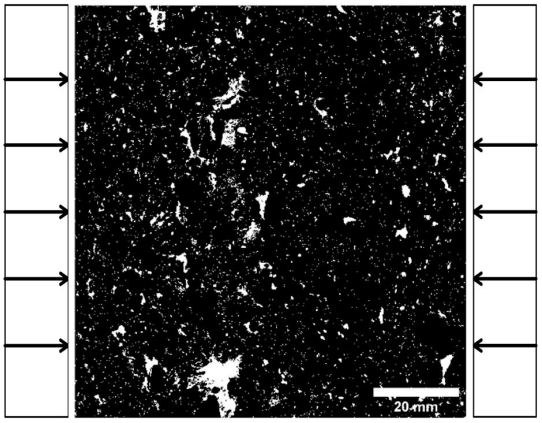

Tf7-2,5m90deg-1:

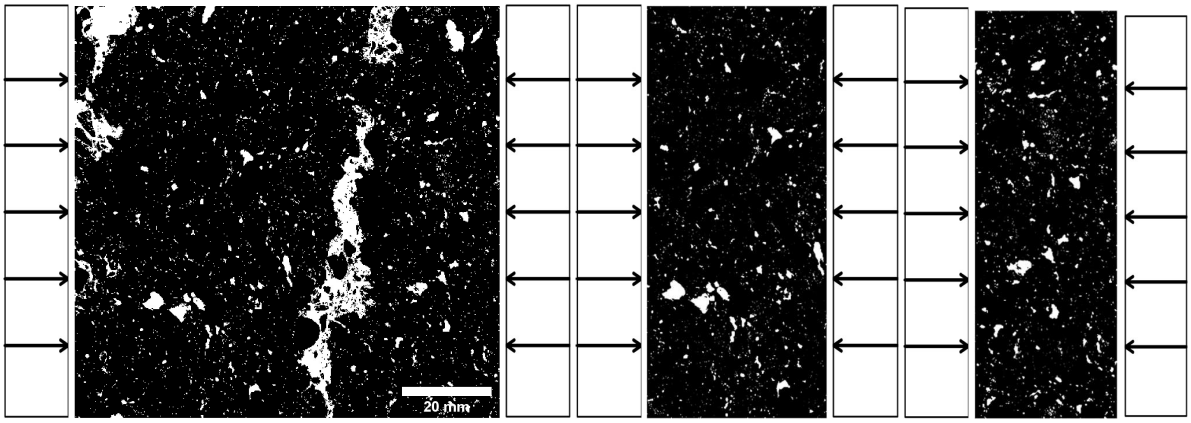

Tf7-2,5m90deg-2:

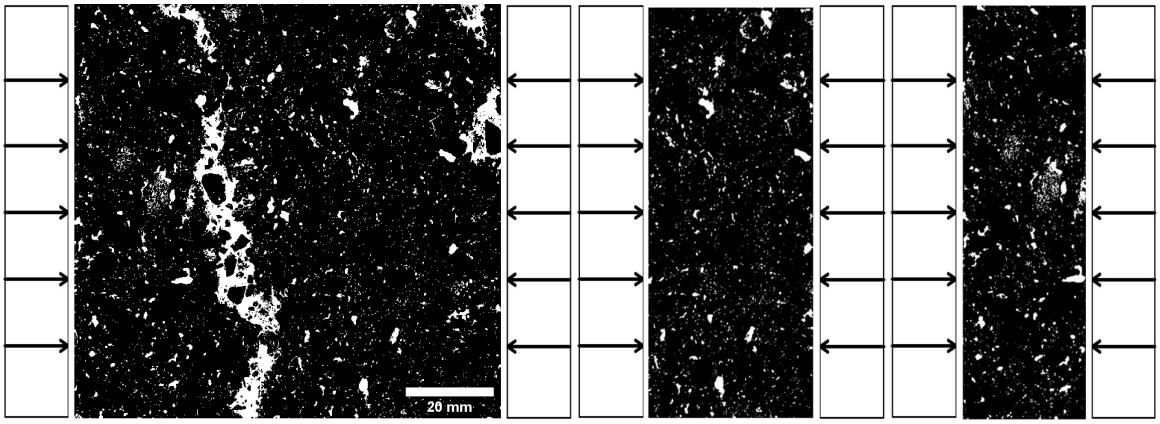

Tf7-3,5m90deg-1:

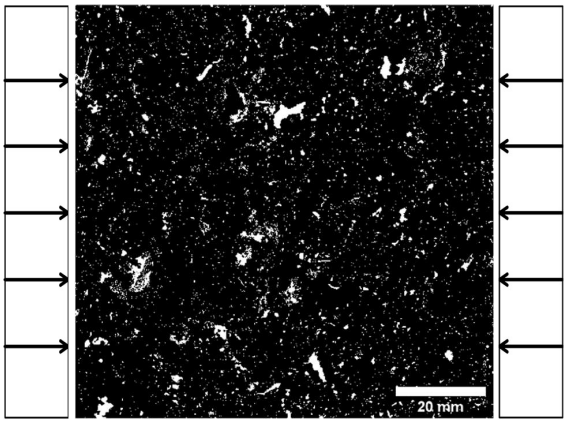

Tf7-3,5m90deg-2:

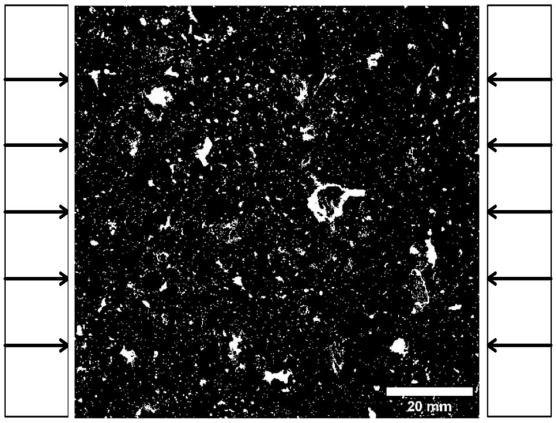

Tf7-1,5m67deg-1:

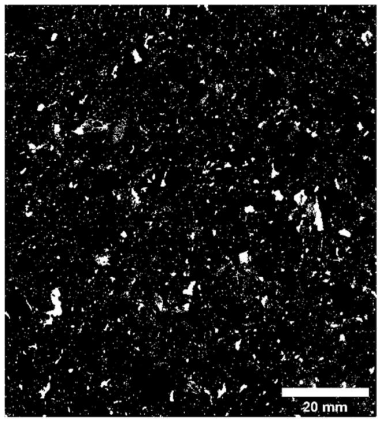

Tf7-1,5m67deg-2:

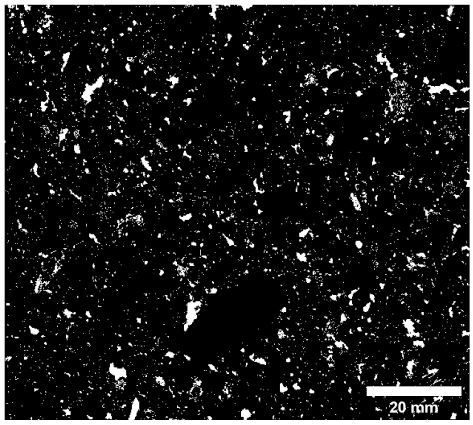

Tf7-1,5m45deg-1:

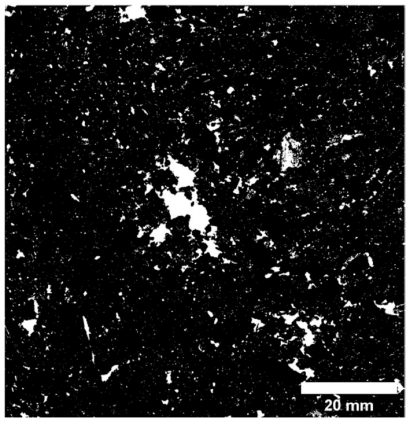

Tf7-1,5m45deg-2:

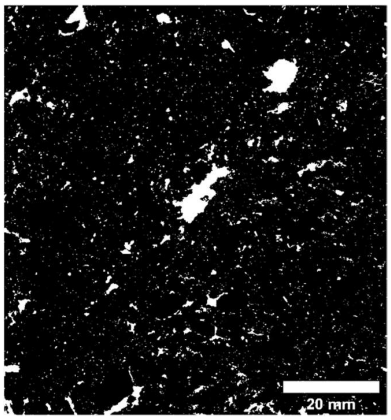

Sf7-1,5m90deg-ref1,1-1:

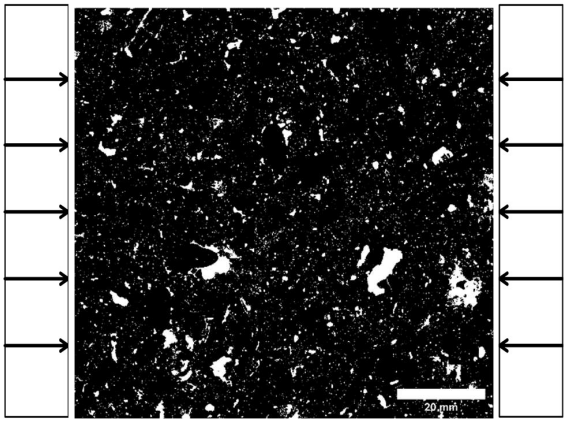

Sf7-1,5m90deg-ref1,1-2:

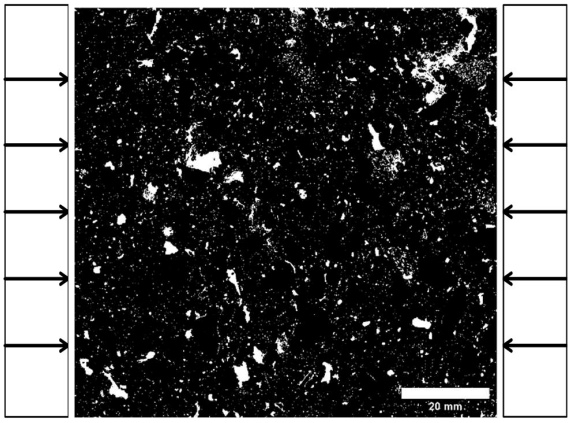

Sf7-1,5m90deg-ref1,2-1:

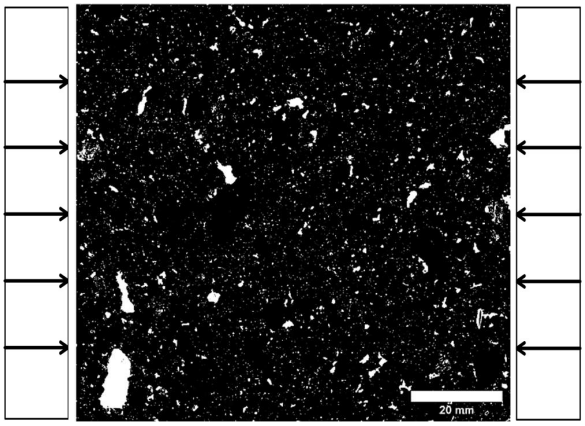

Sf7-1,5m90deg-ref1,2-2:

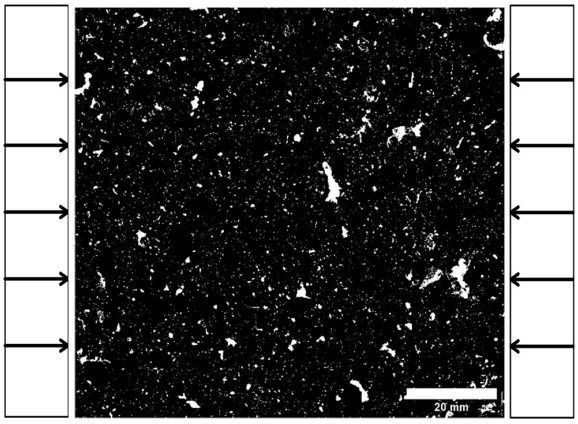

Sf7-1,5m90deg-380M-1

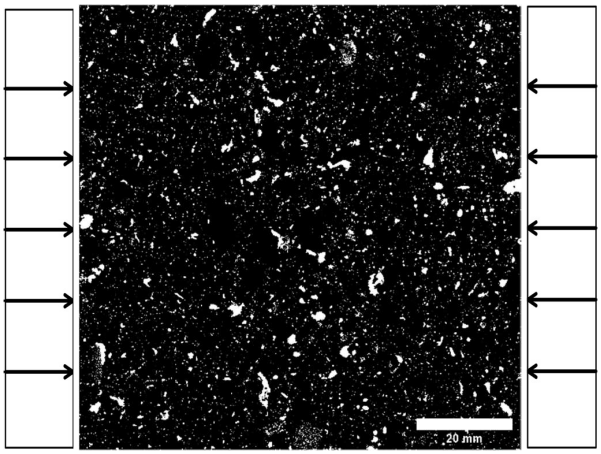

Sf7-1,5m90deg-380M-2

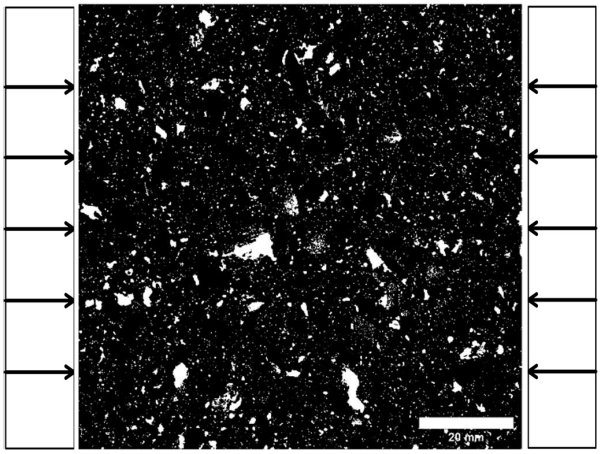

Sf7-1,5m90deg-noSRA-1

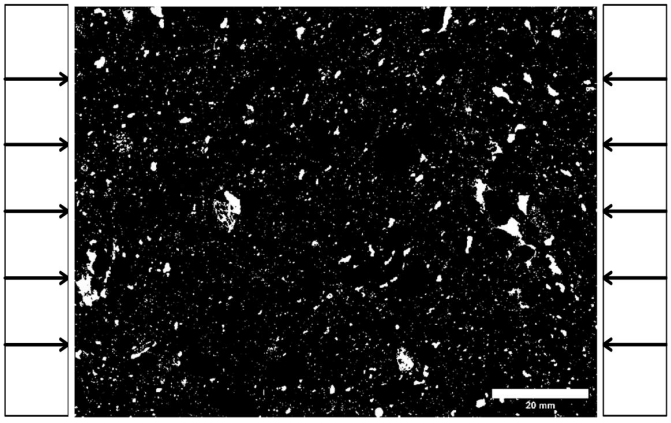

Sf7-1,5m90deg-noSRA-2

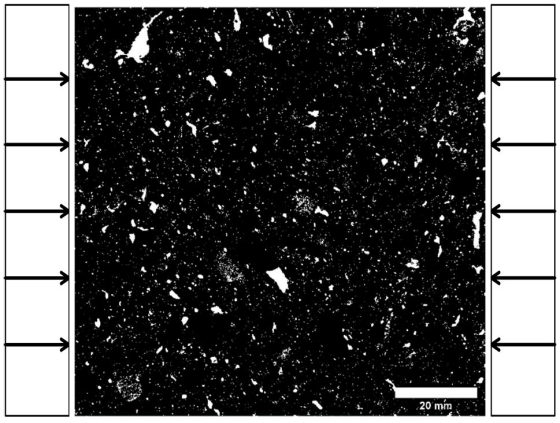

Sf7-1,5m90deg-noHA-1

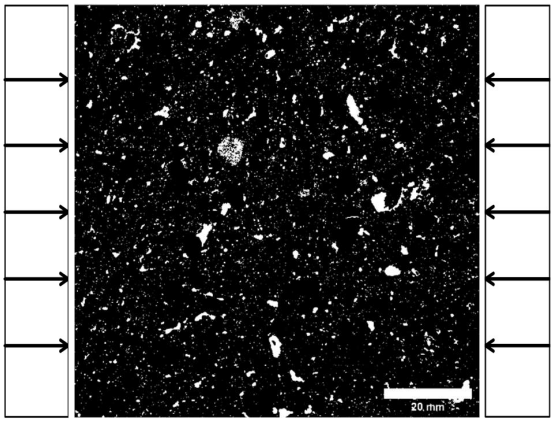

Sf7-1,5m90deg-noHA-2

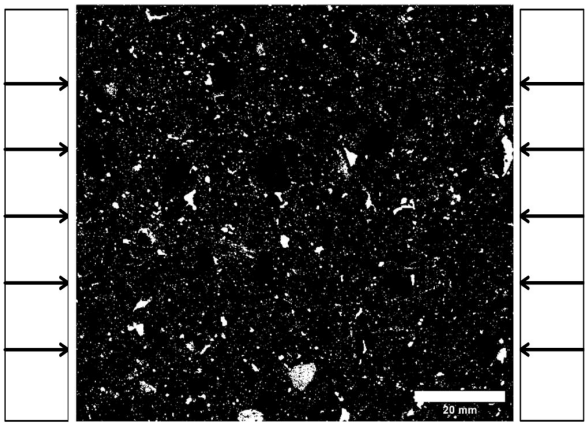

Sf7-1,5m90deg-polymer-1

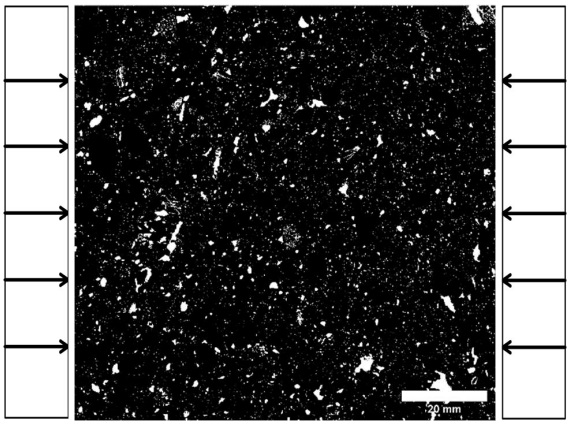

Sf7-1,5m90deg-polymer-2

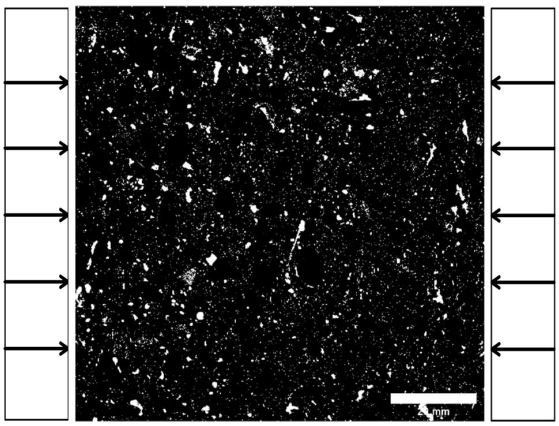

Sf7-1,5m90deg-FA-1

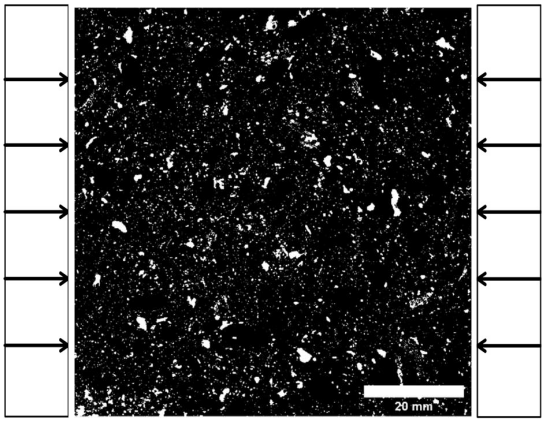

Sf7-1,5m90deg-FA-2

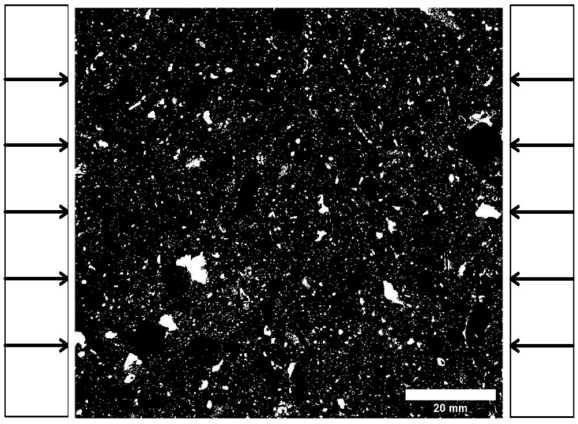

Sf7-1,5m90deg-LF-1

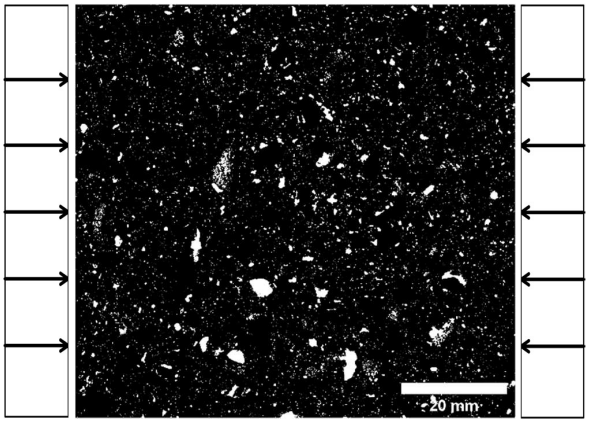

Sf7-1,5m90deg-LF-2

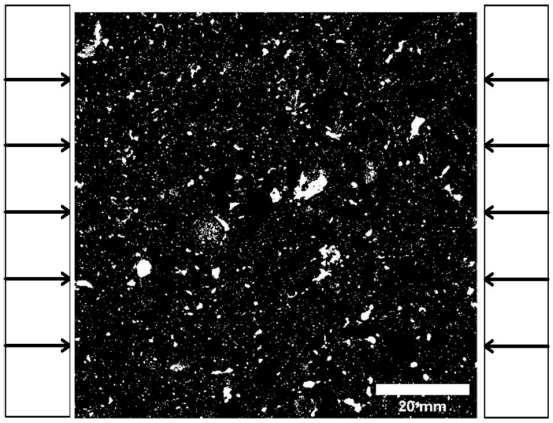

Appendix D Water penetration - complete overview and penetration fronts

D.1 Overview table

Table 30: Overview of all the water penetration tests.

Sample	Pressure $[MPa]$	Time $[h]$	Max penetration $[mm]$	$K_{valenta}$ $[m/s]$	$K_{vuorinen}$ $[m/s]$
3%N2	0.3	72	31	2.7E-12	1.6E-12
3%N4	0.1	48	16	3.2E-12	2.2E-12
3%N5	0.3	72	13	4.7E-13	8.2E-14
3%N6	0.3	72	41	4.7E-12	4.2E-12
3%P1	0.5 (70h) and 0.7 (24h)	94	10	1.2E-13	7.4E-15
3%P2	0.3	72	0	-	-
3%P3	0.5	3	23	2.1E-11	5.6E-11
3%P4	0.1	48	14	2.4E-12	1.4E-12
3%P5	0.3	72	0	-	-
3%P6	0.3	72	0	-	-
3%P7	0.5	70	6	6.1E-14	2.5E-15
3%P8	0.5 (70h) and 0.7 (24h)	94	11	1.4E-13	1.0E-14
10%N2	0.1	1.75	84	2.0E-09	1.4E-07
10%N3	0.1	1.75	67	1.4E-09	7.1E-08
10%N4	0.1	24	>100	>2.1E-10	>2.9E-09
10%N5	0.1	1.75	96	3.1E-09	2.9E-07
10%P1	0.3	6.33	70	1.3E-10	1.3E-09
10%P2	0.3	6.33	80	1.7E-10	2.0E-09
10%P3	0.1	1.75	19	1.0E-10	8.7E-10
10%P4	0.1	24	26	1.4E-11	2.8E-11
10%P5	0.1	1.75	5	6.6E-12	7.6E-12
10%P6	0.1	1.75	14	5.3E-11	2.7E-10
S1 (Ref1.2)	0.5	70	0	-	-
S2 (Ref1.2)	0.5	70	6	5.9E-14	2.3E-15
S3 (Ref1.2)	0.5 (70h) and 0.7 (24h)	94	5	2.7E-14	6.3E-16
S4 (Ref1.2)	0.5 (70h) and 0.7 (24h)	94	11	1.3E-13	9.4E-15

D.2 Penetration fronts

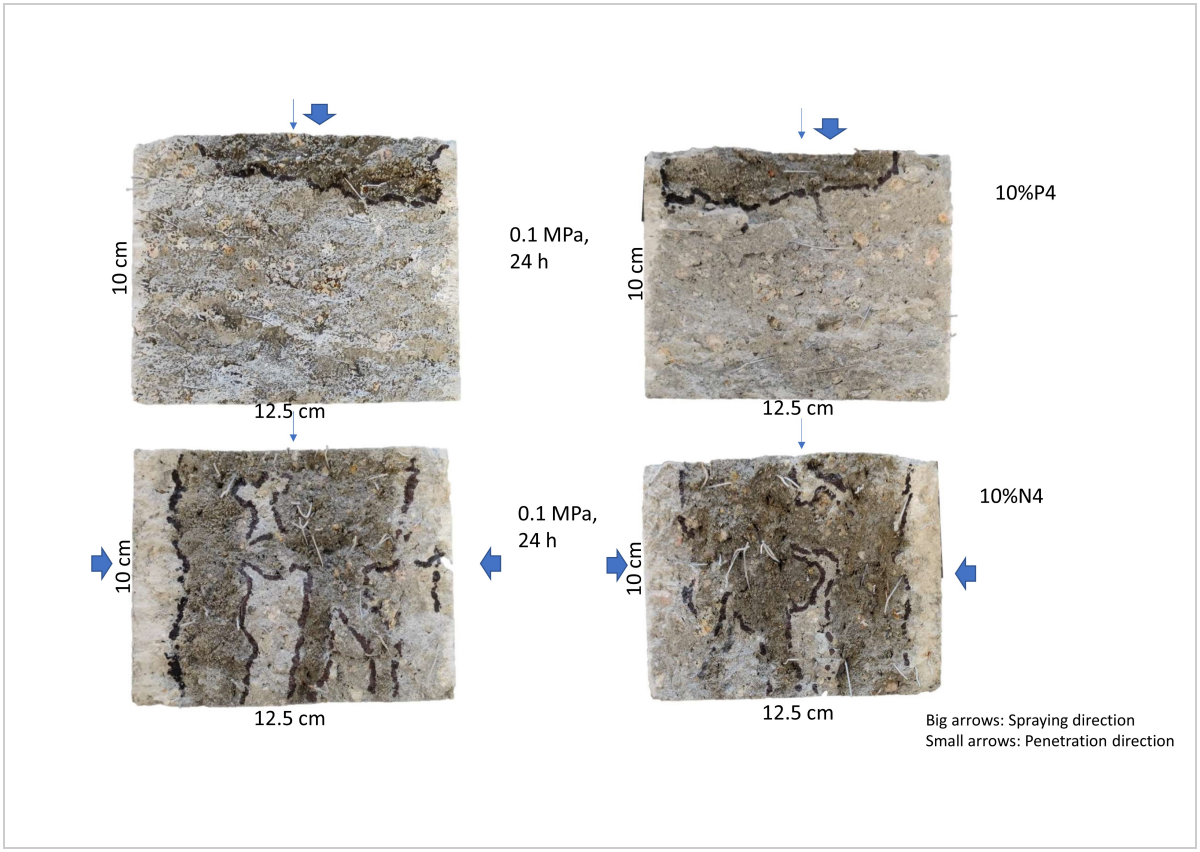

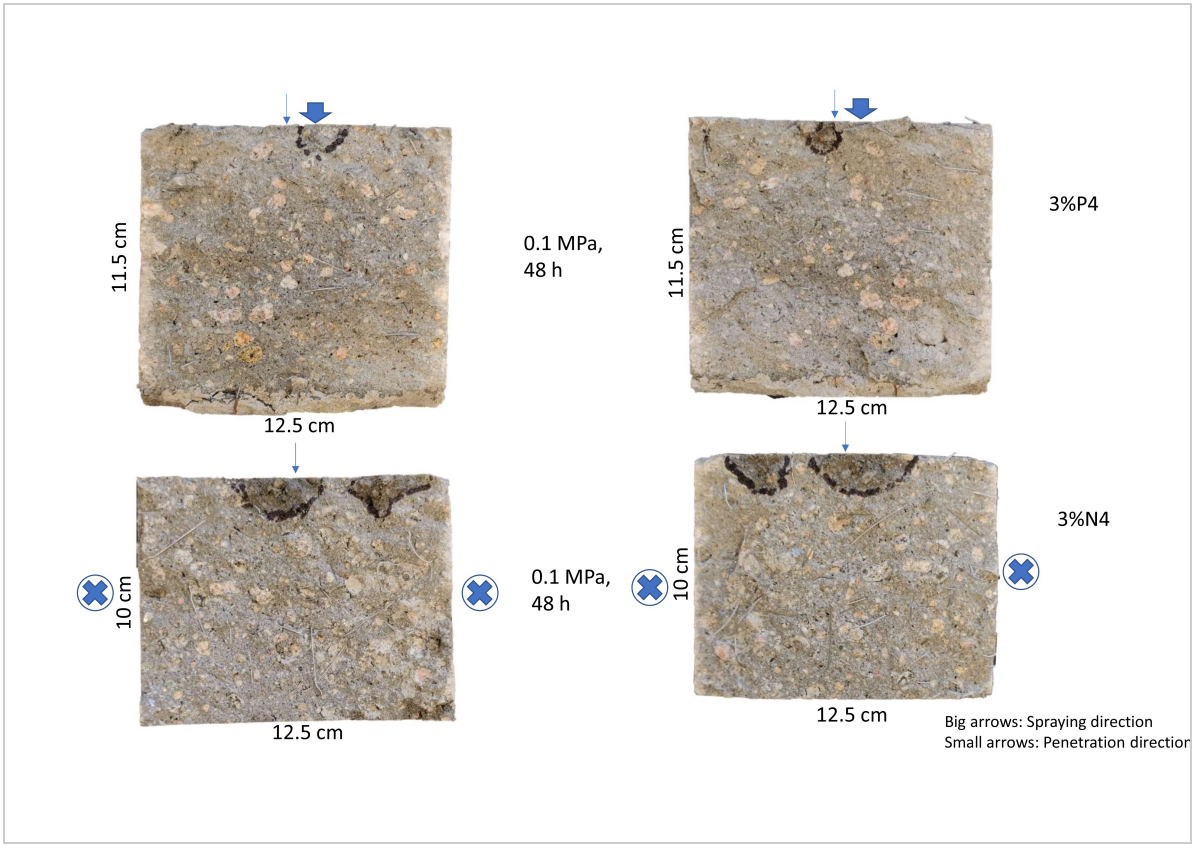

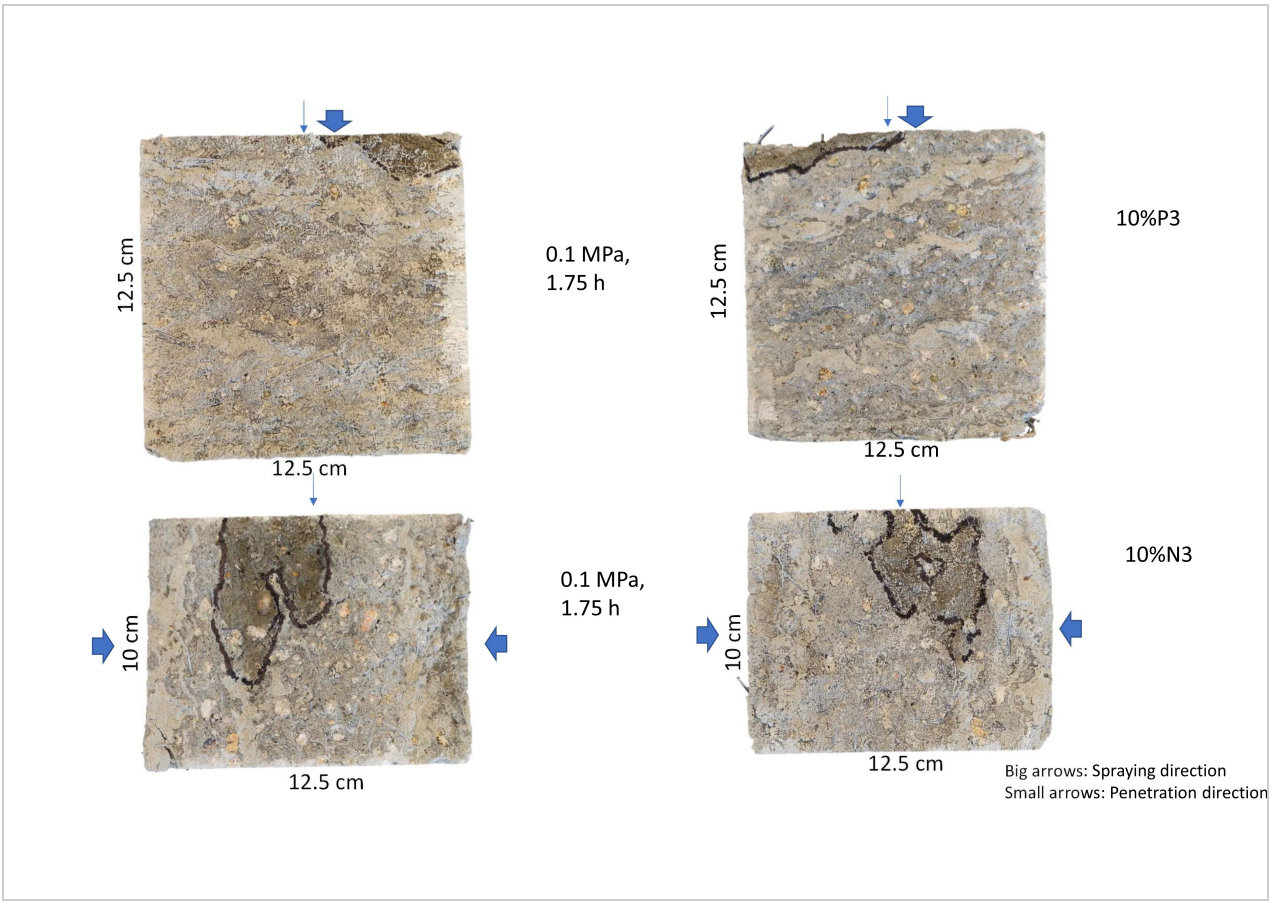
12.5 cm
12.5 cm
0.1 MPa,
1.75 h
12.5 cm
12.5 cm
10%P3
10 cm
12.5 cm
0.1 MPa,
1.75 h
10 cm
12.5 cm
10%N3
Big arrows: Spraying direction
Small arrows: Penetration direction

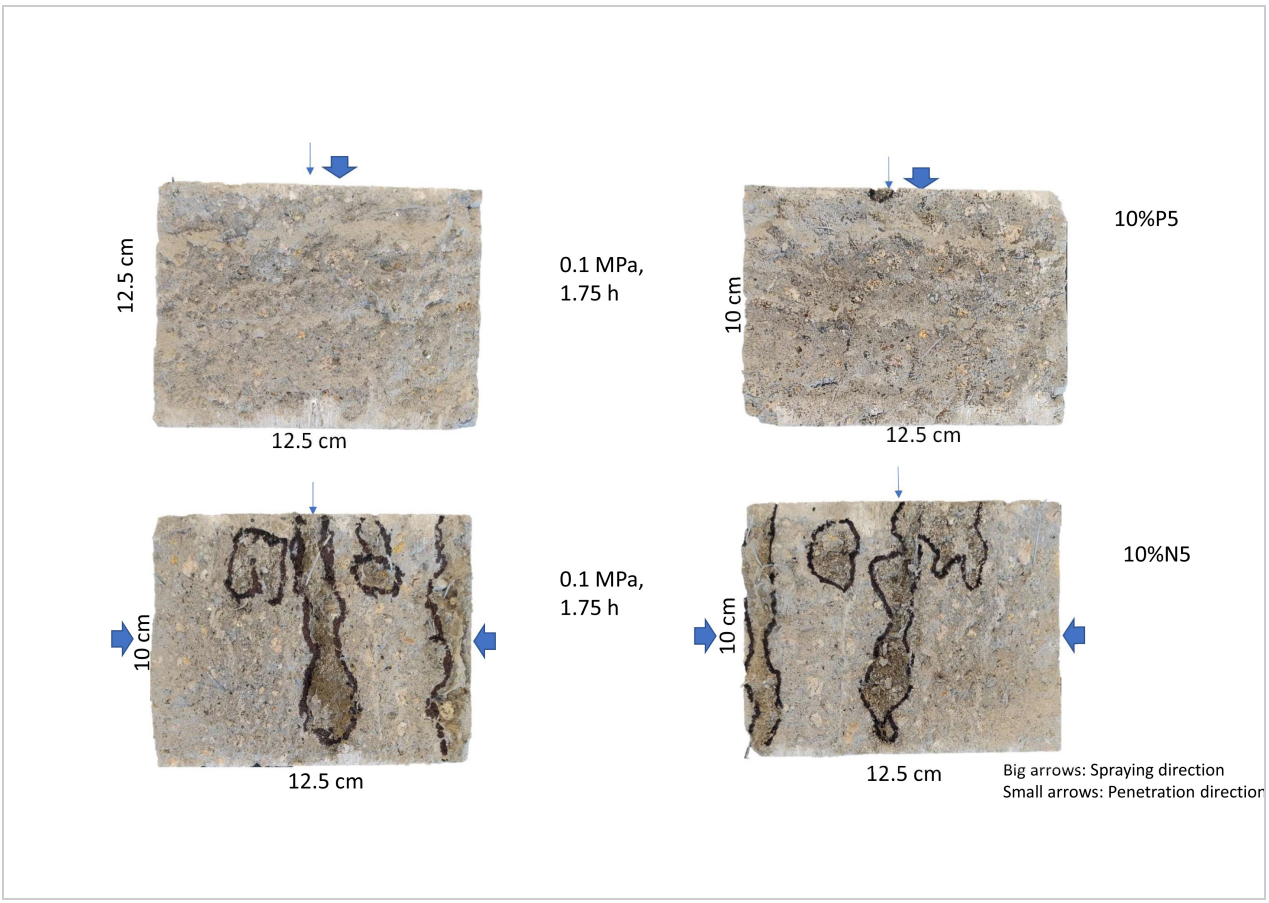
12.5 cm
12.5 cm
0.1 MPa,
1.75 h
10 cm
12.5 cm
10%P5
10 cm
12.5 cm
0.1 MPa,
1.75 h
10 cm
12.5 cm
10%N5
Big arrows: Spraying direction
Small arrows: Penetration direction

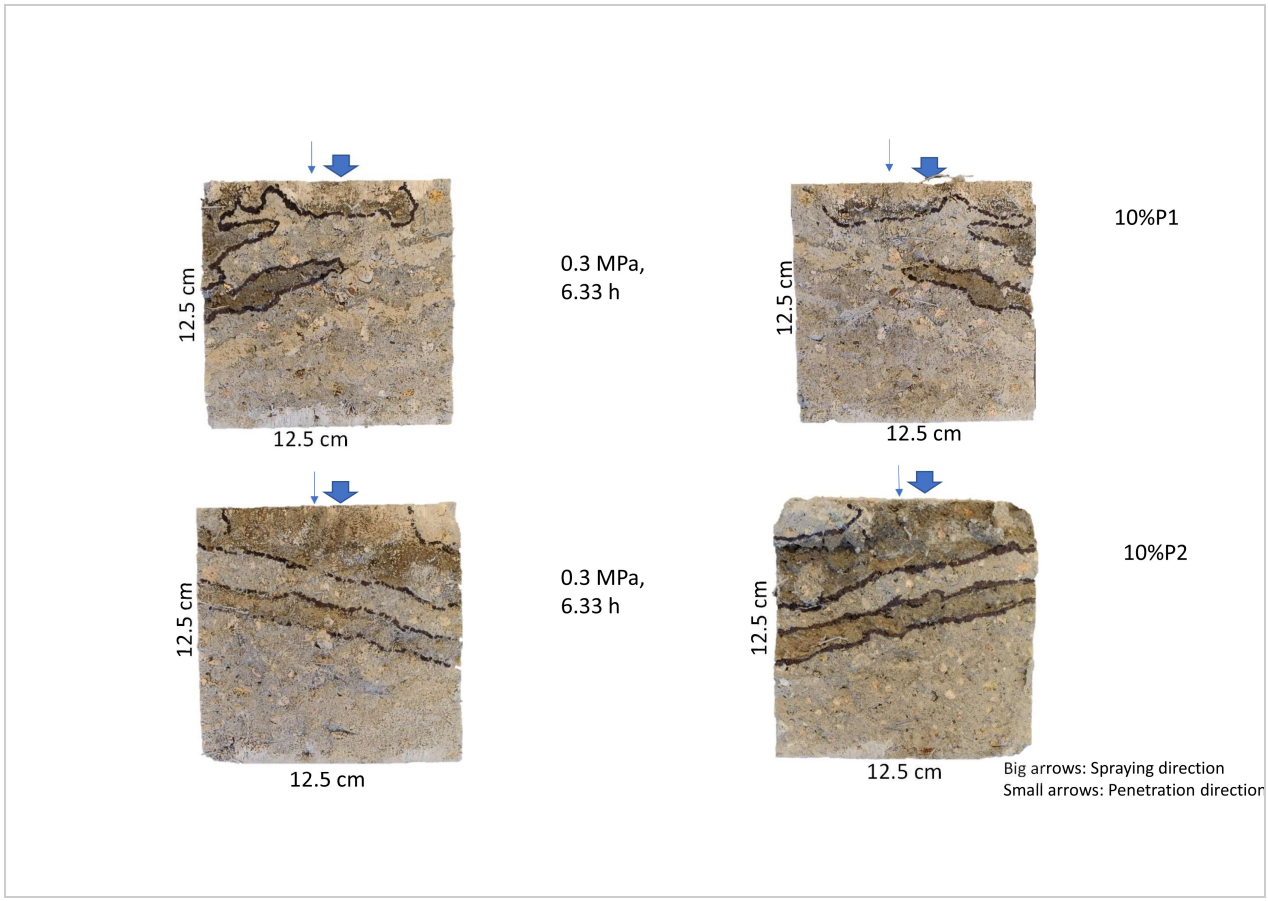
12.5 cm
12.5 cm
0.3 MPa,
6.33 h
12.5 cm
12.5 cm
10%P1
12.5 cm
12.5 cm
0.3 MPa,
6.33 h
12.5 cm
12.5 cm
10%P2
Big arrows: Spraying direction
Small arrows: Penetration direction

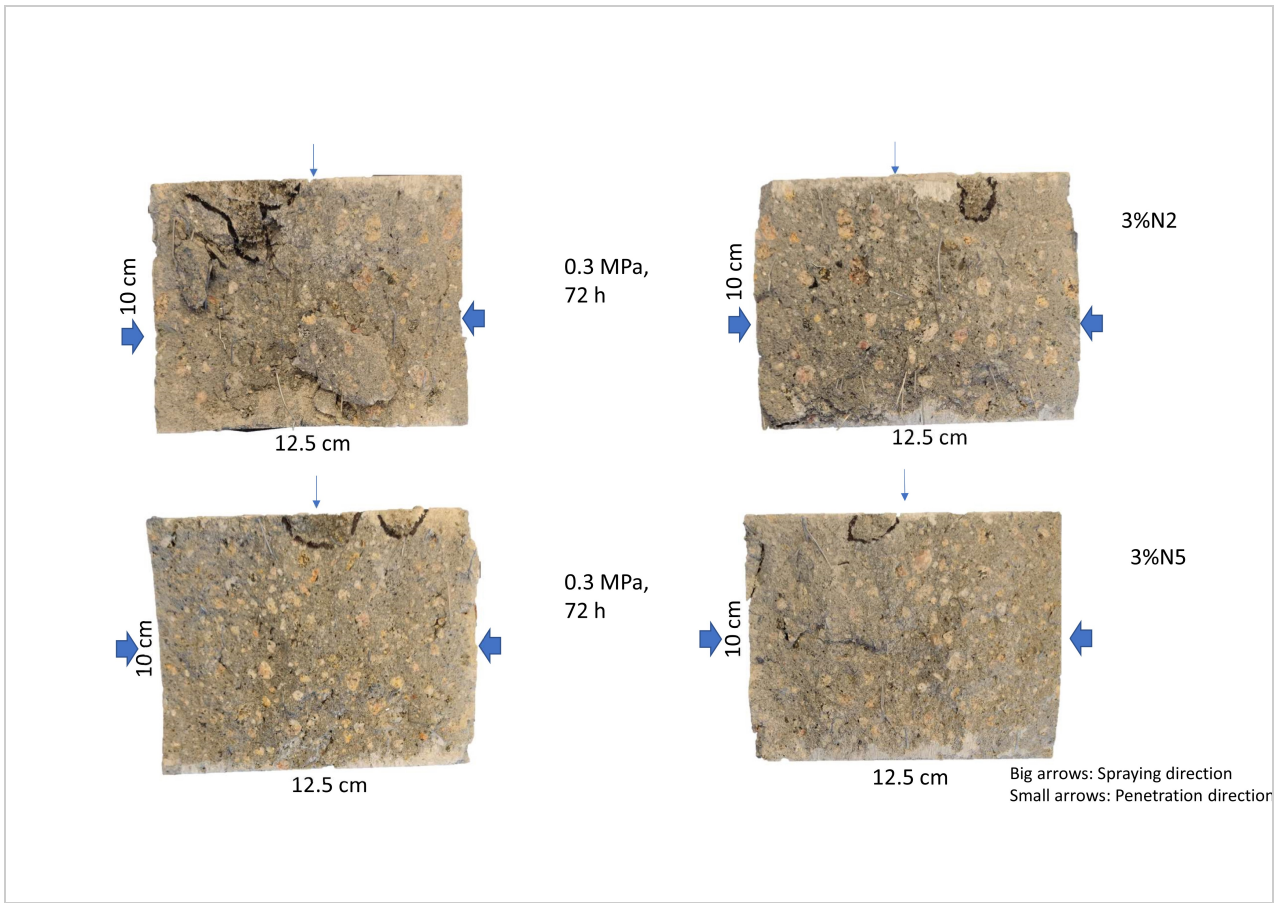
10 cm
12.5 cm
0.3 MPa,
72 h
10 cm
12.5 cm
3%N2
10 cm
12.5 cm
0.3 MPa,
72 h
10 cm
12.5 cm
3%N5
Big arrows: Spraying direction
Small arrows: Penetration direction

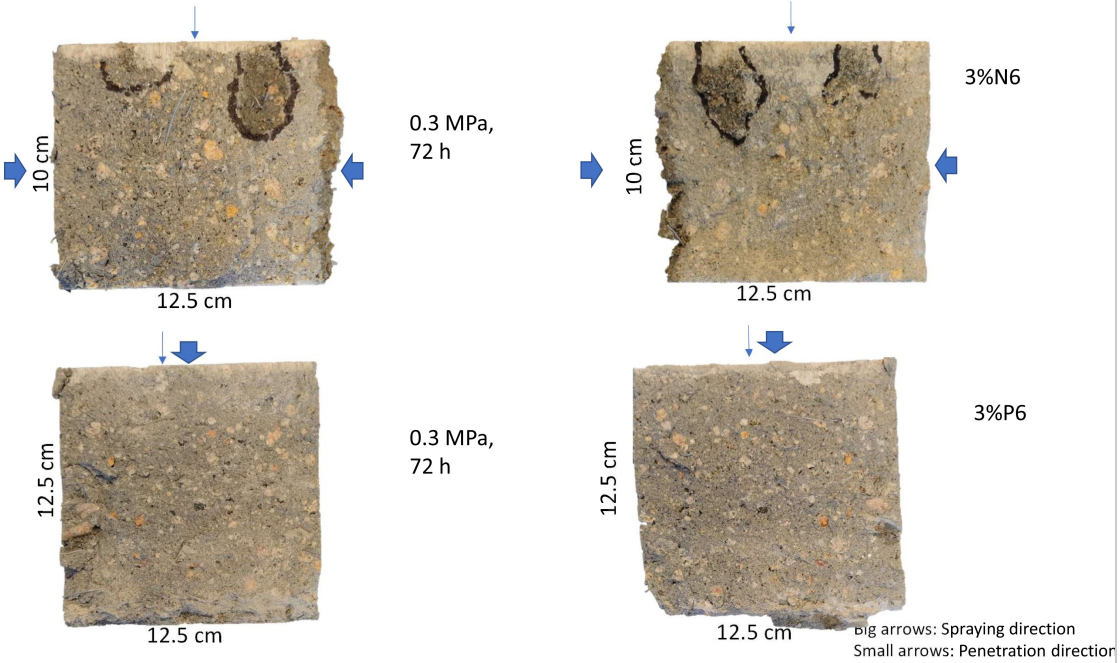
10 cm
12.5 cm
0.3 MPa,
72 h
3%N6
10 cm
12.5 cm
12.5 cm
12.5 cm
0.3 MPa,
72 h
3%P6
12.5 cm
12.5 cm
Big arrows: Spraying direction
Small arrows: Penetration direction

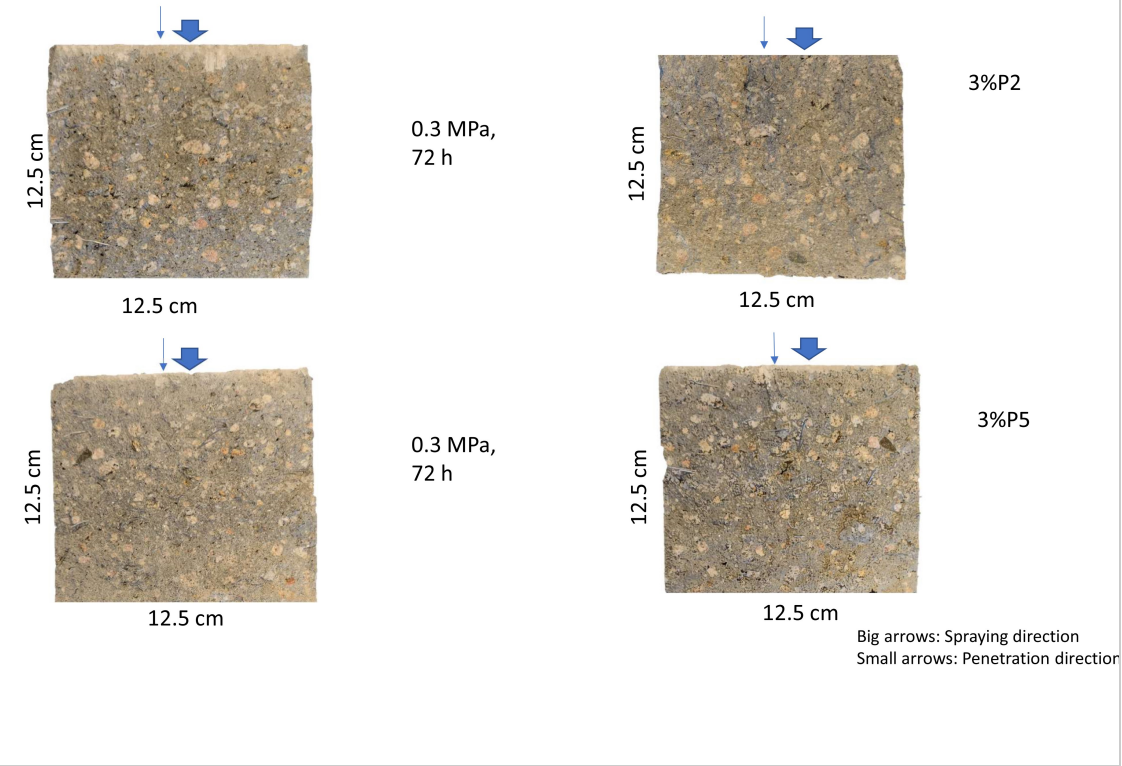
12.5 cm
12.5 cm
0.3 MPa,
72 h
3%P2
12.5 cm
12.5 cm
12.5 cm
12.5 cm
0.3 MPa,
72 h
3%P5
12.5 cm
12.5 cm
Big arrows: Spraying direction
Small arrows: Penetration direction

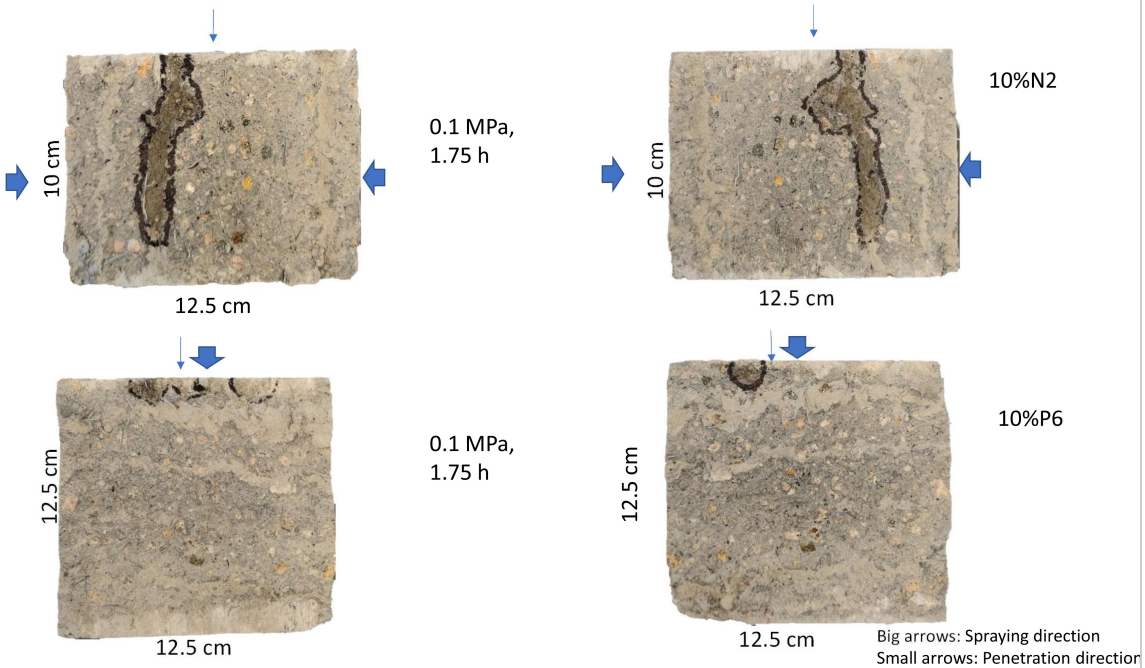
10 cm
12.5 cm
0.1 MPa,
1.75 h
10%N2
10 cm
12.5 cm
12.5 cm
12.5 cm
0.1 MPa,
1.75 h
10%P6
12.5 cm
12.5 cm
Big arrows: Spraying direction
Small arrows: Penetration direction

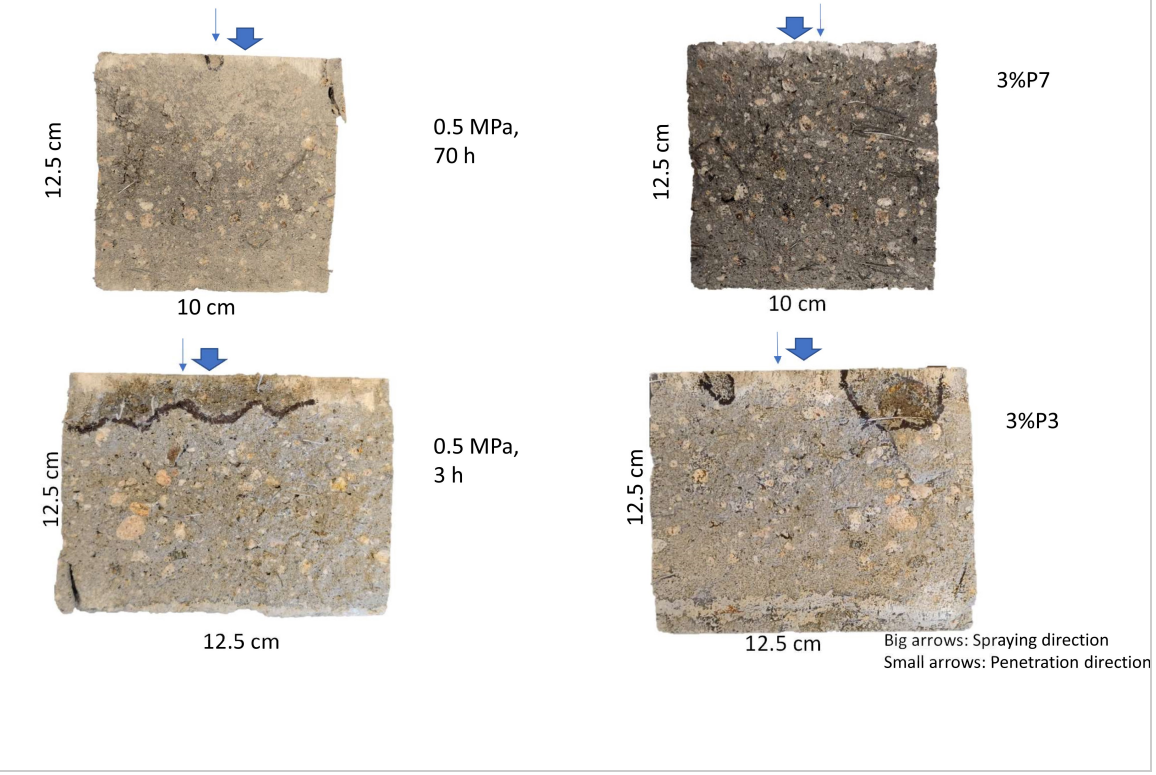
12.5 cm
10 cm
0.5 MPa,
70 h
3%P7
12.5 cm
10 cm
12.5 cm
12.5 cm
0.5 MPa,
3 h
3%P3
12.5 cm
12.5 cm
Big arrows: Spraying direction
Small arrows: Penetration direction

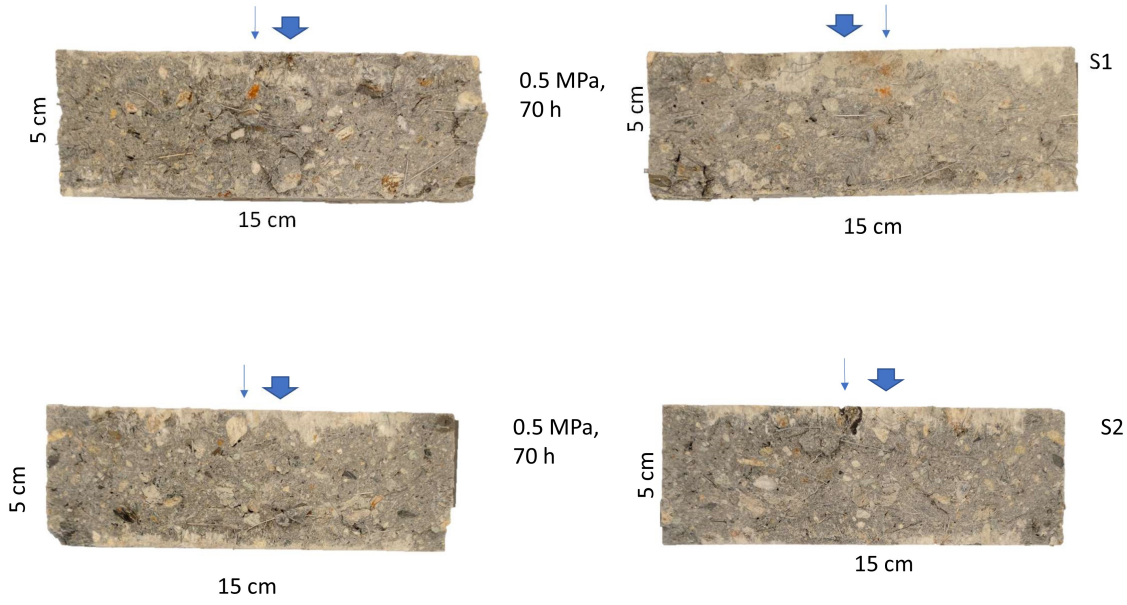
5 cm
15 cm
0.5 MPa,
70 h
S1
5 cm
15 cm
5 cm
15 cm
0.5 MPa,
70 h
S2
5 cm
15 cm
Big arrows: Spraying direction
Small arrows: Penetration direction

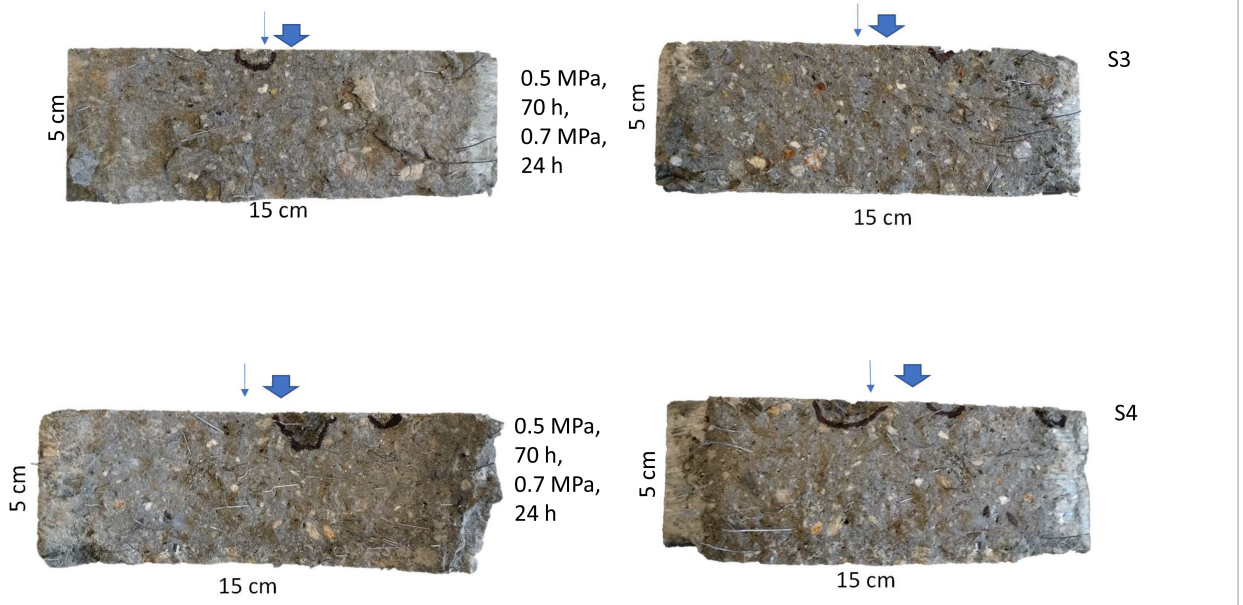
5 cm
15 cm
0.5 MPa,
70 h,
0.7 MPa,
24 h
S3
5 cm
15 cm
5 cm
15 cm
0.5 MPa,
70 h,
0.7 MPa,
24 h
S4
5 cm
15 cm
Big arrows: Spraying direction
Small arrows: Penetration direction

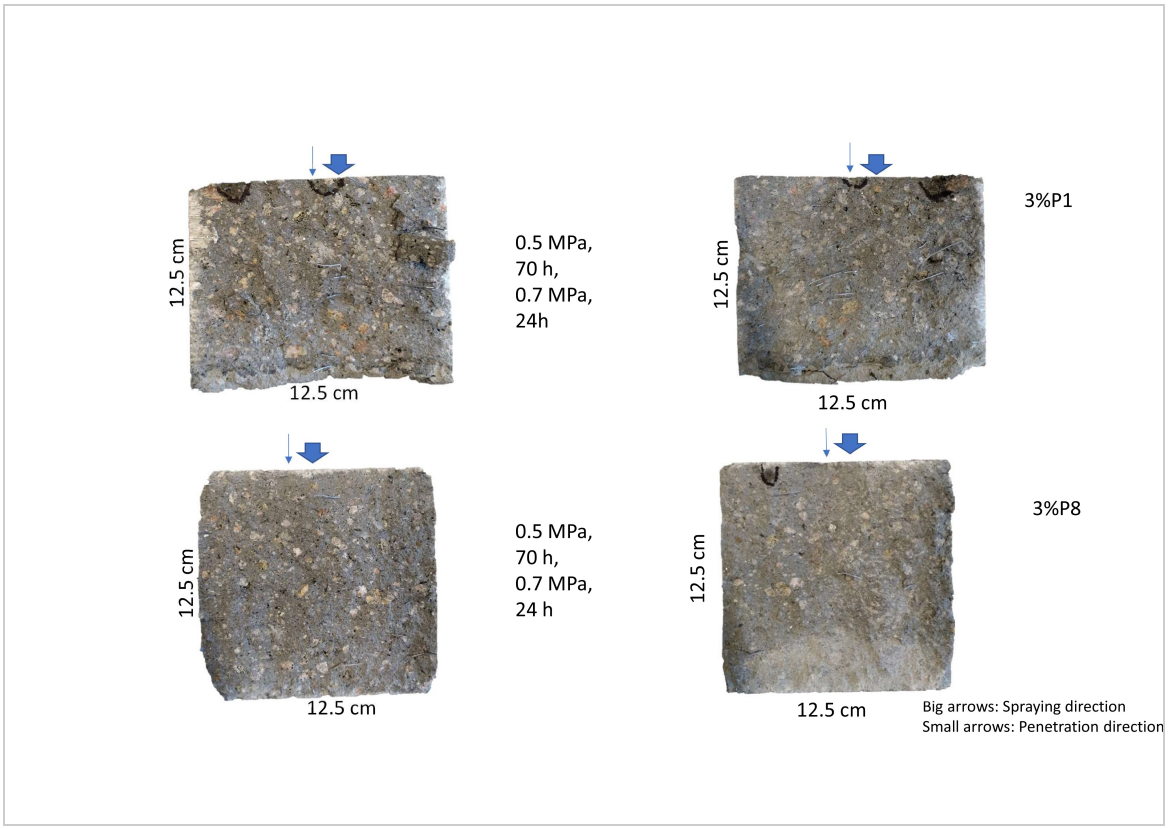
12.5 cm
12.5 cm
0.5 MPa,
70 h,
0.7 MPa,
24h
12.5 cm
12.5 cm
3%P1
12.5 cm
12.5 cm
0.5 MPa,
70 h,
0.7 MPa,
24 h
12.5 cm
12.5 cm
3%P8
Big arrows: Spraying direction
Small arrows: Penetration direction

Magne Stangeland Hårr & Gaute Kjeka

NTNU
Norwegian University of
Science and Technology